# TESTING OZONE SENSITIVITIES USING PROCESS ANALYSIS, CHEMICAL INDICATORS, AND VERY FINE SCALE MODELING WITH CMAQ IN THE PACIFIC NORTHWEST

By

YING XIE

A dissertation submitted in partial fulfillment of
the requirements for the degree of

DOCTOR OF PHILOSOPHY

WASHINGTON STATE UNIVERSITY
Department of Civil and Environmental Engineering

DECEMBER 2008

To the Faculty of Washington State University:

The members of the Committee appointed to examine the dissertation of YING XIE find it satisfactory and recommend that it be accepted.

_____
Chair

_____

_____

_____

# ACKNOWLEDGEMENT

I express my deepest gratitude to my advisor, Brian Lamb, for his continuing guidance, support, and encouragement. I thank him for bringing me into the air quality modeling world, providing sound advice, and giving me the freedom to explore the field. I also thank him for being so kind personally, which gives me the opportunity to balance life and work.

I would like to thank my committee members helped me to finish this work. To Tom Jobson for his thoughtful comments and generous support on data analysis. To Jeff Arnold for providing very helpful scientific guidance and suggestions. To Hal Westberg for volunteering his time and coming back to Pullman for my preliminary exam and defense.

I would like to thank the financial support from the Boeing Endowment and the NW-AIRQUEST Consortium. Many thanks to Rob Elleman for providing data, code, as well as very helpful suggestions throughout many stages of my study. I also would like to thank collaborators at the Washington State Department of Ecology, Puget Sound Clean Air Agency, Oregon Department of Environmental Quality, and Idaho Department of Environmental Quality for data support and sharing resources.

I would like to acknowledge LAR graduate students. Special thank to Jeremy Avise who I learned a lot from and shared wonderful time together as officemate. To Jack Chen,

who gave me the first Unix lesson when I arrived in Pullman and provided many years of modeling support. To Shelley Pressley, Rasa Grivicke, and many more for making LAR a lovely place. I would also like to express my thank to the staff who provided constant help: Tom Weber, Jim Kusznir, Maureen Clausen, Lola Gillespie, Glenda Rogers, Cyndi Whitmore, and Vicki Ruddick.

Finally I would like to thank my family and friends. You are the ones give me the courage to go to graduate school and joyfulness in life. I never would have finished this without you. Special thank goes to Mom and Dad for your deepest love and care.

TESTING OZONE SENSITIVITIES USING PROCESS ANALYSIS, CHEMICAL INDICATORS, AND VERY FINE SCALE MODELING WITH CMAQ IN THE PACIFIC NORTHWEST

Abstract

by Ying Xie, Ph.D.
Washington State University
December 2008

Chair: Brian K. Lamb

This research employed the MM5/SMOKE/CMAQ modeling system to investigate ozone formation and fate in the Pacific Northwest region through three separate studies. In the first study, chemical features of instantaneous ozone production and the behavior of local photochemical indicators were examined with process analysis in CMAQ. Maximum ozone production ($P(O_3)$) rate was 30-40 ppb $hr^{-1}$ downwind of the Portland urban center, with $NO_x$ concentrations of 5-20 ppb and total VOC reactivity above 8 $s^{-1}$. Five indicators ($f_{OH+HC}$, $f_{HO2+NO}$, $P(H_2O_2)/P(HNO_3)$, $O_3/NO_x$, and $L_N/Q$) were found to be useful tools for distinguishing VOC/$NO_x$ sensitive conditions, and the results indicated that the greatest $P(O_3)$ (>30 ppb $hr^{-1}$) occurred at transitional or $NO_x$-limited conditions for the Portland area.

In the second study, the CMAQ model was evaluated for predicted $O_3$-$NO_x$-VOC chemistry by comparing to aircraft measurements collected during a field experiment in western Washington. Results showed that anthropogenic VOC and CO were the major contributors to odd oxygen photochemistry in the morning urban profile, while CO and

oxygenated compounds accounted for two thirds of the measured reactivity in the afternoon aged plume. Peak $O_3$ was associated with VOC-sensitive conditions, but close to the transitional regime. The standard modeling scenario over-predicted the peak $O_3$ and $O_3/NO_y$ slope; these results suggested that the VOC in the current emission inventory might be too high. Modeled $CO/NO_y$ and $VOC/NO_y$ ratios obtained with the current emission inventory were also significantly higher than those observed from morning urban flights, with CO concentrations over-predicted by 80% and the total VOC reactivity over-predicted by 30%. Reducing the VOC emissions by 30% improved model performance for these parameters.

In the last study, the effects of using high resolution (1 km) meteorological and emissions inputs to photochemical simulations of $O_3$ were investigated. Results showed that using high resolution meteorological input alone had a larger impact on the position and peak levels of the $O_3$ plume, with substantial increases in $O_3$ concentrations at places where complex terrain plays an important role. Using high resolution emissions tended to affect small-scale features in $O_3$ concentration patterns mainly within the urban area.

# TABLE OF CONTENTS

# LIST OF TABLES

Page

**CHAPTER ONE:**



**CHAPTER TWO:**



**CHAPTER THREE:**



**CHAPTER FOUR:**

# LIST OF FIGURES

Page

**CHAPTER ONE:**



**CHAPTER TWO:**

**CHAPTER THREE:**

**CHAPTER FOUR:**

# CHAPTER ONE

## Introduction

Tropospheric ozone is formed by complex photochemical reactions between volatile organic compounds (VOCs) and nitrogen oxides ($NO_x$=NO+$NO_2$) in the presence of sunlight. Ozone ($O_3$) has long been a major concern for air quality due to its adverse impact on human health [*Lippman*, 1993] and ecosystems [NRC, 1991] as well as its key role in tropospheric photochemistry and the formation of other pollutants [*Seinfeld and Pandis*, 1997]. It remains as the most troublesome of the criteria pollutants: half of the US population lives in areas where the ozone air quality standard was exceeded in 2007 [http://www.epa.gov/airtrends/sixpoll.html].

Regional $O_3$ levels are governed by the interactions of complex physical and chemical processes, including emissions of precursors, transport and diffusion, photochemical production and loss, as well as dry and wet deposition. For urban areas, ozone control strategies have been developed largely based on 3-D air quality model simulations. Due to the complex nonlinearity of $O_3$-VOC-$NO_x$ chemistry, however, predicted peak $O_3$ levels are not dependent on a unique set of VOC and $NO_x$ concentrations. The effectiveness of using air quality models to design and evaluate control strategy is therefore crucially dependent upon our understanding of the interactions between these nonlinear processes and their representation in the model. For the Pacific Northwest region, the performance of air quality models is also strongly affected by the simulation of regional transport and dispersion, as the region is heavily influenced by complex terrain and unique meteorological conditions within and near the Columbia River Gorge and the Cascade Mountain range.

The goal of this work is to gain a better understanding of ozone formation and fate in the region and to provide insight for future air quality simulation and abatement methods design. This dissertation includes three manuscripts to be published in peer reviewed journals. In the first manuscript:

***VOC/$NO_x$ sensitivity analysis for ozone production using CMAQ process analysis for the Pacific Northwest***

the chemical features of instantaneous ozone production ($P(O_3)$) and behavior of local photochemical indicators are investigated. In the second manuscript:

***Evaluation of $O_3$-$NO_x$-VOC sensitivity predicted with the CMAQ photochemical model using PNW2001 field data***

the Community Multi-scale Air Quality (CMAQ) model is evaluated for predictions of $O_3$-$NO_x$-VOC chemistry by comparing model results to aircraft measurements of CO, $NO_y$ ( = $NO_X$ + $NO_3$ + $HNO_3$ + $HNO_4$ + peroxyacetyl nitrate + other organic nitrates + other lesser contributing oxidized nitrogen compounds), $O_3$, and VOCs collected during the Pacific Northwest field experiment (PNW2001) in terms of cumulative indicator values, emission inventory, and VOC reactivity. In the third manuscript:

***Investigating the impact of high resolution meteorological input and emissions on modeling ozone in the Pacific Northwest***

the effects of using high resolution meteorological and emissions inputs to a photochemical modeling simulation of $O_3$ for the region is explored.

## 1. Ozone chemistry

The relationship between $O_3$, $NO_x$ and VOC can be illustrated by isopleth plot (Figure 1). The plot [*Tonnesen and Dennis*, 2000a] is based on a simple trajectory model simulation for Atlanta, GA. The isopleth lines correspond to the maximum predicted $O_3$ concentrations with different initial $NO_x$ and VOC levels. The heavy line shows the $O_3$ ridgeline, which responds to the maximum $O_3$ levels at given VOC concentrations allowing $NO_x$ concentrations to change ($d[O_3]/dE_{NOx} = 0$). To the left of the ridgeline is the VOC-sensitive regime where $O_3$ increases with increasing VOC concentrations and decreases with increasing $NO_x$ concentrations, whereas to the right of the ridgeline is the $NO_x$-limited regime where $O_3$ increases with increasing $NO_x$ concentrations and is less sensitive to changes in VOC concentrations.

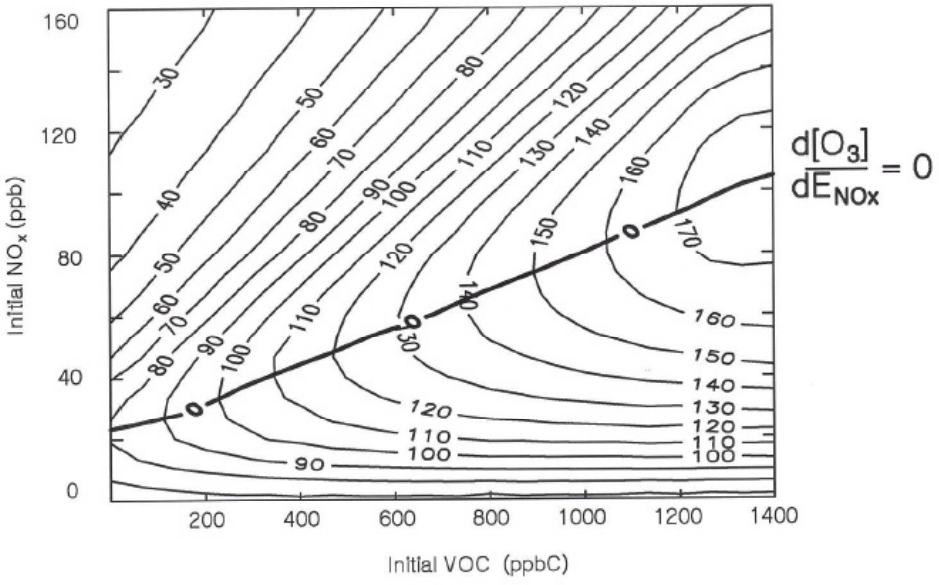


Figure 1. Ozone isopleths (ppb) as a function of VOC and $NO_x$ levels from a simple trajectory model [*Tonnesen and Dennis*, 2000a].

The division between the $NO_x$-sensitive and VOC-sensitive regimes can be explained by the dynamics of $P(O_3)$ and the VOC-OH-$NO_x$ chemistry. $P(O_3)$ is governed by the initiation, propagation, and terminations of a few important radical species in the atmosphere which can be described by the following sets of equations [*Seinfeld and Pandis*, 1997].

Initiation

$$O_3 + h\nu \rightarrow O(^1D) \quad \text{(R1)}$$

$$O(^1D) + H_2O \rightarrow 2OH$$

$$HCHO + h\nu \rightarrow 2HO_2 \quad \text{(R2)}$$

$$HONO + h\nu \rightarrow OH + NO \quad \text{(R3)}$$

Propagation:

$$OH + VOC_i \rightarrow RO_2 \quad \text{(R4)}$$

$$RO_2 + NO \rightarrow NO_2 + HO_2 + \text{intermediate VOC} \quad \text{(R5)}$$

$$HO_2 + NO \rightarrow NO_2 + OH \quad \text{(R6)}$$

$$NO_2 + h\nu \rightarrow NO + O \quad \text{(R7)}$$

$$O + O_2 \rightarrow O_3$$

Termination:

Radical + $NO_x$

$$OH + NO_2 \rightarrow HNO_3 \quad \text{(R8)}$$

$$RO_2 + NO \rightarrow \text{organic nitrate} \quad \text{(R9)}$$

$$CH_3CO_3 + NO_2 \leftrightarrow PAN \quad \text{(R10)}$$

Radical + Radical

$$HO_2 + HO_2 \rightarrow H_2O_2 \quad \text{(R11)}$$

$$RO_2 + HO_2 \rightarrow ROOH \quad \text{(R12)}$$

$$OH + HO_2 \rightarrow H_2O + O_2 \quad \text{(R13)}$$

$$RO_2 + R'O_2 \rightarrow \text{products} \quad \text{(R14)}$$

In the initiation step, free radicals (OH, $HO_2$, and $RO_2$) are formed by splitting chemical bonds through photolysis and ozonolysis reactions. The most important reactions in this step are $O_3$ and HONO photolysis that produce OH radicals and HCHO photolysis that produces $HO_2$ radicals. In the propagation step, OH attacks VOCs forming $RO_2$ and $HO_2$ radicals, which then oxidize NO to $NO_2$. Subsequently, $O_3$ is formed through $NO_2$ photolysis. The cycle completes with the regenerating of OH in reaction R6 and NO in R7. In the termination step, radicals are removed from the system through two categories of reactions: 1) radicals reacting with $NO_x$ and 2) radicals reacting with each other.

OH propagation efficiency ($Pr_{OH}$) and OH chain length are two terms often used to characterize the ozone production cycle. $Pr_{OH}$ is defined as the average fraction of OH radicals which could be recycled in the propagation reactions. OH chain length is defined as the average number of times that a new radical can be recycled before being removed from the system through termination reactions. OH chain length is calculated based on $Pr_{OH}$ as:

$$\text{OH chain length} = 1 + Pr_{OH} + Pr_{OH}^2 + Pr_{OH}^3 + \ldots = 1/(1-Pr_{OH}) \quad (1)$$

OH attacking VOCs is the rate-limiting step in the cycle, and therefore, $P(O_3)$ is roughly proportional to the production rate of OH radicals (P(OH)), which is calculated as the product of new OH and OH chain length:

$$P(OH) = P(newOH)/(1-Pr_{OH}) \quad (2)$$

Although P(OH) is affected by both the newly initiated OH and OH chain length, the latter has a dominant impact since P(OH) changes with the inverse of $Pr_{OH}$ and it has been found that the ozone ridgeline in an ozone isopleth corresponds to the ridgeline of maximum OH chain length [*Tonnesen and Dennis*, 2000a].

Conditions with relatively low VOC/$NO_x$ ratios are found to the left of the ozone ridgeline where $P(O_3)$ is limited by radical availability. Here $NO_2$ competes with VOCs for OH, and radical termination through $HNO_3$ is preferred compared to radical-to-radical self-reaction due to the high $NO_x$ level. P(OH) is low as OH is removed from the system in the form of $HNO_3$. Radial initiation is also low since high NO titrates $O_3$ back to $NO_2$, limiting OH formed from $O_3$ photolysis. In this radical-limited regime, $O_3$ increases with increasing VOC concentrations, but decreases with increasing $NO_x$ concentrations.

Conditions with relatively high VOC/$NO_x$ ratios occur to right of the ridgeline with very different patterns. Here $Pr_{OH}$ is low due to limited NO to react with peroxy radials, and consequently radial-to-radical self-termination forming peroxides is

preferred. In this regime, $NO_x$ is the limiting factor and $O_3$ increases with increasing $NO_x$ concentrations, but is less sensitive to changes in VOC concentrations.

## 2. Theoretical basis of photochemical indicators

The indicator concept was proposed by *Milford et al*. [1994] and *Sillman* [1995, 1997]. They found that in 3-D photochemical models, the ratio of certain species would have different values related to $NO_x$- and VOC-sensitive conditions. Two categories of indicators have been developed including both cumulative ratios such as $O_3/NO_y$, $O_3/NO_z$, $H_2O_2/HNO_3$ [*Sillman*, 1997] and instantaneous ratios such as $P(H_2O_2)/P(HNO_3)$ [*Tonnesen and Dennis*, 2000a] and $L_N/Q$ [*Kleinman* et al., 1997; *Kleinman*, 2005]. In this study, five instantaneous ($f_{OH+HC}$, $f_{HO2+NO}$, $P(H_2O_2)/P(HNO_3)$, $O_3/NO_x$, and $L_N/Q$) and one cumulative ($O_3/NO_y$) indicators are evaluated as summarized in Table 1. The theoretical basis of these indicators is described in the following section.

### 2.1 $P(H_2O_2)/P(HNO_3)$ and $L_N/Q$

*Sillman* [1995] showed that the division between $NO_x$-sensitive and VOC-sensitive regimes is attributed to the relative formation rate of termination products: for conditions with relatively high VOC and low $NO_x$, the formation of peroxides as radical sinks is preferred due to the abundance of free radicals, whereas for conditions with relatively high $NO_x$ and low VOC, $NO_2$ reacting with OH and terminating to nitric acid is preferred. He proposed that the condition of equal sensitivity to $NO_x$ and VOC occurs at:

$$P(HNO_3) = 2(P(H_2O_2)+P(ROOH)) \quad (3)$$

*Kleinman* et al. [1997] and *Kleinman* [2005] showed that the sensitivity of $P(O_3)$ to $NO_x$ concentration, VOC reactivity, and radical production rate (Q) depends on the fraction of radicals that are removed by reactions with $NO_x$ , denoted as $L_N/Q$. Similar to *Sillman* [1995], Kleinman found that the transitional regime occurs at $L_N/Q = 0.5$.

Both formulas are derived based on the steady state balance of radical initiation and termination, where Q is equal to the sum of radical sinks:

$$Q = 2(P(H_2O_2)+ P(ROOH)) + P(HNO_3) + P(PAN) \quad (4)$$

In the derivation, $P(O_3)$ is expressed as a function of $HNO_3/H_2O_2$ or $L_N$, and then solved analytically for specific $HNO_3/H_2O_2$ or $L_N$ values that are associated with conditions for equal sensitivity of $P(O_3)$ to changes in $NO_x$ or VOC concentrations.

## 2.2 $f_{OH+HC}$ and $f_{HO2+NO}$

*Tonnesen and Dennis* [2000a] proposed $f_{OH+HC}$ and $f_{HO2+NO}$ as indicators based on analysis of radical propagation efficiency and OH chain length. $Pr_{OH}$ is expressed as:

$$Pr_{OH} = f_{OH+HC}\, f_{HO2+NO} \quad (5)$$

$f_{OH+HC}$ refers to the faction of OH reacts with VOCs, and can be calculated as:

$$f_{OH+HC} = \frac{\sum k_4 * [HC_i][OH]}{\sum k_4 * [HC_i][OH] + K_8 * [NO_2][OH] + misc.OHreactions} \quad (6)$$

where miscellaneous OH reactions include its reactions with $O_3$, $HO_2$, $SO_2$, etc.

$f_{HO2+NO}$ refers to the faction of $HO_2$ reacts with NO, and can be calculated as:

$$f_{HO2+NO} = \frac{k_9 * [NO][HO_2]}{k_9 * [NO][HO_2] + 2 * (k_{11a} * [HO_2]^2 + k_{11b} * [HO_2]^2[H_20]) + k_{12} * [HO_2][RO_2] + misc.HO_2 reactions} \quad (7)$$

where miscellaneous $HO_2$ reactions include its reactions with $O_3$, OH, etc. Here $f_{OH+HC}$ and $f_{HO2+NO}$ are defined based on the SAPRC99 chemical mechanism [*Carter*, 2000], and therefore, the formulas are slightly different from the original ones in *Tonnesen and Dennis* [2000a] where the RADM2 mechanism was used.

$f_{OH+HC}$ and $f_{HO2+NO}$ values have been related to the ridgeline conditions due to the dependence of $Pr_{OH}$ on these two ratios and their correlations with $NO_x$. As shown in equation 6 and 7, $f_{OH+HC}$ decreases with increasing $NO_2$, while $f_{HO2+NO}$ increases with increasing NO. Therefore, intermediate $NO_x$ levels will maximize the product of the two ($Pr_{OH}$), and subsequently maximize P(OH) and $P(O_3)$, thereby creating the ozone ridgeline.

### 2.3 $O_3/NO_x$

$O_3/NO_x$ was proposed by *Tonnesen and Dennis* [2000a] based on its correlation with OH radical initiation and propagation. At high $O_3/NO_x$ ratios, new OH radicals formed from $O_3$ photolysis is maximized. However, photostationary state equilibrium shifts the system towards low NO and high $NO_2$, decreasing both $f_{OH+HC}$ and $f_{HO2+NO}$, and therefore reducing OH chain length. On the other hand at low $O_3/NO_x$ ratios, $Pr_{OH}$ is high due to the high NO and low $NO_2$ levels. However, high NO titrates $O_3$ back to $NO_2$, and consequently, new OH initiated from $O_3$ is low. Intermediate $O_3/NO_x$ values are

thought to maximize the P(OH) from radical initiation and propagation, and therefore, are related to the ozone ridgeline.

## 2.4 $O_3/NO_y$

$O_3/NO_z$ ($NO_z = NO_y - NO_x$) and $O_3/HNO_3$ were proposed by *Sillman* [1995]. By assuming radical sources are proportional to $O_3$ concentration, these two indicators are derived with methods similar to $P(H_2O_2)/P(HNO_3)$. Subsequently, *Tonnesen and Dennis* [2000b] identified the same indicators based on radical propagation efficiency and OH chain length. $O_3/NO_y$ is related to $NO_x$- and VOC-sensitive conditions as it combines the effects of $O_3/NO_x$ and $O_3/NO_z$.

Table 1. Indicators and the changes associated with VOC- vs. $NO_x$-limited regimes.

| **Indicators** | **VOC-limited** | **$NO_x$-limited** |
|---|---|---|
| $f_{HO2+NO}$ | high $f_{HO2+NO}$, sufficient NO to react with $HO_2$, less $HO_2$ react with $HO_2$+$RO_2$ and peroxides formation | low $f_{HO2+NO}$, less NO react with $HO_2$, more $HO_2$ react with $HO_2$+$RO_2$ and peroxides formation |
| $f_{OH+HC}$ | low $f_{OH+HC}$, less OH react with HC, more OH react with $NO_2$ and $HNO_3$ formation | high $f_{OH+HC}$, more OH react with HC, less OH react with $NO_2$ and $HNO_3$ formation |
| $O_3/NO_x$ | low $O_3/NO_x$, low $O_3$, high NO, low $NO_2$, inhibited P(newOH) but increased $Pr_{OH}$ | high $O_3/NO_x$, high $O_3$, low NO, high $NO_2$, maximize P(newOH) but reduce $Pr_{OH}$ |
| $P(H_2O_2)/P(HNO_3)$ | low $P(H_2O_2)/P(HNO_3)$, more $HNO_3$ formation | high $P(H_2O_2)/P(HNO_3)$, more peroxides formation |
| $L_N/Q$ | high $L_N/Q$, more $HNO_3$ formation | low $L_N/Q$, more peroxides formation |
| $O_3/NO_y$ | low $O_3/NO_y$, more $HNO_3$ formation | high $O_3/NO_y$, more peroxides formation |

**References**


Carter, W. P. L. (2000), *Documentation of the SAPRC-99 Chemical Mechanism for VOC Reactivity Assessment*, No. 92 – 329, 95 – 308, Final Report to California Air Resources Board, Calif. Air Resour. Board, Riverside Calif. (Available at http://www.engr.ucr.edu/~carter/absts.htm#saprc99)

Kleinman, L. I., P. H. Daum, J. H. Lee, Y.-N. Lee, L. J. Nunnermacker, S. R. Springston, L. Newman, J. Weinstein-Lloyd, and S. Sillman (1997), Dependence of ozone production on NO and hydrocarbons in the troposphere, *Geophys Res. Lett., 24*, 2299–2302.

Kleinman, L. I. (2005), The dependence of tropospheric ozone production rate on ozone precursors, *Atmos. Environ., 39*, 575–586.

Lippmann, M. (1993), Health effects of tropospheric ozone: review of recent research findings and their implications to ambient air quality standards*, J. Expo. Anal. Environ. Epidemiol., 3*, 103-129.

Milford, J. B., D. Gao, S. Sillman, P. Blossey, and A. G. Russell (1994), Total reactive nitrogen ($NO_y$) as an indicator of the sensitivity of ozone to reductions in hydrocarbon and $NO_x$ emissions, *J. Geophys. Res., 99*(D2), 3533–3542.

National Research Council (1991), *Rethinking the Ozone Problem in Urban and Regional Air Pollution*. National Academy Press, Washington, District of Columbia.

Sillman, S. (1995), The use of $NO_y$, $H_2O_2$, and $HNO_3$ as indicators for $O_3$-$NO_x$-hydrocarbon sensitivity in urban locations, J. *Geophys. Res., 100*, 14,175–14,188, 1995.

Sillman, S., D. He, C. Cardelino, and R. E. Imhoff (1997), The use of photochemical indicators to evaluate ozone-$NO_x$-hydrocarbon sensitivity: Case studies from Atlanta, New York and Los Angeles, *J. Air Waste Manage.* Assoc*., 47*, 642– 652.

Seinfeld, J.H., and S.N. Pandis (1997), Atmospheric Chemistry and Physics—From Air Pollution to Climate Change, Wiley-Interscience, New York.

Tonnesen, G. S., and R. L. Dennis (2000a), Analysis of radical propagation efficiency to assess ozone sensitivity to hydrocarbons and $NO_x$, 1, Local indicators of instantaneous odd oxygen production sensitivity, *J. Geophys. Res*., *105*, 9213– 9226.

Tonnesen, G. S., and R. L. Dennis (2000b), Analysis of radical propagation efficiency to assess ozone sensitivity to hydrocarbons and $NO_x$, 2, Longlived species as indicators of ozone concentration sensitivity, *J. Geophys. Res., 105*, 9227– 9242.

# CHAPTER TWO

## VOC/$NO_x$ sensitivity analysis for ozone production using CMAQ process analysis for the Pacific Northwest

Ying Xie and Brian Lamb
*Washington State University, Department of Civil and Environmental Research*

## Abstract

As a way to improve our understanding of ozone formation in the Pacific Northwest, we have investigated the chemical features of ozone production rate ($P(O_3)$) and its sensitivity to changes in $NO_x$ and VOC emissions using process analysis in CMAQ for an ozone episode in Portland, OR that occurred during July, 1998. The analyses were conducted in three steps: 1) examining the chemical features of $P(O_3)$ and its relationship with $O_3$ precursors, 2) evaluating the behavior of five instantaneous indicators ($f_{OH+HC}$, $f_{HO2+NO}$, $P(H_2O_2)/P(HNO_3)$, $O_3/NO_x$, and $L_N/Q$), and 3) investigating the sensitivity of $P(O_3)$ to changes in $NO_x$ and VOC concentrations with these indicators. The maximum $P(O_3)$ was 30-40 ppb $hr^{-1}$ downwind of the Portland urban center, with $NO_x$ concentrations of 5-20 ppb and total VOC reactivity above 8 $s^{-1}$. Evaluated with mid-day values, all five indicators clearly distinguished $NO_x$- and VOC-sensitive conditions for ozone event days, but the different indicators were less consistent for the days with lower photochemical production. The indicator values associated with isopleth ridgeline conditions marking the transition from $NO_x$- to VOC-limited were similar to results from previous studies. The indicators were also useful for determining the temporal variations of ozone sensitivity, as their daytime values generally reflected the dynamic changes in the sensitivity. We evaluated the sensitivity of $P(O_3)$ to changes in $NO_x$ and VOC emissions with these indicators, and we found that the indicators provided an overall consistent picture and showed that the greatest $P(O_3)$ (>30 ppb $hr^{-1}$) mostly occurred at transitional or $NO_x$-limited conditions for the Portland area.

## 1. Introduction

The Cascadia region of the Pacific Northwest periodically experiences elevated $O_3$ levels downwind of the Portland, OR and Seattle, WA urban areas. Despite emission reductions in $O_3$ precursors, $O_3$ levels have not decreased to the same extent. Most of the modeling studies conducted in the region have involved direct comparisons of predicted and measured $O_3$ levels [*Barna et al*., 2000; *Vaughan et al*., 2004; *O'Neill et al*., 2005; *Chen et al.*, 2008]. It is well known that photochemical production of $O_3$ is a highly nonlinear system where the predicted peak $O_3$ level is not dependent on a unique set of $NO_x$ and VOC concentrations, and therefore, models might predict incorrect sensitivities to changes in precursors even while correctly predicting $O_3$ levels [*Sillman*, 1995].

The uncertainties in ozone sensitivity have led to the development of various indicators [*Milford et al*., 1994; *Sillman*, 1995; *Sillman et al*., 1998; *Kleinman et al*., 1997; *Tonnesen and Dennis*, 2000a, b] including both cumulative indicators for ozone concentrations and instantaneous indicators for local ozone production rate. *Sillman* [1995] and *Kleinman et al.* [1997] found that $NO_x$ and VOC sensitivity could be attributed to the relative formation rate of peroxides and nitric acid as radical sinks. The theoretical basis is that for conditions with relatively high VOC and low $NO_x$, the formation of peroxides as radical sinks is preferred due to the abundance of free radicals, whereas for conditions with relative high $NO_x$ and low VOC, $NO_2$ reacting with OH and terminating to nitric acid is preferred. In their studies, cumulative indicators such as the $H_2O_2/HNO_3$ and $O_3/NO_y$ were suggested based on a steady state balance of radical initiation and termination. In comparison to the cumulative ratios, *Tonnesen and Dennis*

[2000a] proposed instantaneous indicators such as I($NO,RO_2$) which approximates the fraction of $HO_2$ that reacts with NO, using a slightly different approach based on radical propagation efficiency. Also based on a steady state balance, *Kleinman* et al. [1997] and *Kleinman* [2005] reported that the sensitivity of $P(O_3)$ to $NO_x$ concentration, VOC reactivity, and radical production rate depends on the fraction of radicals that are removed by reactions with $NO_x$. The general thought is that those measurable indicators would have different values related to $NO_x$- and VOC-sensitive conditions, so that model-predicted sensitivity could be evaluated by comparing to measured indicator values or ozone sensitivity could be evaluated directly from measurements.

Although there have been a number of studies [*Sillman*, 1995; *Sillman et al*., 1997; *Kleinman et al.,* 1997; *Sillman et al*., 1998; *Tonnesen and Dennis*, 2000a, b; *Sillman and He,* 2002; *Sillman et al.*, 2003] of these indicators, there is considerable concern about how the indicators might behave under different conditions and geophysical settings, and with different models and photochemical mechanisms. Contradictory results have been reported by *Lu and Chang* [1998] and *Chock et al.* [1999]. For the Pacific Northwest region, these indicators haven't been widely tested, and, therefore, it is unclear whether the range of values related to ozone sensitivity are similar or different compared to other urban areas.

Cumulative and instantaneous indicators have complementary strengths for understanding accumulated and instantaneous ozone production. In this paper, we focus on examining the chemical features of $P(O_3)$ and studying the behavior of five instantaneous indicators ($f_{OH+HC}$, $f_{HO2+NO}$, $P(H_2O_2)/P(HNO_3)$, $O_3/NO_x$, and $L_N/Q$ ) as identified in previous studies [*Tonnesen and Dennis*,2000a; *Kleinman* et al., 1997;

*Kleinman*, 2005]. Our specific objectives are: 1) to investigate the chemical features of $P(O_3)$ and its relationship with $O_3$ precursors in the Pacific Northwest, 2) to investigate the behavior of local indicators for instantaneous odd oxygen production rate ($P(O_x)$), and 3) to evaluate the sensitivity of $P(O_3)$ to changes in $NO_x$ and VOC emissions in the region with these indicators.

Section 2 presents meteorological and photochemical modeling and data analysis methods. Section 3 presents the results. We begin with investigating the chemical features of $P(O_3)$ and its relationship with $O_3$ precursors, followed by examining the behavior of instantaneous indicators in terms of both spatial and temporal variability. We further evaluate the sensitivity of $P(O_3)$ to changes in $NO_x$ and VOC emissions by using these indicators, and finally present conclusions in Section 4.

## 2. Methodology

### 2.1 Modeling domain and episodes selection

The Mesoscale Meteorological model Version 5 [MM5, *Grell et al*., 1994] was used to provide the 3-D meteorological field for air quality modeling. Three one-way nested domains with grid cell horizontal sizes of 36 km, 12 km, and 4 km were applied. The two outer domains consisted of 95 x 98 and 151 x 133 grid cells, respectively. The innermost domain consisted of 94 x 151 grid cells which extended from north of Vancouver, British Columbia to south of Salem, Oregon and from the Pacific coast on the west to the Cascade Mountain range on the east. Vertically, 38 sigma layers were specified. The CMAQ modeling domain was slightly smaller than the MM5 innermost domain with 81 x 138 horizontal grid cells and 22 layers in the vertical.

The ozone episode during 25-28 July 1998 was selected for this study. Multiple exceedances of both the 1-hour and 8-hour ozone standards occurred between 26 and 28 July at Washington and Oregon air quality monitoring sites. There were elevated temperatures over most of the period and light NW winds during the episode. As summarized by *Barna et al*. [2000], the typical synoptic conditions conducive to high $O_3$ concentrations in the region are characterized by the building of an upper-level ridge of high pressure over the west coast of North America and a thermal trough extending northward from California along the coast. This pattern was apparent in the surface weather map for 27 July 1998 [*Lamb et al*., 2006].

## 2.2 MM5

MM5 version 3.7 was used to develop the 3-D meteorology fields. NCEP ETA model analysis (40 km grid cells) was used to initialize the simulation and provide boundary conditions. Analysis nudging was applied in the coarse domains (36 km, 12 km) and observational nudging was applied in the inner 4 km domain. For analysis nudging, 3D nudging was employed for winds, temperature, and moisture, with the boundary layer excluded for temperature and moisture. Surface nudging was applied for winds only. For observational nudging, wind speed and direction observations from about 50 surface stations were used. Data from a small number of surface stations were withheld from the nudging analysis so that an independent evaluation could be conducted at these sites. For the 4 km domain, 30-s the USGS global terrain and land use database was applied to resolve the terrain features and surface categories.

The MM5 physics options applied in the run included the Kain-Fritsch 2 cumulus parameterization scheme [*Kain*, 2004], the MRF PBL scheme [*Hong and Pan*, 1996],

Reinser 1 moisture [*Reisner et al*., 1998], CCM2 radiation [*Hack et al*., 1993], and Noah Land Surface Model [*Chen and Dudhia*, 2001].

Output from MM5 was processed with the Meteorology-Chemistry Interface Processor (MCIP) version 3.0 to provide the correct input to CMAQ. During the MCIP run, all planetary boundary layer (PBL) parameters and radiation fields were passed through from MM5 without re-calculation.

### 2.3 Emissions

The Sparse Matrix Operator Kernel Emissions (SMOKE) processor version 2.0 (http://www.smoke-model.org/index.cfm) was used to process area, on-road mobile, non-road mobile, and point source emissions. Point sources and area sources were based on the EPA 1999 National Emission Inventory (NEI) without back-casting. Local emissions estimates were used to update the 1999 NEI where appropriate. Non-road mobile sources such as lawn and garden and commercial construction equipment were estimated for year 1998 using EPA NONROAD model [*US. EPA*, 2005]. For non-road mobile sources that were not included in the NONROAD model (ships, locomotives, and aircraft), 1999 NEI estimates were used. For on-road vehicles, EPA MOBILE-6 [*US. EPA*, 2003] was used to determine emission factors with changes due to area-dependent Reid Vapor Pressure (RVP) and Inspection and Maintenance (I/M) plan taken into account. The resulting emission factors were assigned on a county level, and then multiplied by Average Daily Vehicle Miles Traveled (ADVMT) for year 1998. For British Columbia, Year 2000 emissions data provided by the Greater Vancouver Regional District and Environment Canada [*GVRD*, 2002] were used directly for all anthropogenic source categories.

Initial anthropogenic emissions in annual estimates were temporally allocated by

hour in SMOKE according to temporal profiles consisting of month, day of week, and hour of day. Spatially, emissions were allocated by surrogates such as population, land use and land cover, mileage on roadways, railroads, and major airports. Based on source category and pollutants type, the SAPRC99 chemical mechanism [*Carter*, 2000] was used to speciate the emissions.

Biogenic emissions from trees, plants, and crops were processed by the Biogenic Emissions Inventory System (BEIS) version 3.12. The model estimates VOC emissions from vegetation based on land-use categories and nitric oxide emissions from microbial activity based on soil types. The 1-km Biogenic Emissions Landcover Database, version 3 (BELD3), was used to generate normalized emissions, which were then used along with meteorological data and speciation profiles to compute gridded and speciated hourly biogenic emissions.

## 2.4 CMAQ

The U.S. EPA Models-3 Community Multi-scale Air Quality (CMAQ) Modeling System [*Byun and Schere*, 2006] version 4.5 was used for photochemical air quality modeling. It incorporates the output fields from the MM5/MCIP meteorological simulations and emissions derived from SMOKE, and then simulates the chemical transport using the CMAQ Chemical Transport Model (CCTM).

The SAPRC99 photochemical mechanism including aqueous chemistry and aerosol dynamics was employed. The ROS3 solver was applied to solve the chemical kinetics equations. The global mass-conserving scheme (yamo) was used as the advection scheme. This scheme uses the Piecewise Parabolic Method (ppm) in horizontal and drives the vertical velocity at each grid cell from the continuity equation.

Multi-scale and eddy diffusion were applied as horizontal and vertical diffusion algorithms, respectively.

CMAQ boundary conditions were extracted from the MOZART-2 global atmospheric chemistry-transport model by matching the CMAQ boundary with the MOZART cells. The July average MOZART-2 values were derived by averaging over ten years of July runs (1990-1999) based upon a long-term climate simulation conducted as part of a separate analysis of the impact of global change on regional air quality at WSU [*Avise et al*., 2008]. Since MOZART-2 and CMAQ use different vertical grid structures, MOZART and CMAQ output were first converted to equivalent pressure coordinates, and then MOZART mixing ratios were linearly interpolated to CMAQ vertical layers [*personal communication, Jeremy Avise*]. The model simulation included a spin-up period of 4 days and then 4 days of valid runs from 25 July until 28 July 1998.

Photochemical grid models are normally configured to output the concentrations of species due to the cumulative effects of physical and chemical processes such as emissions, chemical reaction, and advection without knowing the impact of individual processes. Process analysis has been developed by previous researchers [*Jeffries and Tonnesen*,1994; *Tonnesen*, 1995] to output information quantifying the effects of individual processes upon species concentrations. In CMAQ, information on contributing processes can be made available by invoking process analysis in two ways: integrated process rate (IPR) analysis and integrated reaction rate (IRR) analysis. IPR deals with separating the effects of various physical processes and the net effect of chemistry. IRR deals with quantifying the contributions of selected chemical reactions. The IRR analysis was used in this study to output the production rate of selected species

such as ozone, odd oxygen, new radicals, as well as important propagation and termination pathways.

## 2.5 Base case evaluation

For meteorological parameters, MM5 was evaluated against surface measurements of winds, temperature, and relative humidity from about 170 stations. Table 1 summarizes the domain-wide statistical performance in terms of mean bias, mean absolute error, and index of agreement. The index of agreement is defined as:

$$I = 1 - \frac{\sum_{i=1}^{N} (P_i - O_i)^2}{\sum_{i=1}^{N} (|P_i - \overline{O}| + |O_i - \overline{O}|)^2} \quad (1)$$

An index of agreement value of 1 indicates perfect agreement between model prediction and observation, and a value of 0 means no correlation between the two. The mean bias is defined as:

$$MB = \frac{1}{N} \sum_{i=1}^{N} (P_i - O_i) \quad (2)$$

and the mean absolute error is defined as:

$$MAE = \frac{1}{N} \sum_{i=1}^{N} |P_i - O_i| \quad (3)$$

where N= sample size, P = prediction, and O = observation.

The results showed that the MAE was about 3°C for 2 m temperatures, 1 m/s for wind speed, and 50° for wind direction. This performance is generally comparable to the real-time forecast system operated at the University of Washington

(http://www.atmos.washington.edu/~qcreport/verification_index.psp) and other air quality simulations in the Pacific Northwest [*Barna and Lamb*, 2000; *O'Neill and Lamb*, 2005]. Note that the statistics for wind direction and wind speed were calculated separately for the overall stations and those withheld from observational nudging; the results showed that model performance was similar for these two groups of stations. Model performance was also evaluated on an hourly basis (Figure 1) for MB and MAE. Results showed that surface temperatures were generally warmer than the observed. Wind speeds tended to be under-predicted during the day while over-predicted at night and early morning. For both temperature and wind direction, the errors were greatest in the early morning and less in the afternoon and early evening.

For CMAQ performance, the mean normalized bias (MNB) and mean normalized gross error (MNGE) are often used as standard methods for model evaluation. They are defined as:

$$MNB = \frac{1}{N}\sum_{i=1}^{N}\left(\frac{(P_i - O_i)}{O_i}\right)\cdot 100\% \quad (4)$$

$$MNGE = \frac{1}{N}\sum_{i=1}^{N}\left(\frac{|P_i - O_i|}{O_i}\right)\cdot 100\% \quad (5)$$

MNB and MNGE were calculated to be 5% and 22% for 8-hr average $O_3$ concentrations and 5% and 21% for daily maximum 8-h (DM8H) values at all available ground stations within the modeling domain. Compared to the other air quality simulations in the region [*Smyth et al.*, 2006; *O'Neill et al.*, 2006, *Chen et al.*, 2008], the CMAQ run produced fairly good performance here. In terms of performance for the two metropolitan areas within the domain, the model captured the peak ozone events better in Portland compared

to Seattle [*Lamb et al.*, 2006]. Therefore, the data analysis in this study focused on the Portland area only.

### 2.6 Ozone precursors

We investigated the chemical features of $P(O_3)$ by examining $O_3$ precursors, which include radical precursors, VOCs and $NO_x$. $P(O_3)$ is defined as the difference between the gross photochemical ozone production rate and photochemical loss rate. Radical precursor production is calculated as the sum of the production rate of new radicals and is denoted as Q here. It includes photolysis of $O_3$, HCHO, as well as that of HONO, $H_2O_2$, organic proxides, and various ozonolysis reactions. VOCs are represented by total VOC reactivity ($VOC_R$) and calculated based on OH reactivity:

$$VOC_R = \Sigma k_i[VOC_i] \quad (6)$$

where $VOC_i$ are the model-predicted concentrations of individual VOC including all model species that react with OH radical and produce peroxy radicals. Reaction rates ($k_i$) are calculated based on the rates defined in SAPRC99 mechanism with temperature and pressure effects taken into account. $NO_x$ is defined as the sum of NO and $NO_2$.

### 2.7 Instantaneous indicators

We evaluated the behavior of five instantaneous indicators $f_{OH+HC}$, $f_{HO2+NO}$, $P(H_2O_2)/P(HNO_3)$, $O_3/NO_x$, and $L_N/Q$. Using similar definition as *Tonnesen and Dennis* [2000a] and *Kleinman et al*. [1997], these indicators are defined:

$$f_{OH+HC} = \frac{\sum k_i * [HC_i][OH]}{\sum k_i * [HC_i][OH] + k_{28} * [NO_2][OH] + misc.OHreactions} \quad (7)$$

where $f_{OH+HC}$ is the fraction of OH reacts with hydrocarbons

$$f_{HO2+NO} = \frac{k_{34} * [NO][HO_2]}{k_{34} * [NO][HO_2] + 2 * (k_{40a} * [HO_2]^2 + k_{40b} * [HO_2]^2 [H_2 0]) + \sum k_j * [HO_2][RO_{2,j}] + misc.HO_2 reactions} \quad (8)$$

where $f_{HO2+NO}$ is the fraction of $HO_2$ reacts with NO

$$P(H_2O_2)/P(HNO_3) = (k_{40a} * [HO_2]^2 + k_{40b} * [HO_2]^2 [H_2O])/(k_{28} * [OH][NO_2]) \quad (9)$$

$$L_N/Q = k_{28} * [OH][NO_2]/(newOH + newHO_2 + \sum newRO_{2,j}) \quad (10)$$

where $L_N/Q$ is the fraction of free radicals removed by reactions with $NO_x$. The various rate constants (k) are correspondent to those defined in the mech.def file of SAPRC99_ae4_aq mechanism in CMAQv4.5. Miscellaneous OH reactions include its reactions with $O_3$, $HO_2$, $SO_2$, etc. Miscellaneous $HO_2$ reactions include its reactions with $O_3$, OH, etc. $RO_2$ radicals include various peroxy radicals defined in the SAPRC99 chemical mechanism. Note that the formulas here are specifically defined for SAPRC99, so that there are small differences from the previous study [*Tonnesen and Dennis*, 2000a] in which RADM2 was used.

To evaluate if these indicators have different values related to $NO_x$- and VOC-sensitive conditions, two model sensitivity runs were conducted by decreasing the anthropogenic VOC and $NO_x$ emissions by 30% from the base case. The resulting percentage change in $P(O_x)$ versus percentage change in either VOC or $NO_x$ emissions was then calculated. In this study, we defined $O_x$ as $O_x = O_3 + O^3P + O^1D + NO_2 + 2*NO_3 + 3*N_2O_5 + HNO_4 + PAN + PAN_2 + PBZN + MA\_PAN + RNO_3 + HNO_3$, where

PAN, $PAN_2$, PBZN, and MA_PAN refer to PAN and its analogues, and $RNO_3$ refers to organic nitrates.

$\partial P(O_x)/\partial E_{VOC}$ and $\partial P(O_x)/\partial E_{NOx}$ ) were calculated as:

$$\frac{\partial P(O_x)}{\partial E} = \frac{(P(O_x)_{base} - P(O_x)_{-30\%})/P(O_x)_{base}}{30\%} \quad (11)$$

The model grid cells were assigned to VOC- or $NO_x$-sensitive regimes according to the following criteria. Grid cells with $\partial P(O_x)/\partial E_{NOx} = 0$ are close to ridgeline conditions. $NO_x$-sensitive cells are associated with $\partial P(O_x)/\partial E_{NOx} > 0$, whereas VOC-sensitive cells are linked to $\partial P(O_x)/\partial E_{NOx} < 0$. When $\partial P(O_x)/\partial E_{NOx} = \partial P(O_x)/\partial E_{VOC}$, equal sensitivity is thought to occur in these grid cells.

## 3. Results and discussion

### 3.1 Chemical features of $P(O_3)$ and its relationship with $O_3$ precursors

We investigated the chemical features of $P(O_3)$ and its relationship with $O_3$ precursors by first examining their spatial features with the results on 27 July at 13 LST when the maximum $P(O_3)$ occurred. On this day, conditions were mostly sunny with above normal temperatures around 35-38°C and light north and northwesterly winds around the Portland area. The model predicted large areas with elevated $O_3$ levels above 100 ppb along the I-5 corridor, with a maximum level close to 140 ppb downwind of Portland. Contour plots of $P(O_3)$ are shown in Figure 2a and 2b, where 2a includes the southern part of the domain and 2b displays a smaller sub-domain covering the Portland urban area and the regions with relatively large $P(O_3)$. This sub-domain is used for most

of the data analysis in the following sections. We show contour maps of Q, new OH radicals from $O_3$ photolysis, and new $HO_2$ radicals from HCHO photolysis in Figure 3a - 3c. Contour maps of $VOC_R$ and $NO_x$ concentrations are shown in Figures 4 and 5, respectively.

The maximum $P(O_3)$ (~35 ppb $hr^{-1}$) was predicted to occur slightly downwind of Portland and the high $NO_x$ concentrations at the urban center resulted in negative values there. For Q, the model showed large areas around Portland with values close to 7 ppb $hr^{-1}$. $O_3$ photolysis accounted for about 60% of radical production with the highest rate downwind of the urban center, while HCHO photolysis contributed up to 20% close to the urban core. For $VOC_R$, the predicted levels were between 8-14 $s^{-1}$ for the metropolitan area, whereas a broader range of values occurred in the rural environment due to abundant biogenic emissions. For $NO_x$ concentrations, elevated values between 8 and 20 ppb were predicted in the urban area as a result of large anthropogenic emissions.

The correlations between $P(O_3)$ and its precursors were examined for two high ozone days: 27 and 28 July. Similar to the conditions on the previous day, 28 July had very active photochemical production. The winds were lighter, and as a result, slightly higher precursors levels and peak $O_3$ (~160 ppb) were predicted. In Figure 6, we plot $P(O_3)$ as a function of $VOC_R$ and $NO_x$ concentrations as color-coded symbols using the data within the Portland sub-domain at 13 LST. Only cells with positive $P(O_3)$ are displayed. The results showed that low $P(O_3)$ data points (<10 ppb $h^{-1}$) (shown in light and dark blue) existed at both low and high end of $VOC_R$ and $NO_x$ values. On the other hand, high $P(O_3)$ data points (>20 ppb $h^{-1}$) (shown in red and orange) appeared to generally follow an upward slope, indicating similar $VOC_R/NO_x$ ratios between those

grid cells. For the data points with the maximum $P(O_3)$ (>30 ppb $h^{-1}$), $VOC_R$ was mostly above 8 $s^{-1}$ and $NO_x$ ranged between 5-20 ppb. *Kleinman et al*. [2005] reported high $P(O_3)$ (>25 ppb $h^{-1}$) occurred with $NO_x$ concentrations between 5-25 ppb and $VOC_R$ above 5 $s^{-1}$ in five major U.S. metropolitan areas using calculations with a steady state box model based on observed concentrations. The ranges of precursor concentrations associated with high $P(O_3)$ reported by Kleinman are very similar to the results of our study.

### 3.2 Behavior of instantaneous indicators

#### 3.2.1 Spatial variability

We investigated the behavior of five indicators ($f_{OH+HC}$, $f_{HO2+NO}$, $P(H_2O_2)/P(HNO_3)$, $O_3/NO_x$, and $L_N/Q$) to see whether they are related to $NO_x$- or VOC-sensitive conditions using the model results at 13 LST within the Portland sub-domain. In order to test their behavior under different conditions, the analysis was conducted separately for 27-28 July when the model predicted high $O_3$ levels and 25-26 July when there was less active photochemical production. During 25 to 26 July, the peak $O_3$ levels were predicted to be around 90 ppb for the region, due to lower temperatures on the first and extensive cloud coverage on the second day.

Two sensitivity runs were conducted by decreasing either the anthropogenic VOC or $NO_x$ emissions by 30%. We plot percentage change in $P(O_x)$ versus percentage change in either VOC or $NO_x$ emissions as a function of the base case indicator values. Positive values are related to $P(O_x)$ reductions with reduced emissions, whereas negative values suggest increased $P(O_x)$ values with emissions controls. The results for the two

high ozone days (27 and 28 July) are displayed in Figure 7, and those for the two less productive days (25 and 26 July) are shown in Figure 8.

For the two ozone event days, the indicator values associated with $NO_x$- and VOC-sensitive conditions are summarized in Table 2 and compared to those derived from previous studies [*Tonnesen and Dennis*, 2000a; *Kleinman* et al., 1997; *Kleinman*, 2005]. For $f_{HO2+NO}$, there was a narrow range of values associated with $\partial P(O_x)/\partial E_{NOx} = 0$, primarily between 0.96-0.97, indicating ridgeline conditions. This ridgeline value is very close to the results of *Tonnesen and Dennis* [2000a]. They found ridgeline values of 0.95-0.97 with indicator $I(RO_2,NO)$ which is an approximation of $f_{HO2+NO}$. Cells with values greater than 0.97 were mainly VOC-limited, whereas cells with values less than 0.92 were mostly $NO_x$-limited. Values between 0.92-0.96 were linked to cells having equal sensitivity to $NO_x$ and VOC.

For $f_{OH+HC}$, values between 0.76-0.78 appeared to be associated with ridgeline conditions. VOC-sensitive conditions occurred when values were smaller than 0.76, and $NO_x$-sensitive condition occurred when values were greater than 0.82. $\partial P(O_x)/\partial E_{NOx}$ was approximately equal to $\partial P(O_x)/\partial E_{VOC}$ between 0.79-0.82, indicating equal $NO_x$ and VOC sensitivity. Compared to the previous identified ridgelines values (0.77-0.85) by *Tonnesen and Dennis* [2000a], the values here exhibited a smaller range. The difference is partly due to $I(HC,NO_2)$, which is an approximation of $f_{OH+HC}$, that was used in the previous study. A slightly narrower range was also seen in that study when the pathway fraction ($f_{OH+HC}$) was used as compared to the approximated values ($I(HC,NO_2)$).

Similar to the results from *Tonnesen and Dennis* [2000a], $P(H_2O_2)/P(HNO_3)$ appeared to be a precise indicator due to the narrow range of values associated with

ridgeline conditions. Compared to their ridgeline values (0.06-0.07), lower values (0.02-0.03) were obtained here. As pointed out by *Tonnesen and Dennis* [2000b], the ridgeline values might change for indicators involving $H_2O_2$, $HNO_3$, and organic peroxides due to the differences in model representation of miscellaneous $HO_2$ and OH termination pathways and the differences in ambient $O_3$ and VOC, and $NO_x$ concentrations. We expect the difference here might mainly be due to the different chemical mechanism used in this work (SAPRC99) as compared to the previous study (RADM2).

For $O_3/NO_x$, ridgeline values were around 8-10. Values between 10-14 showed approximately equal $NO_x$ and VOC sensitivity, similar to those (12-16) reported by *Tonnesen and Dennis* [2000a]. Values greater than 14 were clearly $NO_x$-limited, while those less than 8 were primarily VOC-limited.

For $L_N/Q$, the results suggested that cells with $L_N/Q$ greater than 0.68 were VOC-limited, and less than 0.5 were primarily $NO_x$-limited. Ridgeline values appeared to be associated with values around 0.66-0.68, and values between 0.5-0.6 were approximately with equal $NO_x$ and VOC sensitivity. These values are in good agreement with those derived by *Kleinman et al.* [1997] and *Kleinman* [2005].

While all five indicators appeared to be able to distinguish $NO_x$- and VOC-sensitive conditions on the two days with very active photochemical production, the results from the two lower ozone days suggested that these indicators were still linked to $NO_x$- and VOC-sensitive conditions, but with more scatter. For example, in contrast to the narrow ridgeline values of $L_N/Q$ (0.66-0.68) on the two high ozone days, the values for the lower ozone days extended from 0.6 to 0.7.

### 3.2.2 Temporal variations

We have shown that the indicators correlated well with the VOC- and $NO_x$-sensitive conditions around noon when photochemistry was most active. We further investigated the temporal variations of these indicators and evaluated if they are related to the VOC/$NO_x$ sensitivity at two selected grid cells for a number of days. As shown in Figure 2b, one cell was selected close to Vancouver, WA, and the other slightly downwind of Portland urban core and close to where the maximum $P(O_3)$ occurs. The daytime (8:00 LST to 18:00 LST) changes in $P(O_x)$ with 30% reduction in $NO_x$ emissions from 25 July to 28 July are shown in Figure 9 for the Vancouver cell and Figure 10 for the downwind cell. Positive $\Delta P(O_x)$ values are related to $P(O_x)$ reductions with reduced $NO_x$ emissions, whereas negative values suggest increased $P(O_x)$ values with $NO_x$ controls. In the same plot, we show the corresponding $P(O_x)$ and $O_3$ levels on the right axis. Time series of indicator values extracted from each location are plotted with the horizontal line corresponding to the ridgeline values identified from the previous section. Within the five indicators, we plot the inverse values of $L_N/Q$ and $f_{HO2+NO}$ so that the increase in all five indicator values corresponds to increased sensitivity to $NO_x$.

For the Vancouver cell, $P(O_x)$ was below 20 ppb $hr^{-1}$ on the first two days, and showed significantly higher values (~40 ppb $hr^{-1}$) on the next two. For $O_3$, there was a similar pattern, with low levels (< 70 ppb) on the first two days, moderate (~90 ppb) on the third and relatively high (~120 ppb) on the last day. $P(O_x)$ increased with reduced $NO_x$ emissions as $\Delta P(O_x)$ was negative for all four days, indicating predominantly VOC-sensitive conditions in this cell. In terms of indicator response, values of $L_N/Q$ were less than its ridgeline values for almost all hours except for early morning of the first and last

day, suggesting it might not perform well at this time of the day. For the other four indicators, levels were below ridgeline values for the entire period, responding correctly to VOC-sensitive conditions.

At the downwind cell, $P(O_x)$ was slightly lower but showed a similar pattern as in the suburban cell. $O_3$ levels were generally higher with peak levels around 80 ppb on the first two days and reaching 120 ppb and 150 ppb on the following two. On the first two days, $\Delta P(O_x)$ was negative all the time, indicating VOC sensitivity conditions. On the third day, $\Delta P(O_x)$ started with negative values in the morning, but approached zero at noon and was positive in the afternoon, reflecting an evolution from VOC-sensitive to $NO_x$-sensitive conditions. On the last day, $\Delta P(O_x)$ was positive throughout the day, indicating $NO_x$-sensitive conditions. $L_N/Q$ values were below ridgeline values on the first day, correctly responding to VOC-sensitive conditions. On the second day, $L_N/Q$ had low values most of the time except for the last hour in the evening. Since the inverse of $L_N/Q$ is plotted, the high value corresponds to a high $Q/L_N$, which is caused by increased Q as a result of more $RO_2$ production in the evening hours. Nighttime chemistry has relatively large effects on this cloudy day, and the results suggest that $L_N/Q$ might not be suitable for such conditions. On the third day, $L_N/Q$ had below ridgeline values in the morning and approached to above ridgeline values around noon, correlating well with the transition from VOC- to $NO_x$-sensitive conditions on this day. On the last day, $L_N/Q$ had above ridgeline values all the time, correctly reflecting $NO_x$-sensitive conditions.

Values of $f_{OH+HC}$ matched well with the changes in $P(O_x)$ for mid-day values, suggesting VOC-sensitive conditions on the first two days, mixed sensitivity on the third,

and $NO_x$-sensitive conditions on the last day. However, similar to $L_N/Q$, the value at the last hour of the second day suggested mildly $NO_x$-sensitive conditions, while $\Delta P(O_x)$ indicated VOC-sensitive conditions throughout the day.

Values of $f_{HO2+NO}$ and $P(H_2O_2)/P(HNO_3)$ behaved very similarly in their temporal variation, and appeared to be very accurate for the time period we examined. Both of them followed the changes in $P(O_x)$ sensitivity fairly well.

$O_3/NO_x$ also captured the VOC-sensitive conditions on the first two days, transitional from VOC- to $NO_x$-sensitive conditions at noon on the third day, and mostly $NO_x$-sensitive conditions on the last day. Similar to *Tonnesen and Dennis* [2000b], we found low $O_3/NO_x$ values in the late afternoon hours due to decreased $O_3$ but increased $NO_x$ emissions.

### 3.3 Sensitivity of $P(O_3)$ to VOC/$NO_x$ based on indicators

To investigate the sensitivity of $P(O_3)$ to changes in $NO_x$ and VOC emissions using indicators, we plot the indicator values in Figure 11 with the same style as in Figure 6. Data points with $P(O_3) > 30$ ppb $hr^{-1}$ are marked with black circles. With the values identified from the previous section, pink points are related to ridgeline values, light green are associated with equal sensitivity to $NO_x$ and VOC, orange are linked to VOC-limited, and blue are linked to $NO_x$-limited conditions.

The five indicators gave identical results for strongly VOC- or $NO_x$-limited conditions, while they suggested some minor differences for locations associated with transitional regimes. For example, the points associated with ridgeline conditions as indicated by $L_N/Q$ were much less than those indicated by $f_{OH+HC}$, since the former had a more precise ridgeline value. Despite these minor differences, these indicators showed a

generally consistent picture for $P(O_3)$ sensitivity. The data points with the maximum $P(O_3)$ (>30 ppb $hr^{-1}$) appeared to be mostly related to transitional or $NO_x$-limited conditions.

## 4. Conclusions

As a way to improve our understanding of the ozone formation in the Pacific Northwest, we have investigated the chemical features of $P(O_3)$ and its sensitivity to changes in $NO_x$ and VOC emissions with process analysis in CMAQ for an ozone episode that occurred during July, 1998. The analyses were conducted in three steps: 1) examining the chemical features of $P(O_3)$ and its relationship with $O_3$ precursors, 2) evaluating the behavior of five instantaneous indicators ($f_{OH+HC}$, $f_{HO2+NO}$, $P(H_2O_2)/P(HNO_3)$, $O_3/NO_x$, and $L_N/Q$), and 3) investigating the sensitivity of $P(O_3)$ to changes in $NO_x$ and VOC emissions with these indicators.

Maximum $P(O_3)$ was 30-40 ppb $hr^{-1}$ downwind of the Portland urban center, with $NO_x$ concentrations of 5-20 ppb and total VOC reactivity above 8 $s^{-1}$. The ranges of precursor concentrations associated with high $P(O_3)$ predicted here were very close to previously reported values in other U.S. metropolitan areas [*Kleinman et al.,* 2005].

Evaluated with mid-day values, all five indicators clearly distinguished $NO_x$- and VOC-sensitive conditions on ozone event days. On days with less photochemical production, the indicators were less consistent in predicting VOC or $NO_X$ limitations. Ridgeline values we identified in this study were similar to previous work, and the largest difference occurred with $P(H_2O_2)/P(HNO_3)$. The difference might be attributed to the

differences in model representation of miscellaneous $HO_2$ and OH termination pathways as well as the differences in ambient $O_3$ and VOC, and $NO_x$ concentrations.

The indicators also appeared to be useful for examining the temporal variations of ozone sensitivity, as their daytime values generally reflected the dynamic changes in the sensitivity. Some inconsistency occurred when early morning or late afternoon values were used, such as the contradictory results suggested by $L_N/Q$ and $f_{OH+HC}$ at these time periods. The inconsistency was mostly because at these times, nighttime chemistry and heterogeneous reactions have relatively large effects compared to daytime ozone production.

Evaluating the sensitivity of $P(O_3)$ to changes in $NO_x$ and VOC emissions using these indicators, we found that the different indicators suggested identical results for strongly $NO_x$- or VOC-limited conditions, while they showed minor differences for locations associated with transitional regimes. Despite these small differences, these indicators provided overall consistent results and suggested that the greatest $P(O_3)$ (>30 ppb $hr^{-1}$) mostly occurred at transitional or $NO_x$-limited conditions for the Portland area.

All five indicators appear to be able to distinguish $NO_x$- and VOC-sensitive conditions, but some are difficult to measure in the field. As discussed by *Tonnesen and Dennis* [2000a], $f_{OH+HC}$, $f_{HO2+NO}$, and $P(H_2O_2)/P(HNO_3)$ are on the whole not easy to measure, since total $RO_2+HO_2$ is required for $f_{HO2+NO}$, VOC mixture and $NO_2$ for $f_{OH+HC}$, and OH, $HO_2$, and $NO_2$ for $P(H_2O_2)/P(HNO_3)$. For $L_N/Q$, an analytical formula has been developed so that it can be determined from measured or estimated precursors and parameters [*Kleinman et al.*, 2001]. However, the need for $NO_2$, HC mixture, and Q in the formula poses difficulties in getting accurate $L_N/Q$ values. As shown above, $O_3/NO_x$

produces similar results to the other indicators and it is more easily obtained as long as $NO_x$ can be accurately measured. Therefore, $O_3/NO_x$ might be a more useful diagnostic tool for evaluating model-predicted sensitivity.

The results here suggest that indicators are useful tools for distinguishing $NO_x$- and VOC-sensitive conditions. The ridgeline values we identified can be used as reference values in future ozone sensitivity studies, and comparison of measured indicator values with model predictions can provide strong support for validating model predicted sensitivity. Meanwhile, it should also be noted that the indicator values are highly dependent on environmental conditions, removal processes such dry and wet deposition, heterogeneous chemistry, and in particular the representation of photochemical mechanism. It has been shown that the uncertainties in the rate constants and product yields of the chemical mechanisms contribute significantly to the overall uncertainties in $O_3$ predictions. For example, large certainties remain in the rate constants for $RO_2$ reactions that produce organic peroxides [*Stevens et al*., 1997] and $OH+NO_2$ reaction that forms $HNO_3$ [*Russell and Dennis*, 2000]. Therefore, comparisons with results from different photochemical representations and different environment conditions, as well as comparisons with measurements are needed to improve our understanding of the derivation and usefulness of indicators.

**References**


Avise, J., J. Chen, B. Lamb, C. Wiedinmyer, A. Guenther, E. Salathé, C. Mass (2008), Attribution of projected changes in US ozone and $PM_{2.5}$ concentrations to global changes, *Atmos. Chem. Phys. Discuss., 8*, 15131-15163.

Barna, M., and B. Lamb (2000), Improving ozone modeling in regions of complex terrain using observational nudging in a prognostic meteorological model, *Atmos. Environ., 34*, 4889–4906.

Byun, D. W., and K. L. Schere (2006), Review of the governing equations, computational algorithms, and other components of the Models-3 Community Multiscale Air Quality (CMAQ) modeling system, *Appl. Mech. Rev., 59*, 51-77.

Carter, W. P. L. (2000), *Documentation of the SAPRC-99 Chemical Mechanism for VOC Reactivity Assessment*, No. 92 – 329, 95 – 308, Final Report to California Air Resources Board, Calif. Air Resour. Board, Riverside Calif. (Available at http://www.engr.ucr.edu/~carter/absts.htm#saprc99)

Chen, F., and J. Dudhia (2001), Coupling an advanced land surface–hydrology model with the Penn State–NCAR MM5 modeling system. Part I: Model implementation and sensitivity, *Mon. Wea. Rev., 129*, 569–585.

Chen, J., J. Vaughan, J. Avise, S. O'Neill, and B. Lamb (2008), Enhancement and evaluation of the AIRPACT ozone and $PM_{2.5}$ forecast system for the Pacific Northwest, *J. Geophys. Res., 113*, D14305, doi:10.1029/2007JD009554.

Chock, D. P., T. Y. Chang, S. L. Winkler, and B. I. Nance (1999), The impact of an 8 h ozone air quality standard on ROG and $NO_x$ controls in Southern California, *Atmos. Environ., 33*, 2471–2486.

Grell, A. G., J. Dudhia, and D. R. Stauffer (1994), A description of the fifth generation Penn State/NCAR mesoscale model (MM5), in *NCAR Tech. Note 3981STR*, 138 pp., Natl. Cent. Atmos. Res., Boulder, Colo. (Available at http://www.mmm.ucar.edu/mm5)

GVRD Canada (2002), *2000 Emission Inventory for the Lower Fraser Valley Airshed*, Policy and Planning Department Greater Vancouver Regional District, Fraser Valley Regional District, B. C., Canada. (Available at http://www.gvrd.bc.ca/air/inventory_reports.htm)

Hack, J. J., B. A. Boville, B. P. Briegleb, J. T. Kiehl, P. J. Rasch, and D. L. Williamson (1993), Description of the NCAR Community Climate Model (CCM2), *NCAR Tech. Note*, *NCAR/TN-382+STR*, 108 pp., Natl. Cent. for Atmos. Res., Boulder, Colo.

Hong, S.-Y., and H.-L. Pan (1996), Nonlocal boundary layer vertical diffusion in a

medium-range forecast model, *Mon. Wea. Rev., 124*, 2322–2339.

Jeffries, H. E., and S. Tonnesen (1994), A comparison of two photochemical reaction mechanisms using mass balance and process analysis, *Atmos. Environ., 28*, 2991–3003.

Kain, J. S., (2004), The Kain-Fristch convective parameterization: An update, *J. Appl. Meteor., 43*, 170-181.

Kleinman, L. I. (2005), The dependence of tropospheric ozone production rate on ozone precursors, *Atmos. Environ., 39*, 575–586.

Kleinman, L. I., P. H. Daum, J. H. Lee, Y.-N. Lee, L. J. Nunnermacker, S. R. Springston, L. Newman, J. Weinstein-Lloyd, and S. Sillman (1997), Dependence of ozone production on NO and hydrocarbons in the troposphere, *Geophys Res. Lett., 24*, 2299– 2302.

Kleinman, L. I., P. H. Daum, Y.-N. Lee, L. J. Nunnermacker, S. R. Springston, J. Weinstein-Lloyd, and J. Rudolph (2001), Sensitivity of ozone production rate to ozone precursors, *Geophys. Res. Lett., 28*, 2903–2906.

Kleinman, L. I., P. H. Daum, Y.-N. Lee, L. J. Nunnermacker, S. R. Springston, J. Weinstein-Lloyd, and J. Rudolph (2005), A comparative study of ozone production in five U.S. metropolitan areas*, J. Geophys. Res., 110*, D02301, doi:10.1029/2004JD005096.

Lamb, B., Y. Xie, C. Bowman, S. Otterson, D. Schneider, K. Himes, J. Anderson, K. Agyei, and B. Carper (2006), Modeling Analysis of Future Emission Scenarios for Ozone Impacts in the Puget Sound Area, Final report prepared for Puget Sound Clean Air Agency.

Lu, C.-H., and J. Chang (1998), On the indicator-based approach to assess ozone sensitivities and emission features*, J. Geophys. Res., 103*, 3453–3462.

Milford, J. B., D. Gao, S. Sillman, P. Blossey, and A. G. Russell (1994), Total reactive nitrogen ($NO_y$) as an indicator of the sensitivity of ozone to reductions in hydrocarbon and $NO_x$ emissions, *J. Geophys. Res., 99*(D2), 3533–3542.

O'Neill, S. M., and B. K. Lamb (2005), Intercomparison of the community multiscale air quality model and calgrid using process analysis, *Environ. Sci. Technol., 39*(15), 5742–5753.

O'Neill, S. M., et al. (2006), Modeling ozone and aerosol formation and transport in the Pacific Northwest with the Community Multi-Scale Air Quality (CMAQ) modeling system, *Environ. Sci. Technol., 40*, 1286–1299.

Reisner, J., R. M. Rasmussen, and R. T. Bruintjes (1998), Explicit forecasting of supercooled liquid water in winter storms using the MM5 mesoscale model, *Quart. J. Roy. Metero. Soc., 124 B*, 1071-1107.

Russell, A., and R. Dennis (2000), NARSTO critical review of photochemical models and modeling, *Atmos. Environ., 34*, 2283– 2324.

Sillman, S. (1995), The use of $NO_y$, $H_2O_2$, and $HNO_3$ as indicators for $O_3$-$NO_x$-hydrocarbon sensitivity in urban locations, J. *Geophys. Res., 100*, 14,175–14,188, 1995.

Sillman, S., D. He, C. Cardelino, and R. E. Imhoff (1997), The use of photochemical indicators to evaluate ozone-$NO_x$-hydrocarbon sensitivity: Case studies from Atlanta, New York and Los Angeles, *J. Air Waste Manage.* Assoc., *47*, 642– 652.

Sillman, S., D. He, M. R. Pippin, P. H. Daum, D. G. Imre, L. I. Kleinman, J. H. Lee, and J. Weinstein-Lloyd (1998), Model correlations for ozone, reactive nitrogen, and peroxides for Nashville in comparison with measurements: Implications for $O_3$-$NO_x$-hydrocarbon sensitivity, *J. Geophys. Res., 103*, 22,629– 22,644.

Sillman, S., and D. He (2002), Some theoretical results concerning $O_3$-$NO_x$-VOC chemistry and $NO_x$-VOC indicators, *J. Geophys. Res., 107*(D22), 4659, doi:10.1029/2001JD001123.

Sillman, S., R. Vautard, L. Menut, and D. Kley (2003), $O_3$-$NO_x$-VOC sensitivity and $NO_x$-VOC indicators in Paris: Results from models and atmospheric pollution over the Paris area (ESQUIF) measurements, *J. Geophys. Res., 108*(D17), 8563, doi:10.1029/2002JD001561.

Smyth, S. C., W. M. Jiang, D. Z. Yin, H. Roth, and T. Giroux (2006), Evaluation of CMAQ $O_3$ and $PM_{2.5}$ performance using Pacific 2001 measurement data, *Atmos. Environ., 40*, 2735–2749.

Stevens, P. S., et al. (1997), $HO_2$/OH and $RO_2$/$HO_2$ ratios during the Tropospheric OH Photochemistry Experiment: Measurement and theory, *J. Geophys. Res., 102*(D5), 6379–6391.

Tonnesen, G. S. (1995), Development and application of a process analysis method for photochemical oxidant models, Ph.D. dissertation, Dep. of Environ. Eng., Univ. of N. C., Chapel Hill, May.

Tonnesen, G. S., and R. L. Dennis (2000a), Analysis of radical propagation efficiency to assess ozone sensitivity to hydrocarbons and $NO_x$, 1, Local indicators of instantaneous odd oxygen production sensitivity, *J. Geophys. Res., 105*, 9213– 9226.

Tonnesen, G. S., and R. L. Dennis (2000b), Analysis of radical propagation efficiency to

assess ozone sensitivity to hydrocarbons and $NO_x$, 2, Longlived species as indicators of ozone concentration sensitivity, *J. Geophys. Res., 105*, 9227– 9242.

U.S. EPA (2003), User's guide to MOBILE6.1 and MOBILE6.2 (Mobile source emission factor model), in *Rep. EPA420-R-03-010*, Off. of Transp. and Air Qual., Ann Arbor, Mich. (Available at http://www.epa.gov/otaq/m6.htm)

U.S. EPA (2005), Environmental Protection Agency Final 2005 Nonroad Model, [online] http://www.epa.gov/otaq/nonrdmdl.htm#model

Vaughan, J., et al. (2004), A numerical daily air quality forecast system for the Pacific Northwest, *Bull. Am. Meteorol. Soc., 85*, 549– 561.

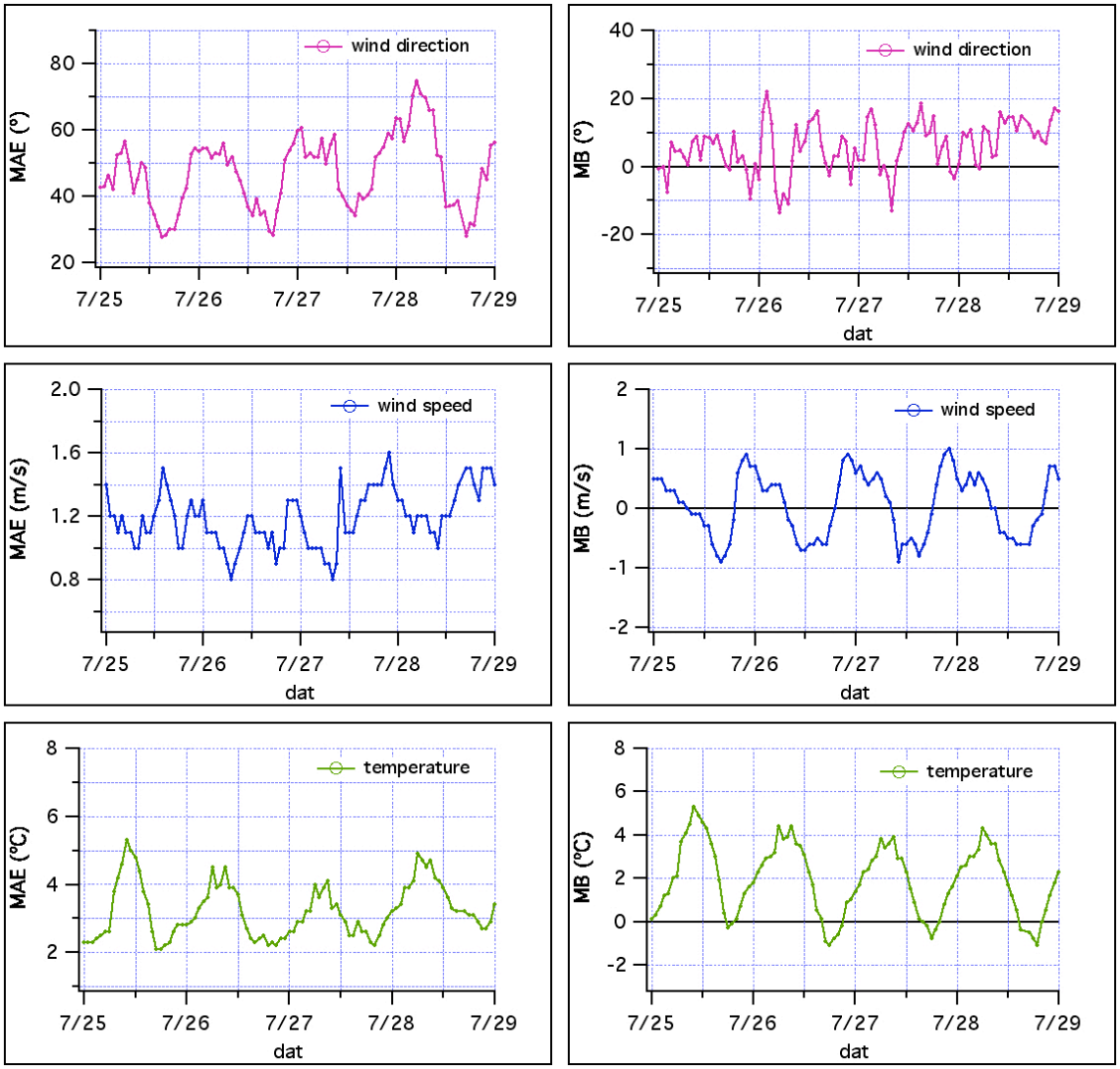


Figure 1. The MAE and MB for wind direction, wind speed, and temperature during 25-28, 1998.

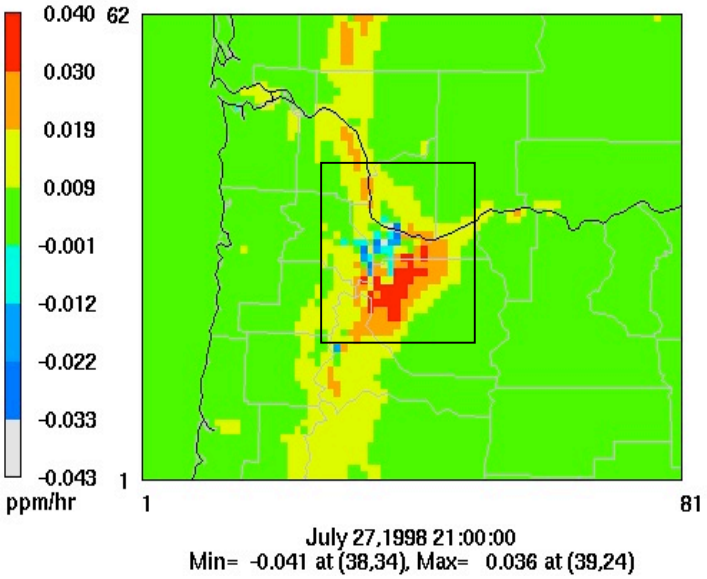


Figure 2a. Surface contours of $P(O_3)$ at 13 LST on 27 July 1998 for the southern part of the modeling domain. The inner black box shows the location of Portland sub-domain.

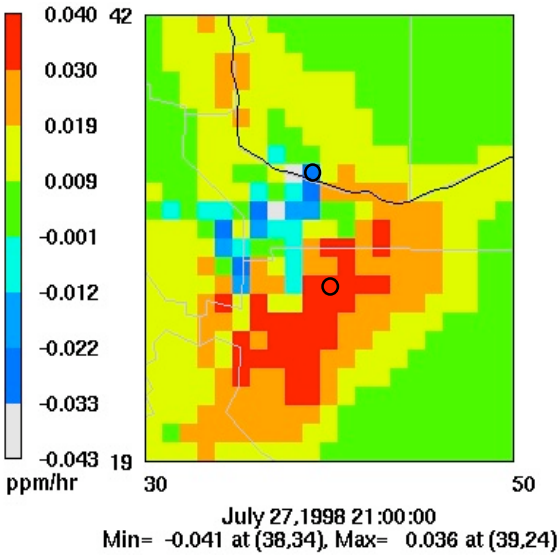


Figure 2b. Surface contours of $P(O_3)$ at 13 LST on 27 July 1998 for the Portland sub-domain. The upper circle shows the Vancouver area cell, and the lower one shows the downwind area cell.

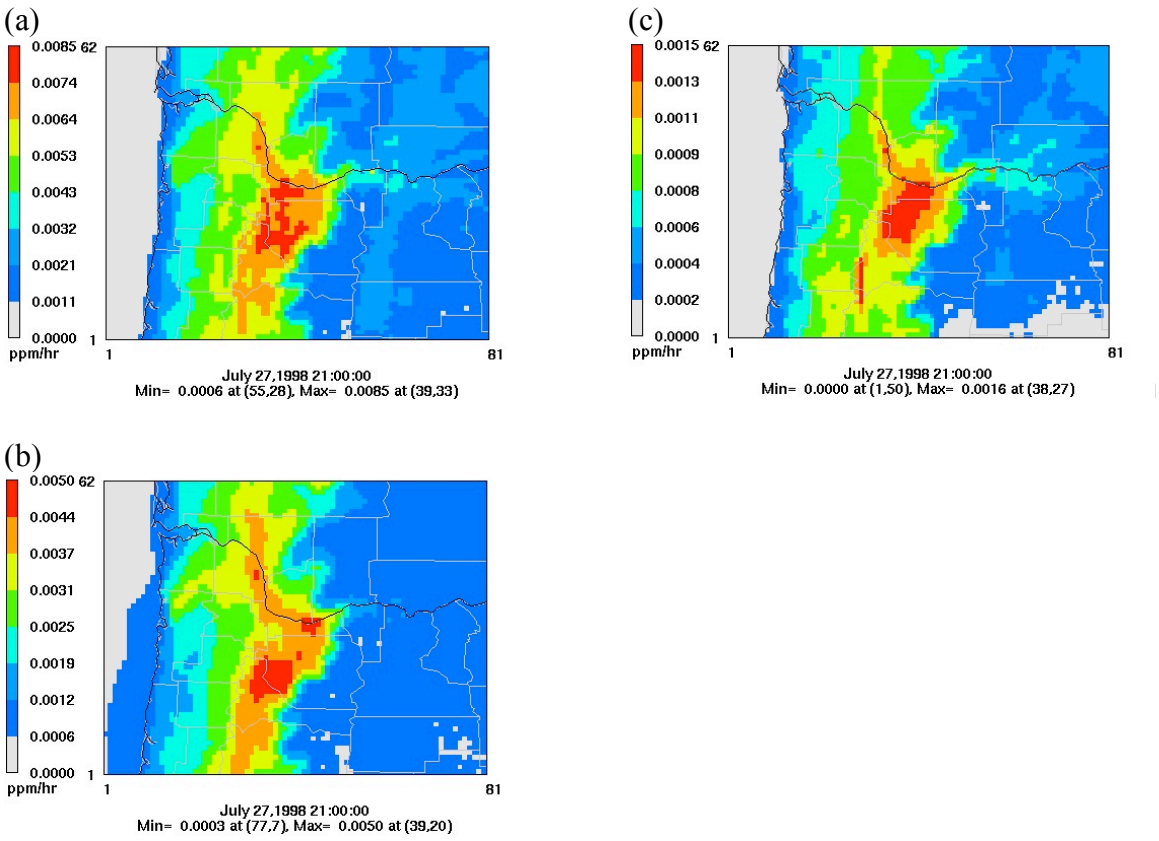


Figure 3. Surface contours of radical production at 13 LST on 27 July 1998 within the southern part of the modeling domain for a) Q, b) OH radicals from $O_3$ photolysis, and c) $HO_2$ radicals from HCHO photolysis.

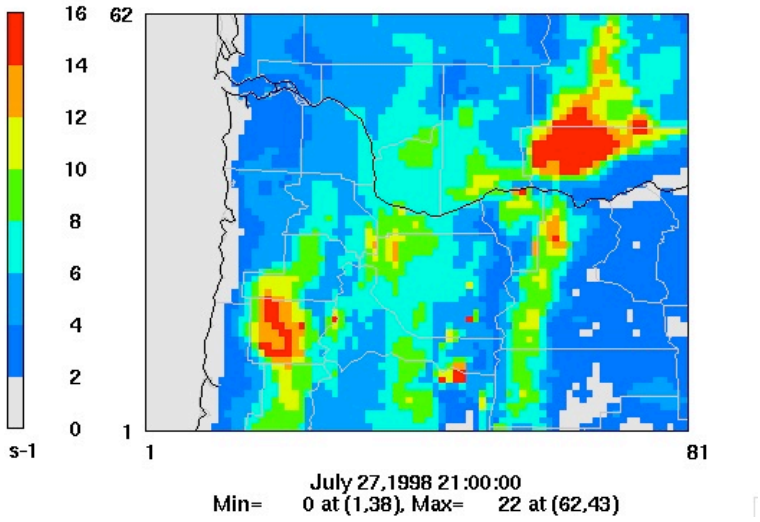


Figure 4. Surface contours of $VOC_R$ at 13 LST on 27 July 1998 for the southern part of the modeling domain.

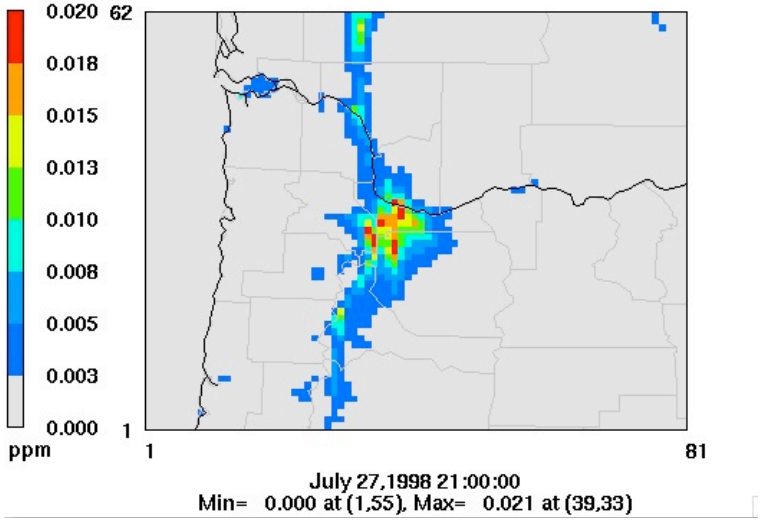


Figure 5. Surface contours of $NO_x$ concentrations at 13 LST on 27 July 1998 for the southern part of the modeling domain.

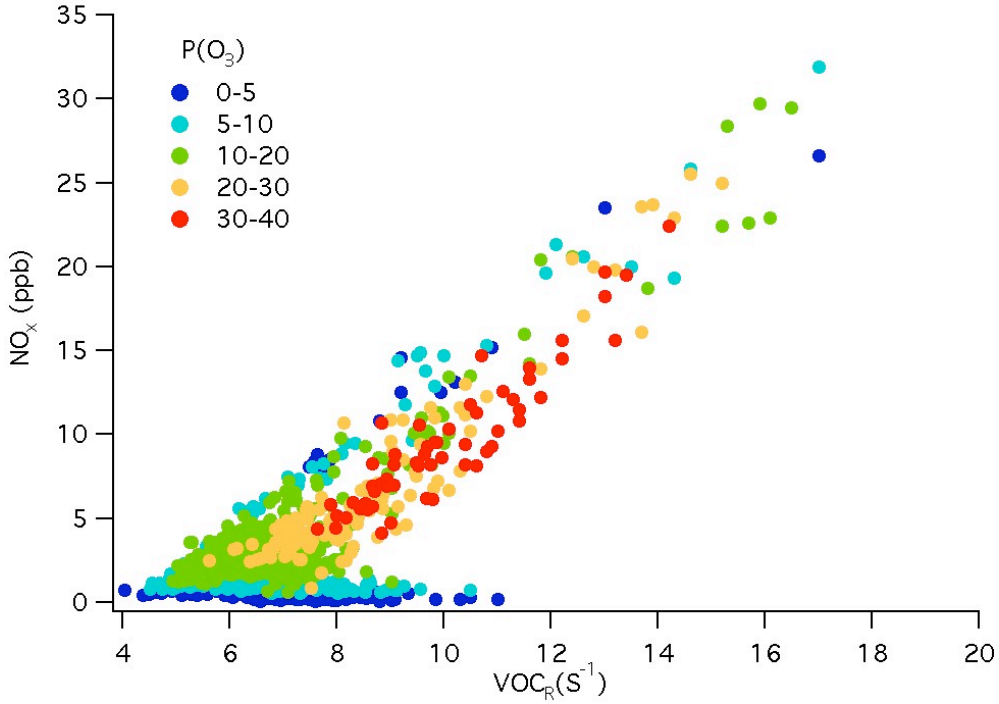


Figure 6. $P(O_3)$ as a function of $NO_x$ and $VOC_R$ at 13 LST on 27-28 July 1998 within the Portland sub-domain. (Only grid cells with $P(O_3) > 0$ are plotted.)

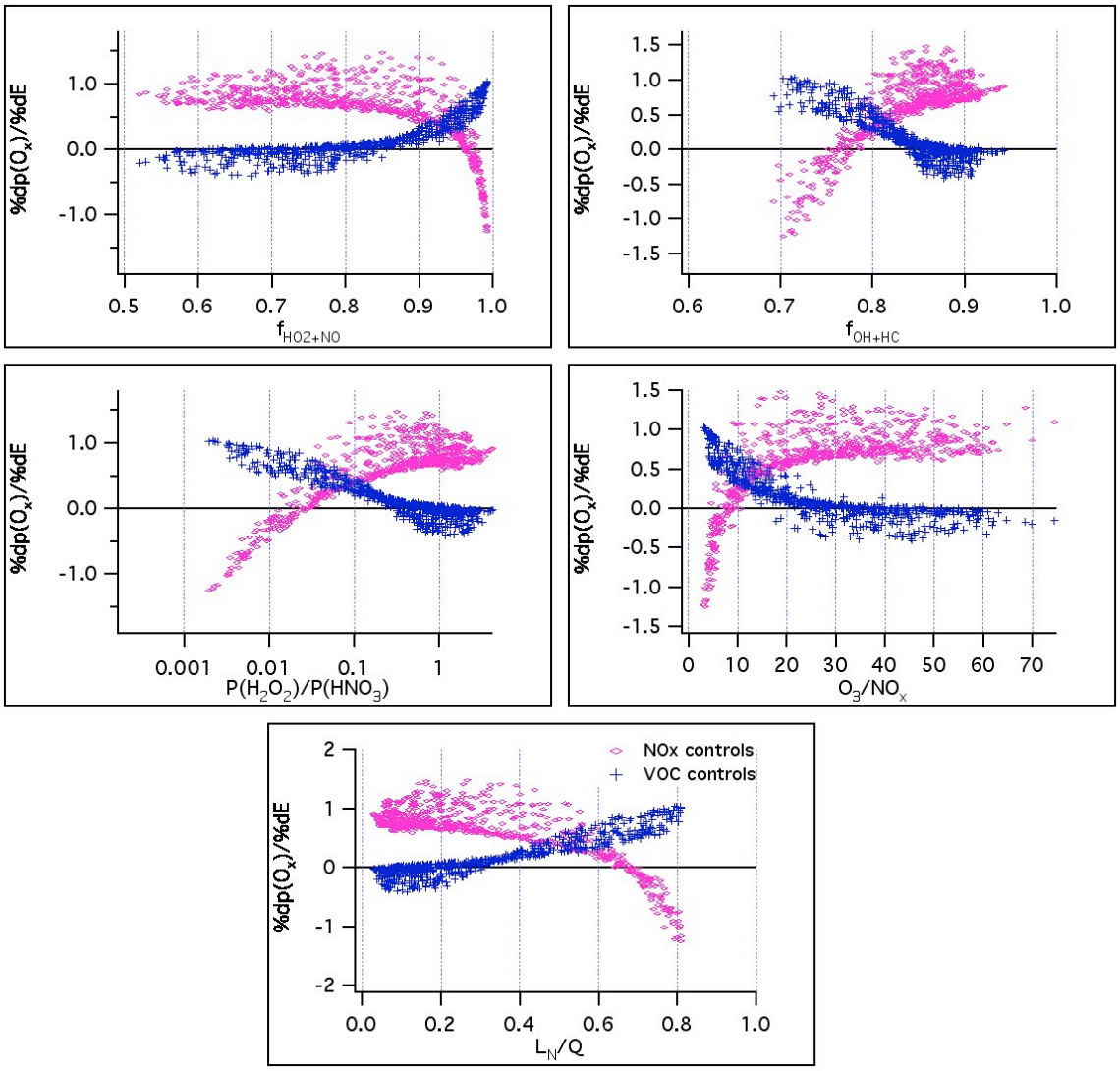


Figure 7. $\partial P(O_x)/\partial E_{NOx}$ (pink diamond) and $\partial P(O_x)/\partial E_{VOC}$ (blue cross) as a function of base case indicator values at 13 LST on 27-28 July 1998 within the Portland sub-domain. (Only cells with $P(O_x)$ greater than 10 ppb $hr^{-1}$ are plotted.)

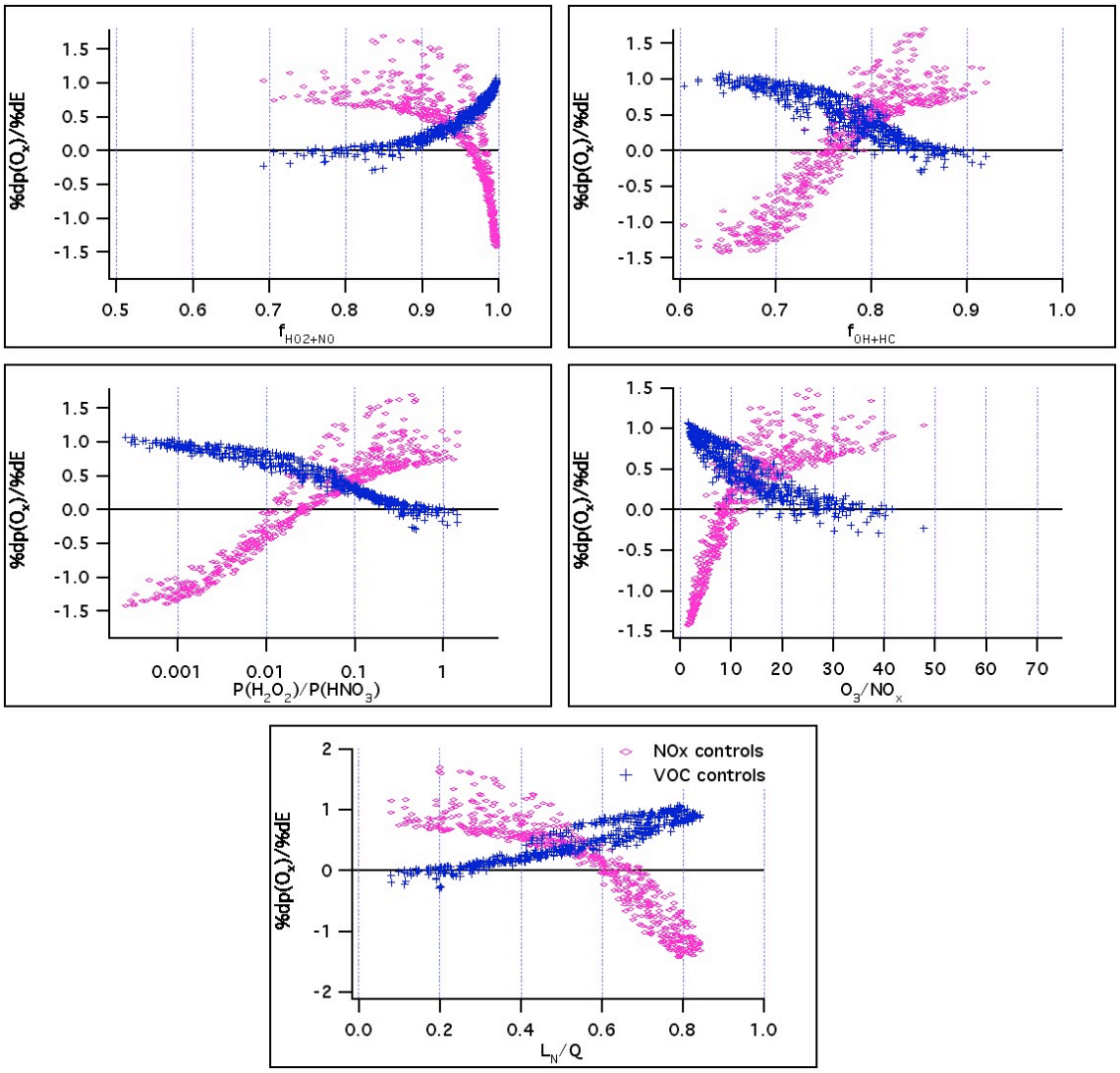


Figure 8. $\partial P(O_x)/\partial E_{NOx}$ (pink diamond) and $\partial P(O_x)/\partial E_{VOC}$ (blue cross) as a function of base case indicator values at 13 LST on 25-26 July 1998 within the Portland sub-domain. (Only cells with $P(O_x)$ greater than 10 ppb $hr^{-1}$ are plotted.)

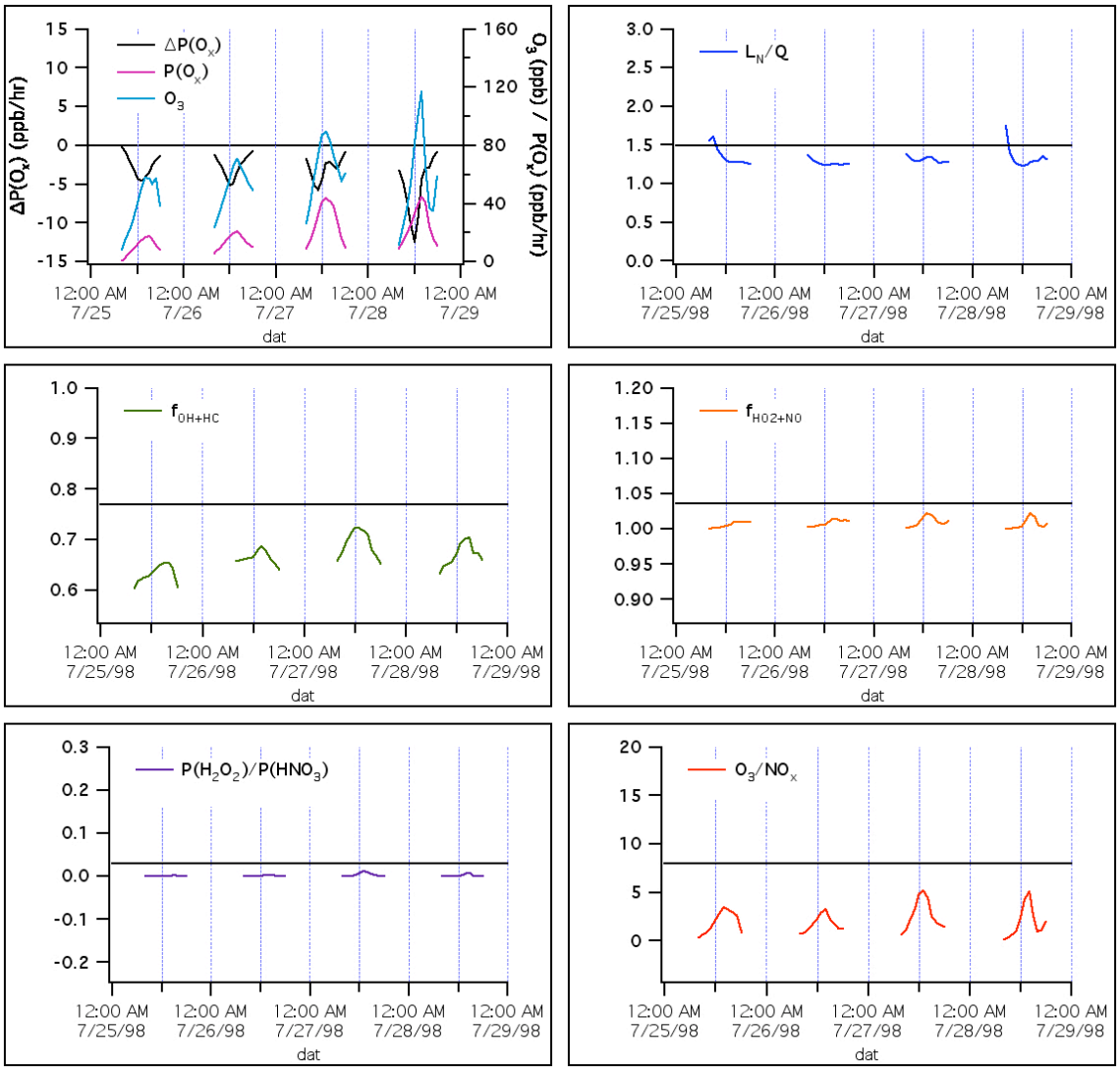


Figure 9. Time series (8:00 LST to 18:00 LST) of $O_3$, $P(O_x)$, $\Delta P(O_x)$, and indicators for the Vancouver area cell.

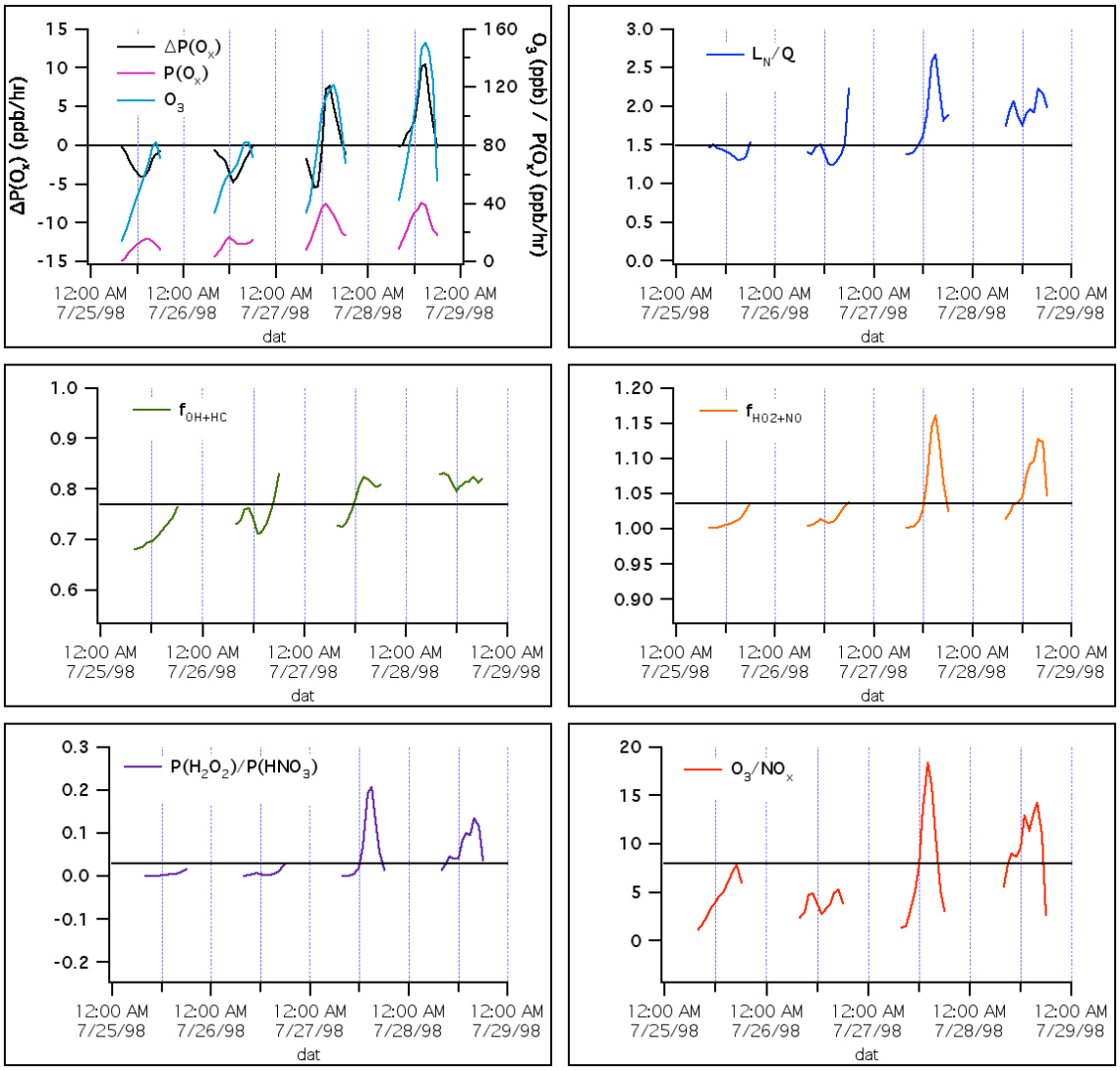


Figure 10. Time series (8:00 LST to 18:00 LST) of $O_3$, $P(O_x)$, $\Delta P(O_x)$, and indicators for the downwind area cell.

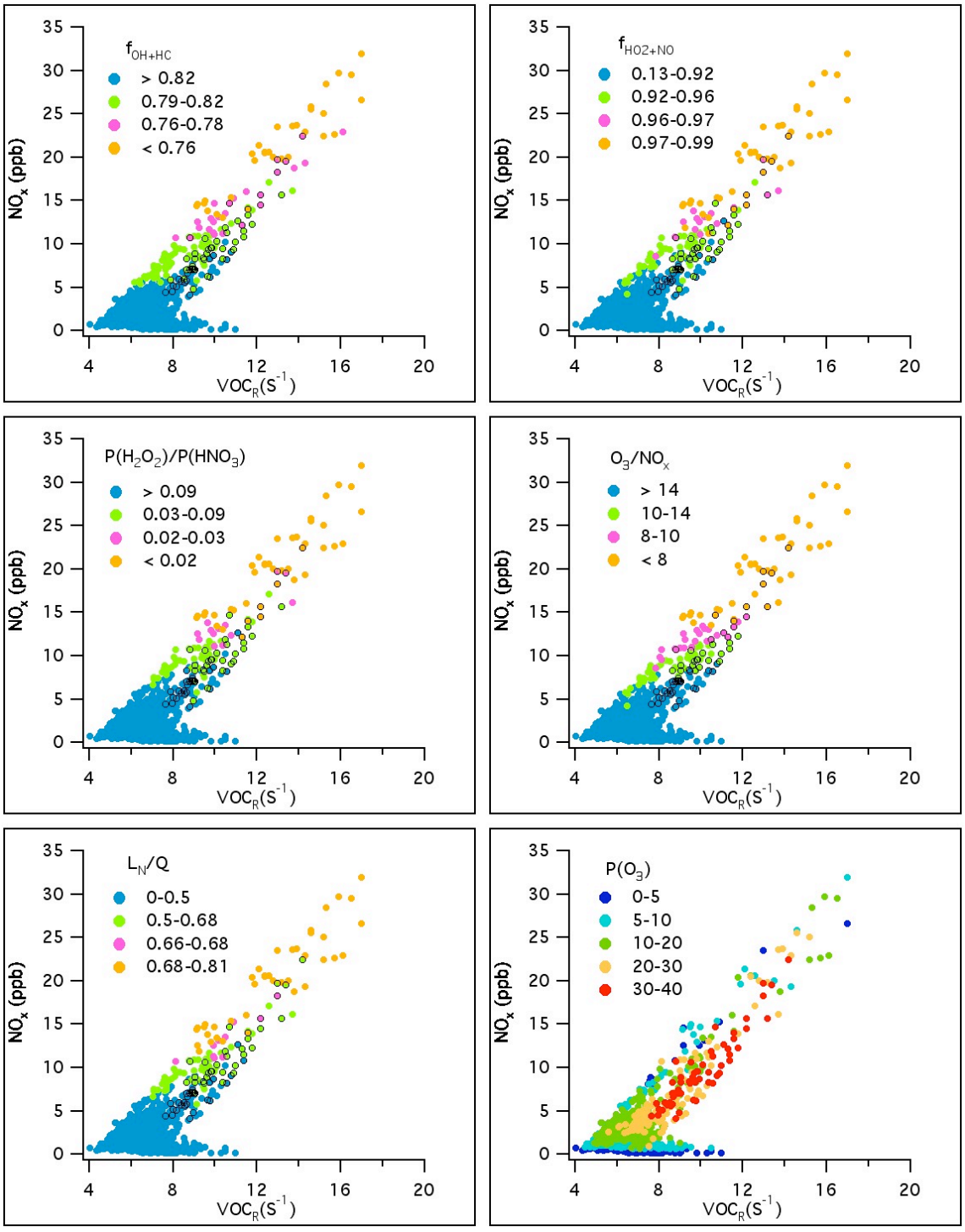


Figure 11. Indicator values and $P(O_3)$ as a function of $NO_x$ and $VOC_R$ at 13 LST on 27-28 July 1998 within the Portland sub-domain. Data points with $P(O_3) > 30$ ppb are marked with black circles and only data with $P(O_3) > 0$ are plotted.

Table 1. Summary of MM5 statistical performance of mean bias (MB), mean absolute error (MAE), and index of agreement (I) for the period of July 25-28, 1998.

| | | MB | MAE | I |
|---|---|---|---|---|
| Temperature | (°C) | 1.9 | 3.2 | 0.75 |
| Wind speed[a] | (m/s) | 0.1 | 1.2 | 0.83 |
| Wind direction[a] | (°) | 6 | 47 | 0.95 |
| Relative humidity | (%) | -1 | 12 | 0.96 |
| Wind speed[b] | (m/s) | 0.3 | 1.2 | 0.79 |
| Wind direction[b] | (°) | 14 | 49 | 0.96 |

[a] includes all surface stations within the modeling domain.
[b] only includes surface stations that withheld from nudging.

Table 2. Indicator values associated with $NO_x$- and VOC-sensitive conditions from this study compared to previously derived values.

| Indicators | VOC-sensitive | Ridgeline | Equal sensitivity | $NO_x$-sensitive |
|---|---|---|---|---|
| $f_{HO2+NO}$[a] | > 0.97 | 0.96-0.97 | 0.92-0.96 | < 0.92 |
| $I(NO,RO_2)$[b] | > 0.97 | 0.95-0.97 | 0.94-0.95 | < 0.94 |
| $f_{OH+HC}$[a] | < 0.76 | 0.76-0.78 | 0.79-0.82 | > 0.82 |
| $I(HC,NO_2)$[c] | < 0.77 | 0.77-0.85 | 0.80-0.85 | > 0.85 |
| $P(H_2O_2)/P(HNO_3)$[a] | < 0.02 | 0.02-0.03 | 0.03-0.09 | > 0.09 |
| $P(H_2O_2)/P(HNO_3)$[d] | < 0.06 | 0.06-0.07 | 0.07-0.12 | > 0.12 |
| $O_3/NO_x$[a] | < 8 | 8-10 | 10-14 | > 14 |
| $O_3/NO_x$[d] | < 12 | 12-14 | 12-16 | > 16 |
| $L_N/Q$[a] | > 0.68 | 0.66-0.68 | 0.5-0.6 | < 0.5 |
| $L_N/Q$[e] | > 0.67 | 0.67 | 0.5 | < 0.5 |

[a] Indicator values from this study.
[b] Indicator values from *Tonnesen and Dennis* [2000a]. Note that $I(NO,RO_2)$ is an approximation of $f_{HO2+NO}$.
[c] Indicator values from *Tonnesen and Dennis* [2000a]. Note that $I(HC,NO_2)$ is an approximation of $f_{OH+HC}$.
[d] Indicator values from *Tonnesen and Dennis* [2000a].
[e] Indicator values from *Kleinman et al.* [1997] and *Kleinman* [2005].

## CHAPTER THREE

# Evaluation of $O_3$-$NO_x$-VOC sensitivity predicted with the CMAQ photochemical model using PNW2001 field data

Ying Xie, Tom Jobson, and Brian Lamb
*Washington State University, Department of Civil and Environmental Research*

Rob Elleman
*U.S. Environmental Protection Agency (EPA) Region 10*

## Abstract

The Community Multiscale Air Quality (CMAQ) model-predicted $O_3$-$NO_x$-VOC chemistry for the Pacific Northwest was evaluated by comparing to aircraft measurements of CO, $NO_y$, $O_3$, and VOCs collected during the Pacific Northwest field experiment in the summer of 2001 (PNW2001) for three aspects: 1) photochemical indicator values ($O_3/NO_y$), 2) emission inventory, and 3) VOC reactivity. The evaluation was performed for two modeling scenarios: a standard scenario and a reduced VOC scenario, which was developed based on the comparisons of measurements with the emission inventory. Results showed that model-predicted $O_3/NO_y$ ratios were closely related to VOC-$NO_x$ sensitive conditions, with transitional values similar to those identified from previous studies. Peak $O_3$ was associated with VOC-sensitive conditions, but these were not far from the transitional regime. The standard modeling scenario over-predicted peak $O_3$ and the $O_3/NO_y$ slope, indicating an overestimation of sensitivity to $NO_x$, probably due to too much VOC in the emission inventory. The reduced VOC scenario resulted in better agreement with measurements in terms of peak $O_3$ as well as $O_3/NO_y$ correlations. Comparisons of observed CO and VOC to $NO_y$ ratios from the morning urban samples with those from the emission inventory also supported an overestimation of VOC in the standard scenario, with CO concentrations over-predicted by 80% and the total VOC reactivity over-predicted by 30%. Anthropogenic VOC and CO were the major contributors to odd oxygen photochemistry in the morning urban profile, while CO and oxygenated compounds accounted for two thirds of the measured reactivity in the afternoon aged plume. The standard modeling scenario substantially overestimated the reactivity from CO. The reduced VOC scenario showed generally

good agreement with observations of the relative contributions to the total VOC reactivity.

## 1. Introduction

Tropospheric ozone is a major concern for air quality due to its adverse impact on human health [*Lippman*, 1993] and ecosystems [*NRC*, 1991]. Ozone remains as the most troublesome of the criteria pollutants: half of the US population lives in areas where the ozone air quality standard was exceeded in 2007 [http://www.epa.gov/airtrends/sixpoll.html]. It is well known that the photochemical production of ozone is a highly nonlinear system: in conditions with relatively high VOC/$NO_x$ ratios, production of $O_3$ is limited by $NO_x$ availability, so it increases with increasing $NO_x$ emissions and is less sensitive to changes in VOC; in conditions with relatively low VOC/$NO_x$ ratios, production of $O_3$ is limited by radical availability and $NO_x$ inhibition, and therefore, $O_3$ increases with increasing VOC and decreases with increasing $NO_x$. For urban areas, ozone control strategies have been developed largely based on 3-D air quality model simulations, where model performance is usually judged by comparing observed and measured $O_3$ levels. Due to the complex nonlinearity of ozone-VOC-$NO_x$ chemistry, however, predicted peak $O_3$ level is not dependent on a unique set of VOC and $NO_x$ concentrations. Therefore, the model might predict incorrect sensitivities to changes in precursors even while correctly predicting $O_3$ levels [*Sillman*, 1995]. In order to gain more confidence in model predictions and control policies, observation-based methods have been developed in recent years. The methods can be divided into two categories [*Sillman*, 1999]: those based on ambient levels of primary emissions of VOC and $NO_x$, and those based on ambient levels of secondary reactants such as reactive nitrogen and peroxides.

For methods based on ambient measurements of direct emissions, a variety of studies have been made for evaluating emission inventories, mostly using species ratios [*Parrish et al*., 1991; *Goldan et al*., 1995; *Harley et al.*, 1997]. Early morning or winter measurements are often used since photochemical conversion and loss are relatively small at the time. For other conditions, concentrations of compounds are still useful when photochemical loss and dilution are properly taken into account [*Mckeen and Liu*, 1993; *Mckeen et al*., 1996]. *Parrish et al*. [1991] made winter and early spring measurements of CO, $SO_2$, and $NO_y$ in Boulder, Colorado and found the observed CO to $NO_y$ ratio consistent with available inventories. At the same site, *Goldan et al*. [1995] measured additional hydrocarbons and oxygenated VOCs in the winter of 1991 and compared the observed compounds to $NO_y$ ratios to those in the 1985 National Acid Precipitation Assessment Program (NAPAP) emission inventory. Their results suggested relatively good performance for CO/$NO_y$, but large over-predictions of many hydrocarbons and significant under-predictions of light alcohols and carbonyls. In contrast to the good agreement in the CO to $NO_y$ ratio from Boulder, *Harley et al.* [1997] found under-predictions of the CO to $NO_x$ ratios in the Los Angeles basin for summer measurements in 1987. More recent studies of CO and $NO_x$ emissions [*Parrish et al*., 2002, *Parrish*, 2006] found a rapid decrease (7-9% per year from 1987 to 1999) in US vehicular CO/$NO_x$ ratios, and a likely overestimation of CO emissions by a factor of two in recent US EPA estimates. Besides species ratios, measured VOC and $NO_x$ have also been used directly to evaluate emissions inventory and model performance [*Harley and Cass*, 1995; *Jacobson et al*., 1996; *Steiner et al*., 2008]. However, when the absolute

values are used alone, it's often unclear how to separate the uncertainties from other processes such as transport, clouds, boundary layer height, etc.

For methods involving secondary reaction products, one of the most important applications relates to the usage of photochemical indicators. The indicator concept was proposed by *Milford et al*. [1994] and *Sillman* [1995, 1997]. They found that in 3-D photochemical models, the ratio of certain species would have different values related to $NO_x$- and VOC-sensitive conditions. Based on steady state balance of radical initiation and termination, *Sillman* [1997] developed indicator ratios including $O_3/NO_y$, $O_3/NO_z$, $H_2O_2/HNO_3$, and other similar ratios related to ozone, reactive nitrogen, and peroxides. In comparison to these cumulative indicators, *Tonnesen and Dennis* [2000a and 2000b] developed local indicators for instantaneous ozone production rate using a slightly different approach based on radical propagation efficiency. Also based on a steady state balance, *Kleinman et al.* [1997] and *Kleinman* [2005] found that the sensitivity of instantaneous ozone production rate to $NO_x$ concentration, VOC reactivity, and radical production rate depends on the fraction of radicals that are removed by reactions with $NO_x$.

The general idea is that since the values of these measurable indicators could be related to $NO_x$- or VOC-sensitive conditions, model predicted sensitivity could be evaluated by comparing to measured indicator values or ozone sensitivity could be evaluated directly from measurements. A number of studies have reported that ambient measurements of indicator values generally show expected behavior in various locations [*Sillman*, 1999]. Values indicating $NO_x$-sensitive conditions were found in the eastern US [*Daum et al*., 1996; *Sillman et al*., 1998], Atlanta [*Sillman et al*., 1995, 1997], and a

rural site in Colorado [*Watkins et al*., 1995], and values indicating VOC-sensitive conditions were measured in Los Angles [*Sillman, 1995*; *Sillman et al*., 1997]. Measured indicator values were also compared with model predictions in Atlanta [*Sillman et al*., 1997], Los Angles [*Sillman et al*., 1997], Nashville [*Sillman et al*., 1998], and Paris [*Sillman et al*., 2003]. It was found that comparisons involving indicator values are more stringent than standard methods based only on ozone performance, and therefore, the uncertainties in ozone sensitivity from model predictions could be reduced.

In 2001, a small field study (the Pacific Northwest 2001 field campaign; PNW2001) was conducted in August in the Puget Sound region. The goal of this study was to better understand ozone and aerosol formation in the region and to provide datasets for air quality model evaluation [*Jobson et al*., 2002]. The U.S. Department of Energy Gulfstream-I (G-I) aircraft was used to measure meteorological conditions, gas phase concentrations, and aerosol properties. Aircraft measurements also included morning "touch-and-go" urban profiles taken at Boeing Field in Seattle. The ambient data from the G-I flights provide a good opportunity for using observation-based methods to evaluate model predicted ozone chemistry and to have a better understanding of ozone formation in the region.

The objectives of this study are to: 1) evaluate model-predicted sensitivity and ozone chemistry by comparing to observed indicator values ($O_3/NO_y$), 2) evaluate the emission inventory using observed compounds versus $NO_y$ ratios in the morning urban profile, and 3) compare observed and model-predicted VOC reactivity. Measurements and photochemical modeling are described in section 2. In section 3, we present the results from comparing observed and predicted $O_3$ and $NO_y$ levels, an examination of the

behavior of modeled $O_3/NO_y$, and an evaluation of the model by comparing to observed $O_3/NO_y$ values. Then from a slightly different perspective, we evaluate the emission inventory and compare measured and modeled VOC reactivity. Finally, we discuss the findings and uncertainties.

## 2. Methodology

### 2.1 PNW2001 field campaign

#### 2.1.1 Flights

Details of the aircraft flights were described in *Elleman* [2007]. Briefly, the U.S. Department of Energy G-I aircraft made five flights during August 2001: 20 August (Monday), 26 August (Sunday), and 27 August (Monday). Both morning and afternoon flights were conducted on 20 and 27 August, while only afternoon flights were made on 26 August. Except for several vertical profiles and morning touch-and-go urban profiles at Boeing Field, the flights were typically at 600 m in the boundary layer west of the Cascades and 1500 m over the mountain range. The three flights on 26 and 27 August are included here for model comparison. As shown in the flight tracks (Figure 1), the morning flight was focused on measuring the Seattle urban area as well as US-Canadian transport, while the afternoon flights were intended to sample the aged urban plume around Puget Sound as well as the background airmass. The meteorology conditions were representative of weak on-shore flow which is frequently seen in the summer. 26 August was characterized by isolated morning stratus clouds followed by sunny and warmer conditions. 27 August was associated with cloudier conditions and cooler temperatures.

### 2.1.2 Instruments

$O_3$ was measured using a commercial UV absorption instrument (Thermo Environmental Instruments, model 49-100) that was calibrated before the field experiment. Uncertainty in the $O_3$ measurement was estimated to be 5%. Carbon monoxide was measured using a nondispersive infrared based monitor (Thermo Environmental Instruments, model 48C). The CO instrument was calibrated before and after each flight with a multipoint calibration. Inflight zeroes were performed in order to track changes in background due to changes in cabin temperature. Estimated uncertainty for a 1 minute average was 30 ppb + 15% of the measured mixing ratio. NO and $NO_y$ were measured with a commercial chemiluminescence instrument (Thermo Environmental Instruments, model 42S). The detector response to NO was calibrated before and after each flight with a multipoint calibration. $NO_y$ was converted to NO using a molybdenum catalyst at 350°C. Detection limits for NO were estimated to be 300 ppt. The uncertainty in the data was 300 ppt + 15% of the measured NO mixing ratio. Instrument response times were 20-30 seconds for the CO, $O_3$, and NO, $NO_y$ instruments.

VOC measurements were made by using a proton transfer reaction mass spectrometer (PTR-MS) and by sampling into canisters for analysis by gas chromatography flame ionization detection (GC-FID). The inlet for the PTR-MS was a rearward facing PFA Teflon tubing inlet through which 1 SLPM was pulled through a low pressure drop mass flow controller by a diaphragm pump. The PTR-MS subsampled this flow at 300 sccm upstream of the mass flow controller. The PTR-MS was calibrated before and after each flight using a multi-component compressed gas standard (Apel-

Reimer Environmental) diluted with humid zero air. Humid zero air was made in-situ by passing ambient air over a heated catalyst (1% Pt on alumina). In-flight zeros were performed by over flowing the inlet with humid zero air. The PTR-MS measured various compounds, in which m/z 33 (methanol), m/z 45 (acetaldehyde), and m/z 59 (acetone) were used here for analysis. Detection limits were ~ 50 -100 ppt depending on the compound.

Canisters were filled with a metal bellows pump sampling from a rearward facing stainless inlet. Canisters were pressurized in 10-15 seconds and returned to Washington State University (WSU) for analysis of $C_3$-$C_{12}$ hydrocarbons by GC-FID. Organics from a 500 mL air sample were cryogenically trapped on glass beads using liquid oxygen. The analysis was performed on a DB-1 column and mixing ratios were determined by referencing responses to a NIST certified standard of 2,2-dimethylbutane. Uncertainty in the canister measurements based on the precision of replicate analysis was the larger of 5% or 10 ppt.

Formaldehyde was measured by in-situ scrubbing and derivitization by DNPH and analysis in flight by HPLC. This system has been described by *Lee et al*. [1996].

## 2.2 Modeling

### 2.2.1 Models and base case evaluation

*Elleman* [2007] performed a series of simulations focused on aerosol predictions using the U.S. EPA Models-3 Community Multi-scale Air Quality (CMAQ) [*Byun and Schere*, 2006] model. In this study, we used Elleman's base case run as the standard modeling scenario. Further details about modeling case design and evaluation can be found elsewhere [*Elleman*, 2007; *Elleman and Covert*, 2008].

The Mesoscale Meteorological model Version 5 (MM5) was run for three one-way nested domains at 36, 12, and 4 km horizontal grid spacing to develop the 3-D meteorology fields. The domain centers on the Pacific Northwest with 38 vertical sigma levels. NCEP 40 km ETA analyses (ETA-221) were used to initialize the atmospheric conditions, and 100 km ETA forecasts (ETA-104) provided 3-hourly boundary conditions. Analysis nudging [*Seaman et al*., 1995] toward the 12-hourly ETA-221 analyses was applied for the 36 and 12 km domains for winds above and within the boundary layer, and for temperature and moisture above the boundary layer. The MM5 physics options included the Kain-Fritsch cumulus parameterization scheme [*Kain and Fritsch*, 1990] at 36 and 12 km domain, the MRF PBL scheme [*Hong and Pan*, 1996], simple ice microphysics, and no shallow cumulus parameterization. Output from the 4 km MM5 simulation was used to provide 3-D meteorological fields for emissions and photochemical modeling.

The area, onroad mobile, non-road mobile, point, and biogenic emissions were processed at WSU using the Sparse Matrix Operator Kernel Emissions (SMOKE) processor (http://www.smoke-model.org/index.cfm). The emission inventory was based on information compiled from the Washington State Department of Ecology, Oregon Department of Environmental Quality, Idaho Department of Environmental Quality, Washington State University, the Western Regional Air Partnership, and Environment Canada. For on-road mobile sources, emissions were based on the Western Regional Air Partnership (WRAP) 2003 inventory with emission factors obtained from EPA MOBILE-6 [*US. EPA*, 2003]. Other mobile sources such as railroad and commercial marine were also included. Point sources were based upon NEI96, with updates for 2001 for

Washington and Oregon. Biogenic emissions from trees, plants, and crops were processed by the Biogenic Emissions Inventory System version 3 (BEIS3). The 1-km Biogenic Emissions Landcover Database, version 3 (BELD3), was used to generate normalized emissions, which were then used in BEIS3 along with meteorological data and speciation profiles to compute gridded and speciated hourly biogenic emissions. The emissions domain is the same as the photochemical modeling domain, which consists of 123 by 183 horizontal grids and encompasses the I-5 corridor of western Washington and Oregon as well as British Columbia. Table 1 summarizes a typical summer weekday emissions in the domain for the standard modeling scenario. For anthropogenic sources, total VOC as wells as its main components (alkane, alkene, aromatics, HCHO, CCHO, acetone, and methanol) are listed in the table. Similar to the previous modeling studies in the Pacific Northwest [*Barna et al*., 2000; *Chen et al*., 2008], anthropogenic sources dominated the $NO_x$ emissions, while biogenic sources accounted for most of the domainwide VOC emissions.

CMAQ version 4.4 was used for photochemical air quality modeling. 21 layers were applied in the vertical with the surface layer about 30 m above the ground and 14 levels between the surface and 800 mb. The SAPRC99 photochemical mechanism [*Carter*, 2000] including aqueous chemistry and aerosol dynamics was employed. The Euler Backward Interactive (EBI) solver was used to solve the chemical kinetic equations. The piecewise parabolic scheme was used as advection scheme and eddy diffusion was used for vertical diffusion algorithms. The Models-3/CMAQ dry deposition model was applied to estimate the deposition velocities of gases and aerosols. CMAQ boundary conditions were based on GEOS-CHEM model [*Bey et al*., 2001] for

most of the gaseous species and representative observations at Cheeka Peak on the Olympic Peninsula [*Anderson et al*., 1999] for aerosols. The only modification from Elleman's base case run was that the north and western boundary conditions for $O_3$ were revised based on the observations at Trinidad Head and Cheeka Peak. The changes mainly affected the western boundary where the $O_3$ concentrations near the surface were increased from 17 to 27 ppb. The model simulation included a spin-up period of 96 hours and then 72 hours of valid runs from 00 UTC 26 August until 00 UTC 29 August 2001.

*Elleman* [2007] evaluated MM5 and CMAQ performance for the standard scenario. For meteorological parameters, MM5 was evaluated against surface measurements of winds, temperature, relative humidity, and sea level pressure from 200 stations. Satellite observation of clouds, vertical profiles from the operational wind profile at the Seattle office of the National Weather Office and from measurements made by the Gulfstream aircraft during PNW2001 were also used for comparison. The results showed that 2 m temperatures were overestimated by 0 to 5°C. The mean error was about 1 m/s for wind speed and 50° for wind direction, which are similar to the performance in the realtime forecasting run operated at the University of Washington (http://www.atmos.washington.edu/mm5rt/mm5info.html). For both temperature and winds, there was a diurnal pattern in the model performance and the errors tend to be greatest in the early morning and less in the afternoon and early evening. Based on the observed profiles from the G-I aircraft, PBL height was overestimated by 400 m and 300-400 m near Enumclaw, 40 km east of Seattle, at 23 UTC (16 PDT) on 26 and 27 August, respectively. For CMAQ performance, Elleman found $O_3$ and photochemistry were

generally over-predicted on 26 August and under-predicted on 27 August. He analyzed the gas phase precursors and meteorology parameters from the model and measurements, but no clear conclusion could be drawn for what caused the errors in predicted photochemistry. Evaluated using standard methods, the normalized mean bias factor and normalized mean error factor for $O_3$ are 28% and 62% for all available ground stations. This error is similar in magnitude to results from previous simulations using CMAQ in the Pacific Northwest [*O'Neill and Lamb*, 2005; *O'Neill et al.*, 2006; *Smyth et al.*, 2006].

### 2.2.2 Modeling scenarios

Two modeling scenarios were conducted. A standard scenario was based on Elleman's base case CMAQ run. A reduced VOC scenario was developed based on the comparisons of observed CO and VOC versus $NO_y$ ratios in the morning urban plume with those in the emission inventory. In the reduced VOC scenario, there were 30% reductions in most of the VOC species with the exception of 44% reduction in CO emissions and factors of 34 and 25 increases in methanol and acetone emissions, respectively. For each scenario, two sensitivity runs were conducted by decreasing either the anthropogenic VOC or $NO_x$ emissions by 30%. Details of the comparisons are discussed in Section 2.2.4 and 3.2.

### 2.2.3 Mapping modeled and observed chemical compounds

When comparing observed and modeled VOCs, measured alkane, alkene, and aromatics were grouped into corresponding lumped model species in SAPRC99 chemical mechanism according to the compounds in a standard urban mixture. *Carter* [1994a, 2000] used this mixture to derive the parameters for lump species in the base mechanism as well as reactivity scales of Carter. Since the lumped species in SAPRC99 generally

include more compounds than those being measured in PNW2001, the lumped groups from CMAQ output were multiplied by the mole fractions of the compounds available from the measurements. Detailed mapping between observation and model output is shown in Table 2.

### 2.2.4 Evaluation of the emission inventory

Ratios of anthropogenic VOC, CO, formaldehyde, acetaldehyde, isoprene, acetone, and methanol with respect to $NO_y$ from the morning touch-and-go profile at Boeing Field on 27 August were compared to those with respect to $NO_x$ from the emission inventory. The emission inventory represents a typical summer weekday, and was extracted from a region that encompasses the Seattle urban area. In the inventory, only the values between 6 and 10 AM were included for comparison. Measurements with elevated $NO_y$ levels (> 30 ppb) from the touch-and-go profile were assumed to be representative of fresh urban emissions and used to calculate the average measured ratios. For this period, there are two hundred data samples for CO and $NO_y$, sixteen samples for acetone, methanol, and acetaldehyde from the PTRMS, six samples for hydrocarbons from canisters, and one sample for formaldehyde. Since VOC were generally collected with much less frequency than $NO_y$, $NO_y$ concentrations were averaged over the VOC sampling periods to compute the ratios.

### 2.2.5 VOC reactivity

Here, we defined the total VOC reactivity ($VOC_R$) as the sum of the OH loss frequency due to reactions with CO, anthropogenic hydrocarbons, oxygenated hydrocarbons (formaldehyde, acetaldehyde, acetone, and methanol), and isoprene.

$$VOC_R = \Sigma k_i[VOC_i] \quad (1)$$

where $k_i$ is the OH rate constant and $VOC_i$ is the measured VOC concentration. OH rate constants come from *Atkinson* [1994].

For modeled VOC reactivity, the same compounds (CO, anthropogenic hydrocarbons, oxygenated hydrocarbons, and isoprene) were included in calculation. For lumped species, model output was multiplied by the mole fractions of the compounds available from the measurements. The OH rate constant of each lumped group was also recalculated based on the relative molar contributions from the measured VOC species (see Table 2).

Measured and predicted VOC reactivities were compared for selected time windows during the three flights, with these time windows shown as shaded areas in Figure 2. For the two afternoon downwind flights, the time windows were selected to cover the peak observed VOC reactivity with each spanning around 15 min. For the morning urban flight, the time window is about eight minutes and covers the touch-and-go profile. Within the time windows, there were four, six, and three canisters collected in the afternoon of 26 August, the morning and afternoon of 27 August, respectively. The observed reactivity was calculated based on the measurement frequency of the canister samples: CO was averaged over the time period when canister samples were collected, while acetone, methanol, acetaldehyde, and formaldehyde were calculated by picking the closest data points coincident with the canister samples.

# 3. Results and discussion

## 3.1 $O_3$ and $NO_y$

### 3.1.1 Aircraft measurements compared with model predictions

As shown in the Figure 1, during the afternoon flight of 26 August, elevated $O_3$ levels close to 80 ppb, about 40 ppb above the regional background, were observed to the south and southeast of Seattle. For the morning flight on 27 August, $O_3$ concentrations were relatively higher in the early part of the flight south of Seattle (around 30 to 50 ppb) as the G-I was mostly between 1000 and 2000 m for this period and captured the concentrations from the residual layer. Most other locations showed levels around 30 ppb except that very low concentrations were measured from the touch-and-go profile at Boeing Field as a result of $NO_x$ titration. This is consistent with the elevated $NO_y$ levels (see Figure 2) in the profile due to the relatively shallow morning boundary layer and abundant rush hour emissions. For the afternoon flight on 27 August, $O_3$ levels were generally lower than the previous day. Background concentrations were around 30 ppb, while slightly higher levels around 40 to 50 ppb were measured at the northern part of Seattle, to the southeast of the city around Enumclaw, and to the west over the Cascade ranges.

Measured $O_3$ and $NO_y$ were compared with the model results from the standard and reduced VOC scenarios for the three flights (see Figure 2 and Table 3). Here the model values were interpolated three-dimensionally in space and in time, so that they were matched in time and GPS location with the aircraft measurements [*Elleman*, 2007].

For the afternoon flight on 26 August, both model runs captured the $O_3$ plume to the southeast of Seattle around Enumclaw, but tended to over-predict to the north and

east of the metropolitan area. For the peak $O_3$ levels, there were large over-predictions in the standard scenario by around 20 ppb, while the reduced VOC scenario showed much closer agreement with the measurements. In terms of $NO_y$, two model runs showed essentially the same results, which was also true for the two flights on 27 August. Both scenarios predicted the $NO_y$ background correctly and the peak levels fairly well except for missing a few spikes, probably because the plumes were too small to be resolved at 4 km grid resolution. For the morning flight on 27 August, both model scenarios showed some under-predictions of $O_3$ levels for the early part of the flight when G-I was well above the morning boundary layer. Good agreement was reached for most of the other locations. The two model runs also predicted $NO_y$ levels relatively well, except for some under-predictions within the touch-and-go profile. This may partly due to the over-predictions of morning surface temperatures and the tendency to over-predict vertical diffusion by the MRF PBL scheme [*Elleman*, 2007]. For the afternoon flight on 27 August, the reduced VOC scenario predicted slightly lower $O_3$ concentrations than the standard run. Both runs captured the background $O_3$ levels well, but over-predicted $NO_y$ concentrations and correspondingly under-predicted the $O_3$ levels to the east of Seattle. The overestimation was also true for primary pollutants such as NO (not shown), CO, and anthropogenic VOC, which are discussed in detail in Section 3.3.2 below.

### 3.1.2 Modeled VOC-$NO_x$ sensitivity and $O_3/NO_y$ values

In order to evaluate CMAQ-predicted sensitivity using indicators, we first examined the behavior of model-predicted $O_3/NO_y$ to see whether it indicates the VOC-$NO_x$ sensitivity of the system. For each modeling scenario, two sensitivity runs were conducted by decreasing either the anthropogenic VOC or $NO_x$ emissions by 30%. In

Figure 3., we plot $O_3$ reductions associated with either VOC or $NO_x$ controls against their base case $O_3/NO_y$ ratios for each scenario. The model results are for 16 PDT on 26 August at layer 9 to match the aircraft measurements. Only the grid cells within a sub-domain which covers the peak $O_3$ plume and the Seattle urban center are plotted. In Figure 3 positive values were related to $O_3$ reductions with reduced emissions, whereas negative values showed increased $O_3$ values with emissions controls. It can be seen that ozone sensitivity was closely related to $O_3/NO_y$ in both modeling scenarios: cells with $O_3/NO_y$ greater than 8 were $NO_x$-limited, and cells with values less than 6 were VOC-limited.

Following the method of *Sillman et al*. [2003], the grid cells were defined as VOC-sensitive if $O_3$ in the 30% reduced VOC case was lower than both the 30% reduced $NO_x$ case and the base case by at least 2 ppb. The grid cells were $NO_x$-sensitive if $O_3$ in the 30% reduced $NO_x$ case was lower than both the 30% reduced VOC case and the base case by at least 2 ppb. If both the reduced VOC and reduced $NO_x$ cases resulted $O_3$ reductions by at least 2 ppb relative to the base case, the grid cells were defined to have mixed sensitivity. *Sillman et al*. [1997, 1998, 2003] used percentile distribution of the indicator values to identify transitional values associated with ozone sensitivity. The 95th percentile of the $O_3/NO_y$ ratios associated with VOC-sensitive locations and the 5th percentile ratios associated with $NO_x$-sensitive locations were chosen as the transitional values. As shown in Table 4, the transitional values were computed accordingly for the two modeling scenarios and compared with the previous studies [*Sillman and He*, 2002]. It appears that for both modeling scenarios, the 5th percentile values for $NO_x$-sensitive conditions were larger than the 95th percentile values for VOC-sensitive conditions. The

results suggest that the transitional values were around 6-8, which is close to most of the previous studies despite the large differences in geographic locations, photochemical models, and chemical mechanisms.

### 3.1.3 Compare observed and modeled indicator ratios ($O_3/NO_y$)

For the afternoon flight on 26 August, observed $O_3$ versus $NO_y$ relationships were compared with predicted values from the standard and reduced VOC scenarios as shown in Figure 4. For each scenario, model grid cells were shown as VOC-sensitive, $NO_x$-sensitive, or mixed sensitivity according to the criteria described above. To minimize the impact from changes in G-I altitude, the analysis here is based on the data around 3:00 – 4:30 PM (PDT), when G-I flew at 600 m except for a vertical profile near Enumclaw. No obvious correlation was found between observed $O_3$ and $NO_y$ in the afternoon flight on 27 August, probably due to the cloudier and cooler conditions.

The standard scenario predicted VOC-sensitive chemistry in the Seattle urban center and $NO_x$-sensitive conditions downwind. Peak $O_3$ was associated with VOC-sensitive conditions, but these were not far from the transitional regime. The model predicted a strong correlation between $O_3$ and $NO_y$ in $NO_x$-sensitive grid cells, with $O_3$ increasing with increased $NO_y$ concentrations. Compared to the observed values, the predicted rate of increase in $O_3$ with $NO_y$ is slightly higher and the $O_3$ peak was substantially overestimated (95 ppb modeled versus 77 ppb measured). In VOC-sensitive grid cells, the model predicted less correlation between $O_3$ and $NO_y$ and showed a large discrepancy with the observations.

The reduced VOC scenario also predicted VOC-sensitive chemistry in the Seattle urban center and $NO_x$-sensitive conditions in the outskirts, although the VOC-limited

area extended slightly further downwind. Similar to the standard scenario, peak $O_3$ was associated with VOC-sensitive and transitional locations. The model predicted lower $O_3$ peaks and slightly lower rate of increase of $O_3$ with $NO_y$, which matched the observations much closer. The correlation between $O_3$ and $NO_y$ in the VOC-sensitive regime was also in much better agreement with the measurements.

Figure 5 shows the observed $O_3$ versus $NO_y$ overlaid with $O_3/NO_y$ transitional value identified from the reduced VOC scenario ($O_3/NO_y$=6.6). Most of the observed values are associated with VOC-sensitive or transitional conditions as sitting below or close to the transitional line. *Sillman et al*. [2003] showed observed $O_3/NO_y$ values from Atlanta, Nashville, and Paris where measurements are mostly above or close to the transitional line. Compared to these cities, Seattle appears to be more associated with transitional and VOC-sensitive conditions.

### 3.2 Comparisons of the emissions inventory

Ratios of CO and VOC with respect to $NO_y$ from the morning urban touch-and-go profile on 27 August were compared to those with respect to $NO_x$ from the emission inventory as shown in Figure 6 and Table 5. The ratio of CO to $NO_y$ was overestimated by 80% (6.5 observed versus 11.6 in the emissions inventory). Overestimation of the CO to $NO_y$ ratio might be due to an overestimation of the CO emissions or an underestimation of the $NO_x$ emissions. As mentioned in Section 3.1.1, we found model predicted $NO_y$ levels were generally in good agreement with the observed concentrations. Recent studies on fuel-based emission inventory in the urban areas [*Parrish*, 2006] also suggest $NO_x$ emissions are reasonably accurate for the mid to late 1990s. Therefore, the overestimation of the CO to $NO_y$ ratio here is most likely due to an overestimation of the

CO emissions. Compared to other datasets, the observed CO/$NO_y$ ratio from G-I (6.5) was close to the reported CO/$NO_x$ ratios in 2000 at Nashville (5.7±0.4), TN, Atlanta, GA (6.5±0.4), and US urban (7.9±0.1) [*Parrish*, 2006]. The CO/$NO_x$ ratio from the Seattle emission inventory (11.6) was also close to U.S. EPA annual average inventory value (10.7 for year 1998) [*Parrish et al.*, 2002]. This suggests that both the observation and the emission inventory for Seattle are close to the U.S. urban average, and CO emissions were substantially overestimated in the recent inventory. Similar results have been reported by *Parrish* [2002] and *Parrish et al*. [2006] where they found CO emissions in U.S. vehicular emissions were overestimated by about a factor of two in the most recent EPA estimates. It should be noted that the uncertainty in the observed CO/$NO_y$ ratio from the G-I here was estimated to be 30% according to the uncertainty in the measurements, and this uncertainty doesn't change the general conclusion we reached.

For anthropogenic VOC (the sum of alkanes, aromatics, and alkenes), the ratio to $NO_y$ was overestimated by about 25%. For its components, the emission inventory predicted the correlation of aromatics to $NO_y$ relatively well, but overestimated alkanes to $NO_y$ ratio by about 30%. With only propene being available from the observed datasets, the ratios of alkenes to $NO_y$ were fairly low in both measured and predicted values. The ratios of oxygenated compounds to $NO_y$ were significantly underestimated, ranging from a factor of 3 for formaldehyde to a factor of 30 for methanol. Similar underestimations were reported for Boulder [*Goldan et al.*, 1995] and Boston/New York and Los Angles [*Warneke et al*., 2007]. These oxygenated compounds are emitted in large quantities from urban areas, but the sources of these emissions are still not well understood [*de Gouw et al*., 2005; *Warneke et al.*, 2007].

As shown in Figure 6 and Table 5, the ratios of these compounds to $NO_y$ were also compared to the emission inventory in a reactivity-weighted manner by multiplying the absolute ratios with the correspondent OH rate coefficient. There was an even split between CO and anthropogenic VOC, each of which accounts for 40% of the total measured reactivity. The contribution from oxygenated compounds was about half of that from CO. For anthropogenic VOC, aromatics played a more important role than alkanes. Compared to the observed ratios, there were about 30%, 80%, and 30% overestimations in anthropogenic, CO, and the total VOC reactivity in the emission inventory. This result also supports that overestimation of VOC in the emission inventory might be the cause for overestimating peak $O_3$ and $O_3/NO_y$ slope in the standard modeling scenario. According to the findings here, we developed the reduced VOC modeling scenario by reducing most of the VOC species by 30% with the exception of reducing CO by 44% and increasing methanol and acetone by factors of 34 and 25.

### 3.3 VOC reactivity

For each time window during the three flights (see shaded areas in Figure 2), median values from the measurements were compared with these from the standard and reduced VOC scenario for the total VOC reactivity and its components (Figure 7) as well as for contributions to the anthropogenic VOC reactivity (Figure 8). More details in bar plot with maximum, minimum, and median values are shown in Figures 9 and 10. The following discussion is based on median values unless noted otherwise.

#### 3.3.1 Measured VOC reactivity

As pointed out in the evaluation of the emission inventory, morning urban VOC reactivity were dominated by anthropogenic VOC and CO, each of which contributed to

about 40% of the measured reactivity. The contribution from oxygenated compounds was about half of that from CO, while the contribution from biogenic sources was minor. Compared to the previous studies in other urban areas, *Kleinman et al*. [2005] also found near equal contributions from anthropogenic VOC and CO in Phoenix and Philadelphia. For the total VOC reactivity, the values measured here had a value around 4 $s^{-1}$, which is in between the median values reported in Phoenix (~1.2 – 5 $s^{-1}$, median =~2 $s^{-1}$) and Philadelphia (~2.6 – 11 $s^{-1}$, median = ~4.5 $s^{-1}$).

For the two afternoon flights, CO was the largest contributor to the total VOC reactivity in the aged plume, accounting for about 40% of the measured values. Compared to morning urban profile, anthropogenic sources showed a reduced contribution (~20% on 26 August and ~30% on 27 August), while the contribution from isoprene increased, as a result of both warmer afternoon temperatures and more abundant emission sources in the downwind area. The isoprene spatial distribution was highly variable, indicated by the large differences between the maximum and median values in Figure 9. The contribution from oxygenated compounds also increased in the aged plume, which accounted for about 36% and 27% of the total VOC reactivity on 26 and 27 August, respectively. The larger contribution from oxygenated compounds on the first day was consistent with higher $O_3$ levels. Compared to the morning urban plume, the overall trend here was reduced values in anthropogenic sources due to loss from chemical reactions and dilution, and increased contributions from biogenic and oxygenated sources as a result of photochemical production of these compounds.

For anthropogenic components (Figure 8), aromatics played the most important role in the morning urban plume on 27 August. In the afternoon aged plume, the

reactivity from aromatics was less than that from alkanes on 26 August and showed comparable values on 27 August. For all flights, alkenes only accounted for a small fraction of the anthropogenic reactivity due to limited data from the measurements.

It should be noted that there were also other unmeasured anthropogenic compounds that also contribute to OH reactivity. Due to the detection limit of the instruments, part of the alkanes, aromatics, and the majority of the alkenes were not available from the canister measurements. In particular, ethene, $C_4$ and $C_5$ alkenes might be important due to their fast reaction rates with OH radicals. *Zweidinger et al.* [1988] measured roadside concentrations including various light alkanes and alkenes. According to their study, the contributions from ethene, and $C_4$ and $C_5$ alkenes are about 40% of the total measured reactivity. *Goldan et al.* [2000] referred to Zweidinger's work to quantify the impact of unmeasured light alkenes on the total reactivity and pointed out that the results from roadway study could be used as an upper limit for aircraft studies due to the fast loss rates of these compounds. Taken into account the possible unmeasured anthropogenic VOC reactivity up to 40%, the contribution from anthropogenic VOC might be greater than that from CO in the morning urban plume and have comparable values in the afternoon aged plumes.

### 3.3.2 Modeled VOC reactivity compared with measurements

For the relative contribution from each component to the total VOC reactivity (see Figure 7), the standard scenario substantially overestimated the contribution from CO, while the reduced VOC run showed much better agreement with the measurements. For anthropogenic VOC, both scenarios showed some under-prediction on 26 August while matching the observations on 27 August relatively well. For formaldehyde and

acetaldehyde, both scenarios showed generally good agreement with observations. For acetone and methanol, there was substantial improvement in the predicted mixing ratios from the reduced VOC scenario where their emission rates were actually increased. However, the changes in VOC reactivity were small, due to their slow reactions with OH radicals. Biogenic sources such as isoprene are difficult to validate due to limited measurements as well as being highly variable in space. It appears that both runs tended to underestimate the role of isoprene, especially in the afternoon of 26 August when biogenic emissions were favored by relative warm temperatures. For the total VOC reactivity, the reduced VOC scenario showed better performance than the standard case in the two flights on 27 August. The standard scenario was in closer agreement with the measured values in the afternoon flight on 26 August, but with the wrong reason: there were large compensating errors from overestimating CO and underestimating anthropogenic and isoprene reactivity.

For anthropogenic VOC (Figure 8), both model scenarios predicted the relative importance of alkanes and aromatics fairly well for each flight. In the afternoon of 26 August, most components of the anthropogenic VOC reactivity were somewhat under-predicted by both scenarios. In the afternoon of 27 August, the reduced VOC run performed better than the standard scenario, but it showed some under-predictions of aromatics in the morning of 27 August. It should be noted that for the afternoon of 27 August even in the reduced VOC scenario, the model tended to overestimate anthropogenic VOC for its maximum values (Figure 9) despite the good agreement in terms of median level (Figure 7). As mentioned previously, the overestimations were also seen for CO, NO, and $NO_y$ along with the underestimation of $O_3$. The discrepancies

between the model and measurements here are likely due to dilution related to meteorological variables as well as model representation of oxidation rates and photochemistry. The primary pollutants might be diluted or reacted away at a faster rate than the model predicted on that cooler and cloudier day, and resulted in lower levels of primary pollutants and higher $O_3$ which couldn't be captured by the model.

### 3.3.3 VOC reactivity and $NO_y$

Correlations between VOC reactivity and $NO_y$ were also compared between the measurements and the two modeling scenarios for anthropogenic VOC and CO as shown in Figure 11. Anthropogenic VOC and CO reactivity both appeared to increase with increased $NO_y$ in the observed and predicted values. For CO, the reduced VOC run showed lower $CO/NO_y$ slopes and much better agreement with observations in all three flights. For anthropogenic VOCs, the reduced VOC scenario showed close or better performance for the two days.

## 3.4 Discussion

The standard modeling scenario overestimated peak $O_3$ and the $O_3/NO_y$ slope, which suggests an overestimation of sensitivity to $NO_x$, probably due to too much VOC in the emission inventory. Comparisons of CO and VOC versus $NO_y$ ratios from the morning urban plume and those from the emission inventory also suggested an overestimation of the total VOC reactivity by about 30%. The reduced VOC scenario was developed based on emission inventory comparison, and resulted in better agreement with the measurements in terms of peak $O_3$ as well as $O_3/NO_y$ correlations. Comparisons of observed and predicted VOC reactivity also showed that the reduced VOC scenario performed generally better than the standard run. CO predictions were substantially

improved with the adjusted emissions, and better agreement with the measured VOC reactivity was reached most of the time.

Except for the errors in the emission inventory, indicator ratios can also be substantially affected by $NO_y$ removal processes such dry and wet deposition, aerosol interactions as well as measurements errors. We found model predicted $NO_y$ concentrations reasonably accurate in both the urban plume and the background airmass. Therefore, the modeled errors in $O_3$ and $O_3/NO_y$ correlations from the standard scenario are mostly likely related to the errors in the emissions instead of those associated with $NO_y$ removal or measurements.

## 4. Conclusions

CMAQ-predicted $O_3$-$NO_x$-VOC chemistry was evaluated by comparing to the measured values from the PNW2001 field campaign. Two modeling scenarios were evaluated: 1) a standard scenario based on the original run from *Elleman* [2007], and 2) a reduced VOC scenario developed based on comparisons of observations with the emission inventory.

We found that $O_3/NO_y$ ratio is a useful indicator for evaluating model-predicted ozone sensitivities. Modeled ratios appeared to be closely related to VOC-$NO_x$ sensitive conditions, with transitional values similar to those identified from previous studies. In the Puget Sound area, peak $O_3$ was associated with VOC-sensitive conditions, but these were not far from the transitional regime. Compared to measured $O_3/NO_y$ values from Atlanta, Nashville, and Paris [*Sillman et al*., 2003], Seattle appeared to be more associated with transitional and VOC-sensitive conditions. The standard modeling

scenario over-predicted peak $O_3$ and the $O_3/NO_y$ slope, which suggested an overestimation of sensitivity to $NO_x$, probably due to too much VOC in the emission inventory. The reduced VOC scenario resulted in better agreement with measurements in terms of peak $O_3$ as well as $O_3/NO_y$ correlations.

Comparisons of observed CO and VOC to $NO_y$ ratios from the morning urban profile with those from the emission inventory also supported an overestimation of VOC in the standard scenario. The results suggested: (1) substantial overestimation of CO emissions by 80%, which is consistent with the recent findings from *Parrish et al.* [2002] and *Parrish* [2006], (2) overestimation of anthropogenic and the total VOC reactivity by 30%, (3) large under-predictions of oxygenated compounds, ranging from a factor of 3 for formaldehyde to a factor of 30 for methanol. Similar underestimations of oxygenated compounds were reported in Boulder [*Goldan et al*., 1995] and Boston/New York and Los Angles [*Warneke et al*., 2007].

In the morning urban plume, anthropogenic VOC and CO appeared to be the most important contributors to odd oxygen photochemistry, while the contribution from oxygenated compounds was about half of that from CO. For the total VOC reactivity, the values measured here was around 4 $s^{-1}$, which is between the median values reported in Phoenix (~1.2 – 5 $s^{-1}$, median =~2 $s^{-1}$) and Philadelphia (~2.6 – 11 $s^{-1}$, median = ~4.5 $s^{-1}$) [*Kleinman et al*., 2005]. In the afternoon downwind plume, CO and oxygenated compounds accounted for two thirds of the total measured reactivity. Anthropogenic sources showed a reduced contribution due to loss from chemical reactions and dilution. Biogenic sources such as isoprene also played an important role in the aged plume, but were difficult to validate due to limited measurements and high spatial variability.

Compared to the measured VOC reactivity, the standard modeling scenario substantially overestimated the reactivity from CO. The reduced VOC scenario showed generally good agreement with observations of the relative contributions of the total measured VOC reactivity.

Our results showed that both CO and oxygenated compounds play an important role in the regional photochemistry, however, their emissions were not well quantified. This has profound implications for modeling regional $O_3$ productions due to the sensitivity to VOC/$NO_x$ ratios. Therefore, better methods should be developed for updating the current CO emission inventory, and more measurements are needed to have a better understanding of the sources of oxygenated compounds.

**References**


Anderson, T. L., D. S. Covert, J. D. Wheeler, J. M. Harris, K. D. Perry, B. E. Trost, D. J. Jaffe, and J. A. Ogren (1999), Aerosol backscatter fraction and single scattering albedo: Measured values and uncertainties at a coastal station in the Pacific Northwest, *J. Geophys. Res., 104*(D21), 26,793–26,807.

Atkinson, R. (1994), Gas-phase tropospheric chemistry of organic compounds, *J. Phys. Chem. Ref. Data Monogr., 2*, 1– 216, 1994.

Barna, M., and B. Lamb (2000), Improving ozone modeling in regions of complex terrain using observational nudging in a prognostic meteorological model, *Atmos. Environ., 34*, 4889–4906.

Bey, I., D. J. Jacob, R. M. Yantosca, J. A. Logan, B. D. Field, A. M. Fiore, Q. Li, H. Y. Liu, L. J. Mickley, and M. G. Schultz (2001), Global modeling of tropospheric chemistry with assimilated meteorology: Model description and evaluation, *J. Geophys. Res., 106*(D19), 23,073–23,095.

Byun, D. W., and K. L. Schere (2006), Review of the governing equations, computational algorithms, and other components of the Models-3 Community Multiscale Air Quality (CMAQ) modeling system, *Appl. Mech. Rev*., *59*, 51-77.

Carter, W. P. L. (1994), Development of ozone reactivity scales for volatile organic compounds, *J. Air Waste Manage. Assoc., 44*, 881– 899.

Carter, W. P. L. (2000), *Documentation of the SAPRC-99 Chemical Mechanism for VOC Reactivity Assessment*, No. 92 – 329, 95 – 308, Final Report to California Air Resources Board, Calif. Air Resour. Board, Riverside Calif. (Available at http://www.engr.ucr.edu/~carter/absts.htm#saprc99)

Chen, J., J. Vaughan, J. Avise, S. O'Neill, and B. Lamb (2008), Enhancement and evaluation of the AIRPACT ozone and $PM_{2.5}$ forecast system for the Pacific Northwest, *J. Geophys. Res., 113*, D14305, doi:10.1029/2007JD009554.

Daum, P. H., L. I. Kleinman, L. Newman, W. T. Luke, J. Weinstein-Lloyd, C. M. Berkowitz, and K. M. Busness (1996), Chemical and physical properties of plumes of anthropogenic pollutants transported over the North Atlantic during the North Atlantic Regional Experiment, *J. Geophys. Res., 101*(D22), 29,029–29,042.

de Gouw, J. A., et al. (2005), Budget of organic carbon in a polluted atmosphere: Results from the New England Air Quality Study in 2002, *J. Geophys. Res., 110*, D16305, doi:10.1029/2004JD005623.

Elleman (2007), Aerosol Size Distribution Modeling for the Pacific Northwest, Ph.D. dissertation, University of Washington, Seattle, Washington.

Elleman, R. A., and D. S. Covert (2008), Aerosol size distribution modeling with the Community Multiscale Air Quality modeling system (CMAQ) in the Pacific Northwest: 1. Model comparison to observations, *J. Geophys. Res*., submitted.

Goldan, P. D., M. Trainer, W. C. Kuster, D. D. Parrish, J. Carpenter, J. M. Roberts, J. E. Lee, and F. C. Fehsenfeld (1995), Measurements of hydrocarbons, oxygenated hydrocarbons, carbon monoxide, and nitrogen oxides in an urban basin in Colorado: Implications for emission inventories, *J. Geophys. Res., 100*, 22,771– 22,784.

Goldan, P. D., D. D. Parrish, W. C. Kuster, M. Trainer, S. A. McKeen, J. Holloway, B. T. Jobson, D. T. Sueper, and F. C. Fehsenfeld (2000), Airborne measurements of isoprene, CO, and anthropogenic hydrocarbons and their implications, *J. Geophys. Res., 105*(D7), 9091–9105.

Harley, R. A. and G. R. Cass (1995), Modeling the atmospheric concentrations of individual volatile organic compounds, *Atmos. Environ., 29*, 905-922.

Harley, R. A., R. F. Sawyer, and J. B. Milford (1997), Updated photochemical modeling for California's South Coast air basin: Comparison of chemical mechanisms and motor vehicle emission inventories, *Environ. Sci. Technol., 31*, 2829– 2839.

Hong, S.-Y., and H. L. Pan (1996), Nonlocal boundary layer vertical diffusions in a medium-range forecast model. *Mon. Wea. Rev., 124*, 2322-2339.

Jacobson, M. Z., R. Lu, R. P. Turco, O. B. Toon (1996), Development and application of a new air pollution modeling system-part I: Gas-phase simulations, *Atmos. Environ., 30*, 1939-1963.

Jobson, T., and coauthors (2002), Airborne measurements of hydrocarbons and aerosols in the Puget Sound airshed, *Eos Trans. AGU, 83*(47), Fall Meet. Suppl., Abstract A71A-0062.

Kain, J. S., and J. M. Fritsch (1990), A one-dimensional entraining/detraining plume model and its application in convective parameterization. *J. Atmos. Sci., 47*, 2784-2802.

Kleinman, L. I., P. H. Daum, J. H. Lee, Y.-N. Lee, L. J. Nunnermacker, S. R. Springston, L. Newman, J. Weinstein-Lloyd, and S. Sillman (1997), Dependence of ozone production on NO and hydrocarbons in the troposphere, *Geophys Res. Lett., 24*, 2299– 2302.

Kleinman, L. I. (2005), The dependence of tropospheric ozone production rate on ozone precursors, *Atmos. Environ., 39*, 575–586.

Kleinman, L. I., P. H. Daum, Y.-N. Lee, L. J. Nunnermacker, S. R. Springston, J. Weinstein-Lloyd, and J. Rudolph (2005), A comparative study of ozone production in five U.S. metropolitan areas, *J. Geophys. Res., 110*, D02301, doi:10.1029/2004JD005096.

Lee, Y.-N., X. Zhou, W. R. Leaitch, and C. M. Banic (1996), An aircraft measurement technique for formaldehyde and soluble carbonyl compounds, *J. Geophys. Res., 101*(D22), 29,075–29,080.

Lippmann, M. (1993), Health effects of tropospheric ozone: review of recent research findings and their implications to ambient air quality standards, *J. Expo. Anal. Environ. Epidemiol., 3*, 103-129.

McKeen, S. A., and S. C. Liu (1993), Hydrocarbon ratios and photochemical history of air masses, *Geophys. Res. Lett., 20*, 2363– 2366.

McKeen, S. A., S. C. Liu, E.-Y. Hsie, X. Lin, J. D. Bradshaw, S. Smyth, G. L. Gregory, and D. R. Blake (1996), Hydrocarbon ratios during PEM-WEST A: A model perspective, *J. Geophys. Res., 101*(D1), 2087–2109.

Milford, J. B., D. Gao, S. Sillman, P. Blossey, and A. G. Russell (1994), Total reactive nitrogen ($NO_y$) as an indicator of the sensitivity of ozone to reductions in hydrocarbon and $NO_x$ emissions, *J. Geophys. Res., 99*(D2), 3533–3542.

National Research Council (1991), *Rethinking the Ozone Problem in Urban and Regional Air Pollution*. National Academy Press, Washington, District of Columbia.

O'Neill, S. M., and B. K. Lamb (2005), Intercomparison of the community multiscale air quality model and calgrid using process analysis, *Environ. Sci. Technol., 39*(15), 5742–5753.

O'Neill, S. M., et al. (2006), Modeling ozone and aerosol formation and transport in the Pacific Northwest with the Community Multi-Scale Air Quality (CMAQ) modeling system, *Environ. Sci. Technol., 40*, 1286–1299.

Parrish, D. D., M. Trainer, M. P. Buhr, B. A. Watkins, and F. C. Fehsenfeld (1991), Carbon monoxide concentrations and their relation to concentrations of total reactive oxidized nitrogen at two rural U.S. sites, *J. Geophys. Res., 96*(D5), 9309–9320.

Parrish, D. D., M. Trainer, D. Hereid, E. J. Williams, K. J. Olszyna, R. A. Harley, J. F. Meagher, and F. C. Fehsenfeld (2002), Decadal change in carbon monoxide to nitrogen oxide ratio in U.S. vehicular emissions, *J. Geophys. Res., 107*(D12), 4140, doi:10.1029/2001JD000720.

Parrish, D. D. (2006), Critical evaluation of US on-road vehicle emission inventories,

*Atmos. Environ., 40*, 2288–2300.

Seaman, N. L, D. R. Stauffer, and A. M. Lario-Gibbs (1995), A multiscale four-dimensional data assimilation system applied in the San Joaquin Valley during SARMAP. Part I: modeling design and basic performance characteristics, *J. Appl. Meteor., 34*, 1739-1761.

Sillman, S. (1995), The use of $NO_y$, $H_2O_2$, and $HNO_3$ as indicators for $O_3$-$NO_x$-hydrocarbon sensitivity in urban locations, J. *Geophys. Res., 100*, 14,175–14,188, 1995.

Sillman, S., et al. (1995), Photochemistry of ozone formation in Atlanta, GA: Models and measurements, *Atmos. Environ., 29*, 3055–3066.

Sillman, S., D. He, C. Cardelino, and R. E. Imhoff (1997), The use of photochemical indicators to evaluate ozone-$NO_x$-hydrocarbon sensitivity: Case studies from Atlanta, New York and Los Angeles, *J. Air Waste Manage.* Assoc., *47*, 642– 652.

Sillman, S., D. He, M. R. Pippin, P. H. Daum, D. G. Imre, L. I. Kleinman, J. H. Lee, and J. Weinstein-Lloyd (1998), Model correlations for ozone, reactive nitrogen, and peroxides for Nashville in comparison with measurements: Implications for $O_3$-$NO_x$-hydrocarbon sensitivity, *J. Geophys. Res., 103*, 22,629– 22,644.

Sillman, S. (1999), The relation between ozone, $NO_x$ and hydrocarbons in urban and polluted rural environments, *Millenial Rev. Ser., Atmos. Environ., 33*, 1821–1845.

Sillman, S., and D. He (2002), Some theoretical results concerning $O_3$-$NO_x$-VOC chemistry and $NO_x$-VOC indicators, *J. Geophys. Res., 107*(D22), 4659, doi:10.1029/2001JD001123.

Sillman, S., R. Vautard, L. Menut, and D. Kley (2003), $O_3$-$NO_x$-VOC sensitivity and $NO_x$-VOC indicators in Paris: Results from models and atmospheric pollution over the Paris area (ESQUIF) measurements, *J. Geophys. Res., 108*(D17), 8563, doi:10.1029/2002JD001561.

Smyth, S. C., W. M. Jiang, D. Z. Yin, H. Roth, and T. Giroux (2006), Evaluation of CMAQ $O_3$ and $PM_{2.5}$ performance using Pacific 2001 measurement data, *Atmos. Environ., 40*, 2735–2749.

Steiner, A. L., R. C. Cohen, R. A. Harley, S. Tonse, D. B. Millet, G. W. Schade, and A. H. Goldstein (2008), VOC reactivity in central California: comparing an air quality model to ground-based measurements, *Atmos. Chem. Phys., 8*, 351-368,

Tonnesen, G. S., and R. L. Dennis (2000a), Analysis of radical propagation efficiency to assess ozone sensitivity to hydrocarbons and $NO_x$, 1, Local indicators of instantaneous odd oxygen production sensitivity, *J. Geophys. Res., 105*, 9213– 9226.

Tonnesen, G. S., and R. L. Dennis (2000b), Analysis of radical propagation efficiency to assess ozone sensitivity to hydrocarbons and $NO_x$, 2, Longlived species as indicators of ozone concentration sensitivity, *J. Geophys. Res.*, *105*, 9227– 9242.

Watkins, B. A., D. D. Parrish, M. Trainer, R. B. Norton, J. E. Yee, F. C. Fehsenfeld, and B. G. Heikes (1995), Factors influencing the concentration of gas phase hydrogen peroxide during the summer at Niwot Ridge, Colorado, *J. Geophys. Res., 100*(D11), 22,831–22,840.

Warneke, C., et al. (2007), Determination of urban volatile organic compound emission ratios and comparison with an emissions database, *J. Geophys. Res., 112*, D10S47, doi:10.1029/2006JD007930.

Zweidinger, R. B., J. E. Sigsby, S. B. Tejada, F. D. Stump, D. L. Dropkin, and W. D. Ray (1988), Detailed hydrocarbon and aldehyde mobile source emissions from roadway studies, *Environ. Sci. Technol., 22*, 956-962.

U.S. EPA (2003), User's guide to MOBILE6.1 and MOBILE6.2 (Mobile source emission factor model), in *Rep. EPA420-R-03-010*, Off. of Transp. and Air Qual., Ann Arbor, Mich. (Available at http://www.epa.gov/otaq/m6.htm)

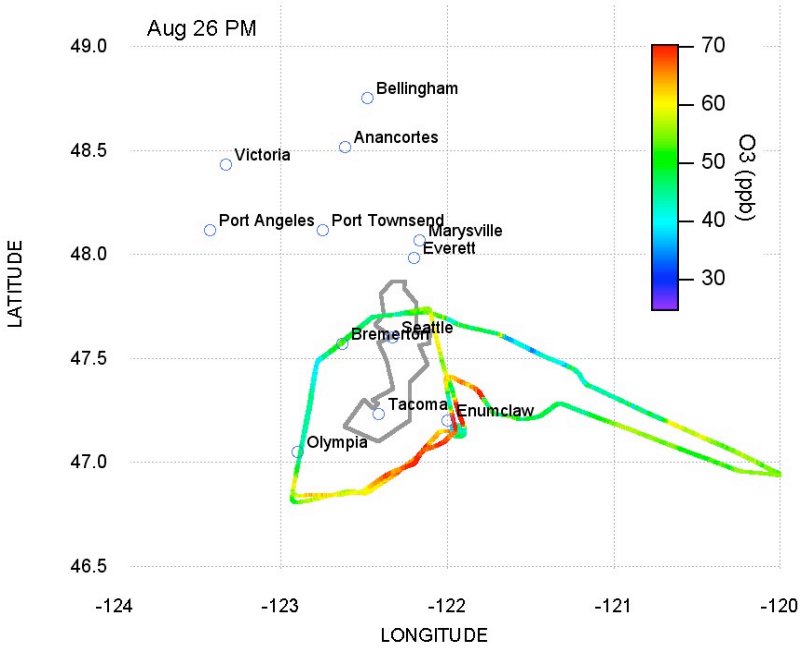
Aug 26 PM
Bellingham
Anancortes
Victoria
Port Angeles
Port Townsend
Marysville
Everett
Seattle
Bremerton
Tacoma
Enumclaw
Olympia
O3 (ppb)
70
60
50
40
30
LATITUDE
LONGITUDE
49.0
48.5
48.0
47.5
47.0
46.5
-124
-123
-122
-121
-120

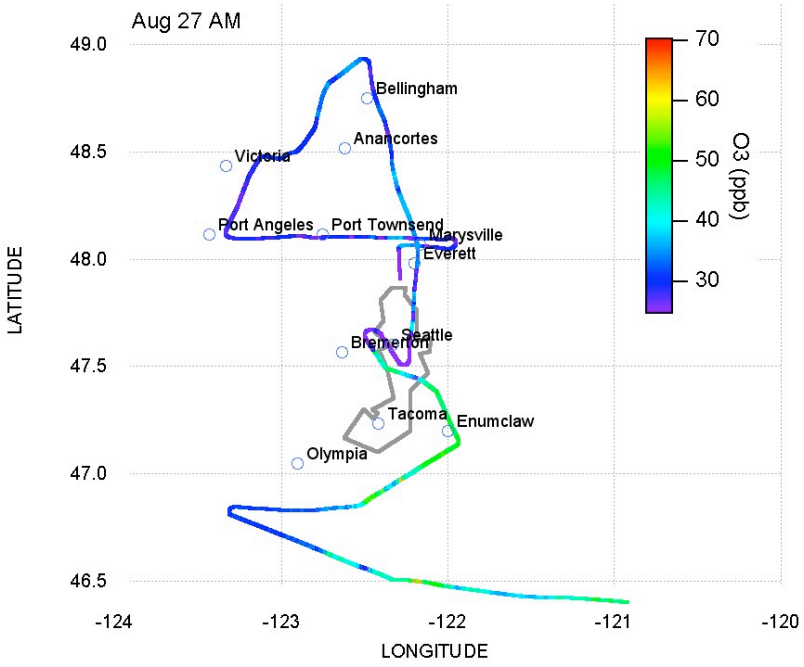
Aug 27 AM
Bellingham
Anancortes
Victoria
Port Angeles
Port Townsend
Marysville
Everett
Seattle
Bremerton
Tacoma
Enumclaw
Olympia
O3 (ppb)
70
60
50
40
30
LATITUDE
LONGITUDE
49.0
48.5
48.0
47.5
47.0
46.5
-124
-123
-122
-121
-120

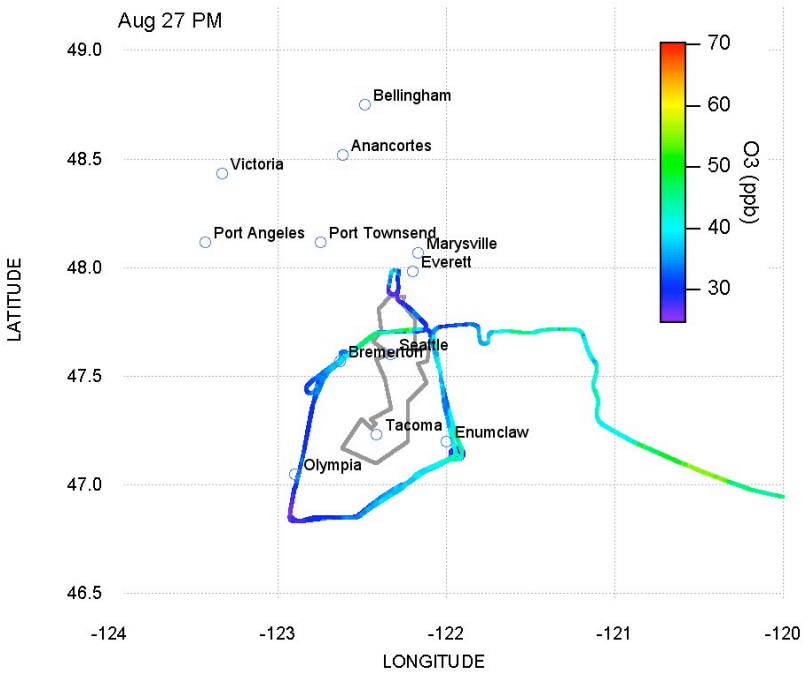


Figure 1. Flight tracks for Aug 26 PM, Aug 27 AM, and Aug 27 PM. Measured $O_3$ concentrations are indicated by the color-coding on the tracks.

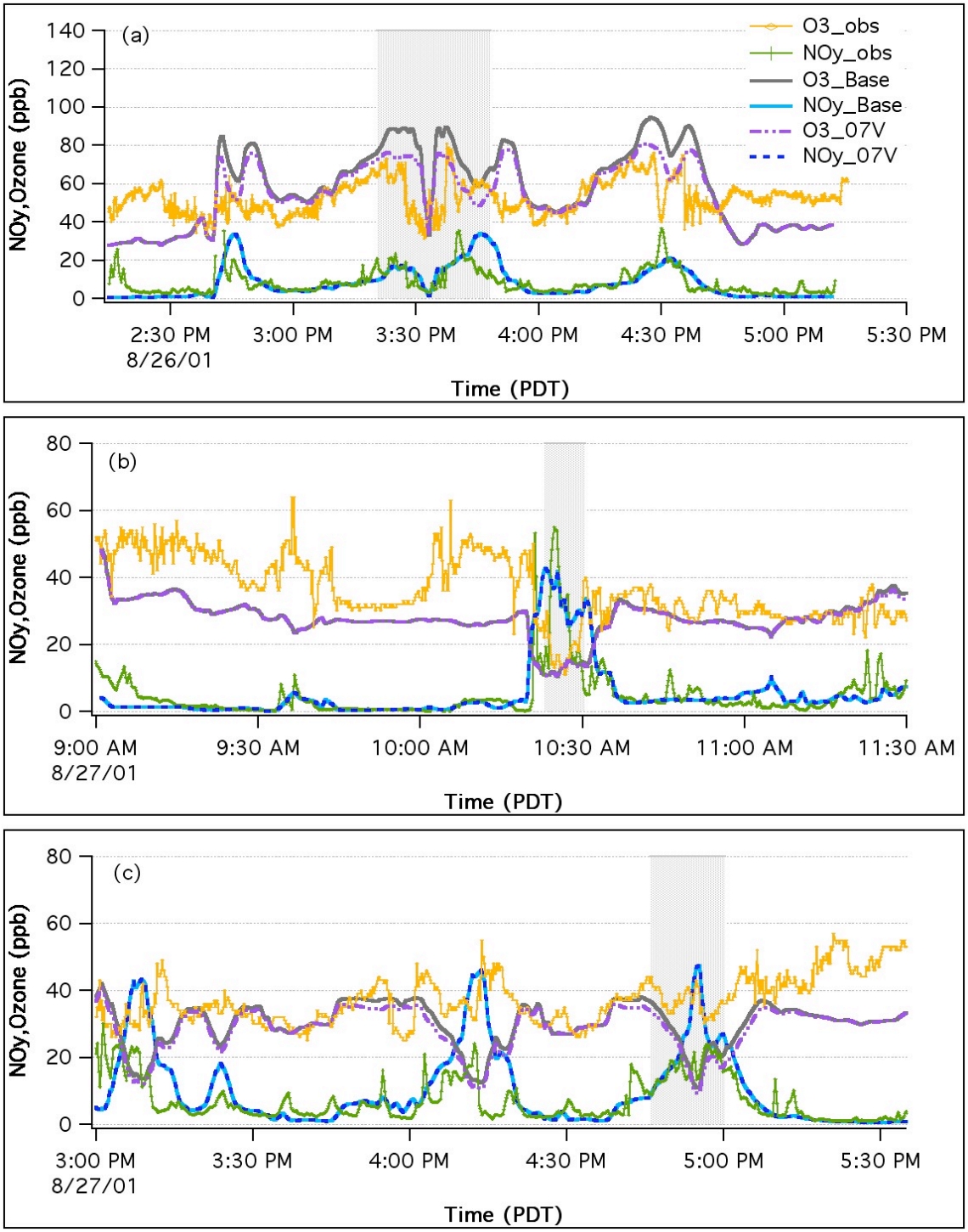


Figure 2. Modeled $O_3$ and $NO_y$ levels compared with observed values for the three flights on: a) Aug 26 PM (Sunday), b) Aug 27 AM (Monday), and c) Aug 27 PM (Monday). Note that "_Base" refers the standard scenario, and "_07V" refers to the reduced VOC scenario.

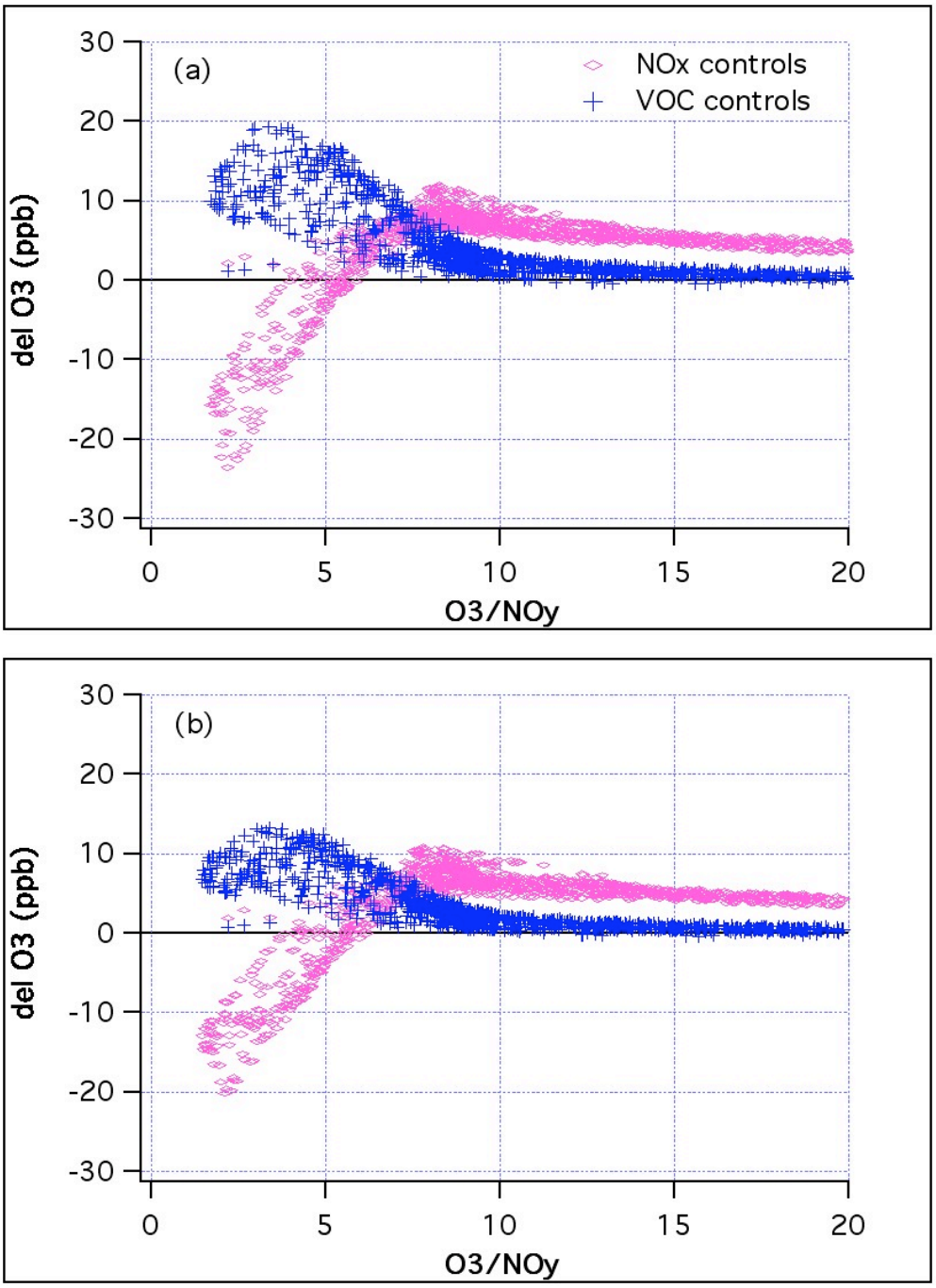


Figure 3. $O_3$ reductions due to a 30% anthropogenic VOC or $NO_x$ emission controls plotted as a function of $O_3/NO_y$ at 16 PDT on 26 August within a Seattle subdomain for a) the standard scenario, and b) the reduced VOC scenario.

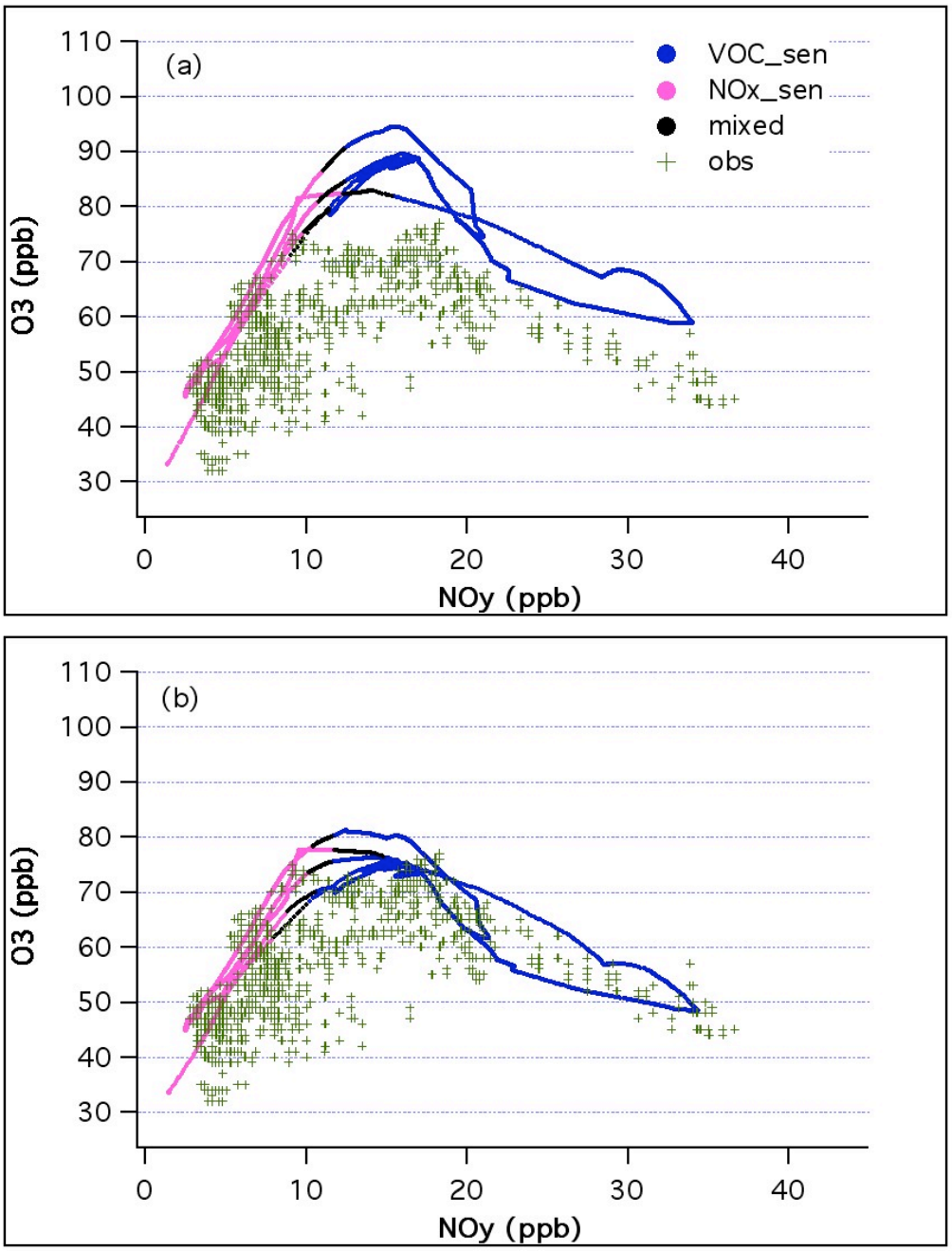


Figure 4. Modeled $O_3$ versus $NO_y$ compared with measured values for the afternoon flight on 26 August for: a) the standard scenario, and b) the reduced VOC scenario. Model grids are marked as VOC-sensitive, $NO_x$-sensitive, or mixed sensitivity based on their response to emission controls.

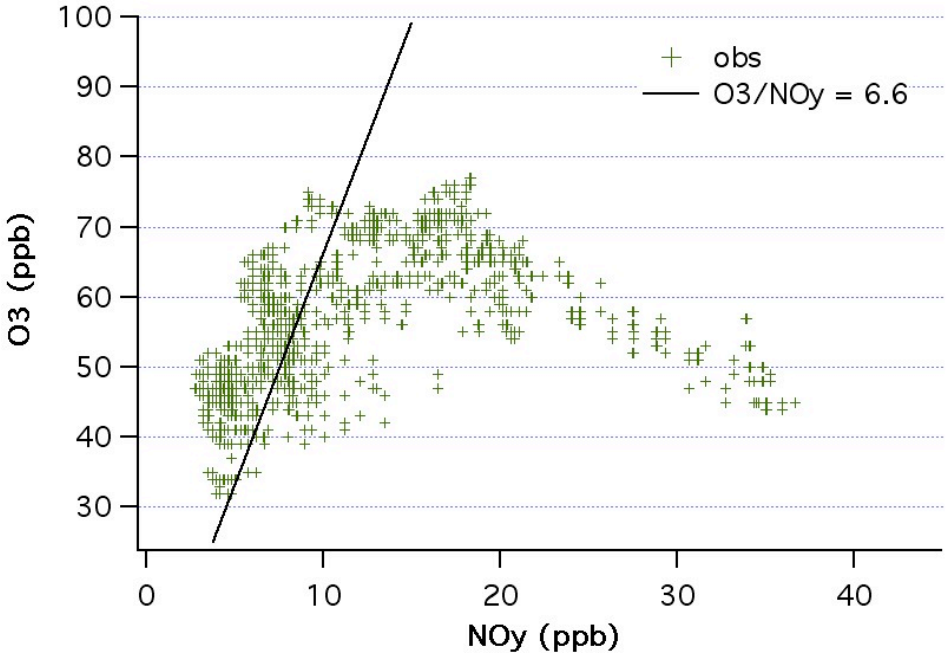


Figure 5. Measured $O_3$ versus $NO_y$ in the afternoon flight of 26 August. The line corresponds to $O_3/NO_y$ ratio of 6.6.

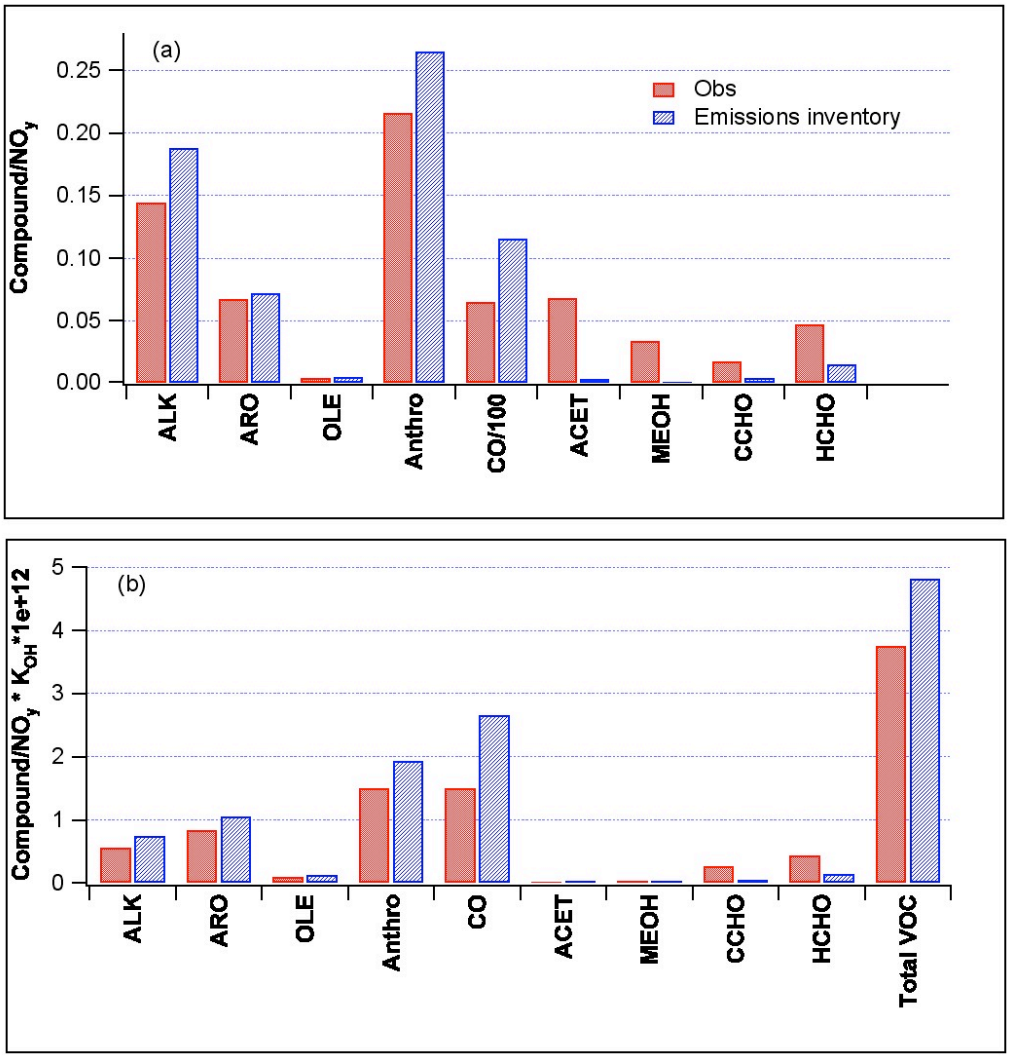


Figure 6. Comparisons of ratios of CO and VOC with respect to $NO_y$ from the morning urban profile on 27 August with those with respect to $NO_x$ from the emission inventory for: a) CO and VOC versus $NO_y$ ($NO_x$) ratios, and b) reactivity-weighted CO and VOC versus $NO_y$ ($NO_x$) ratios.

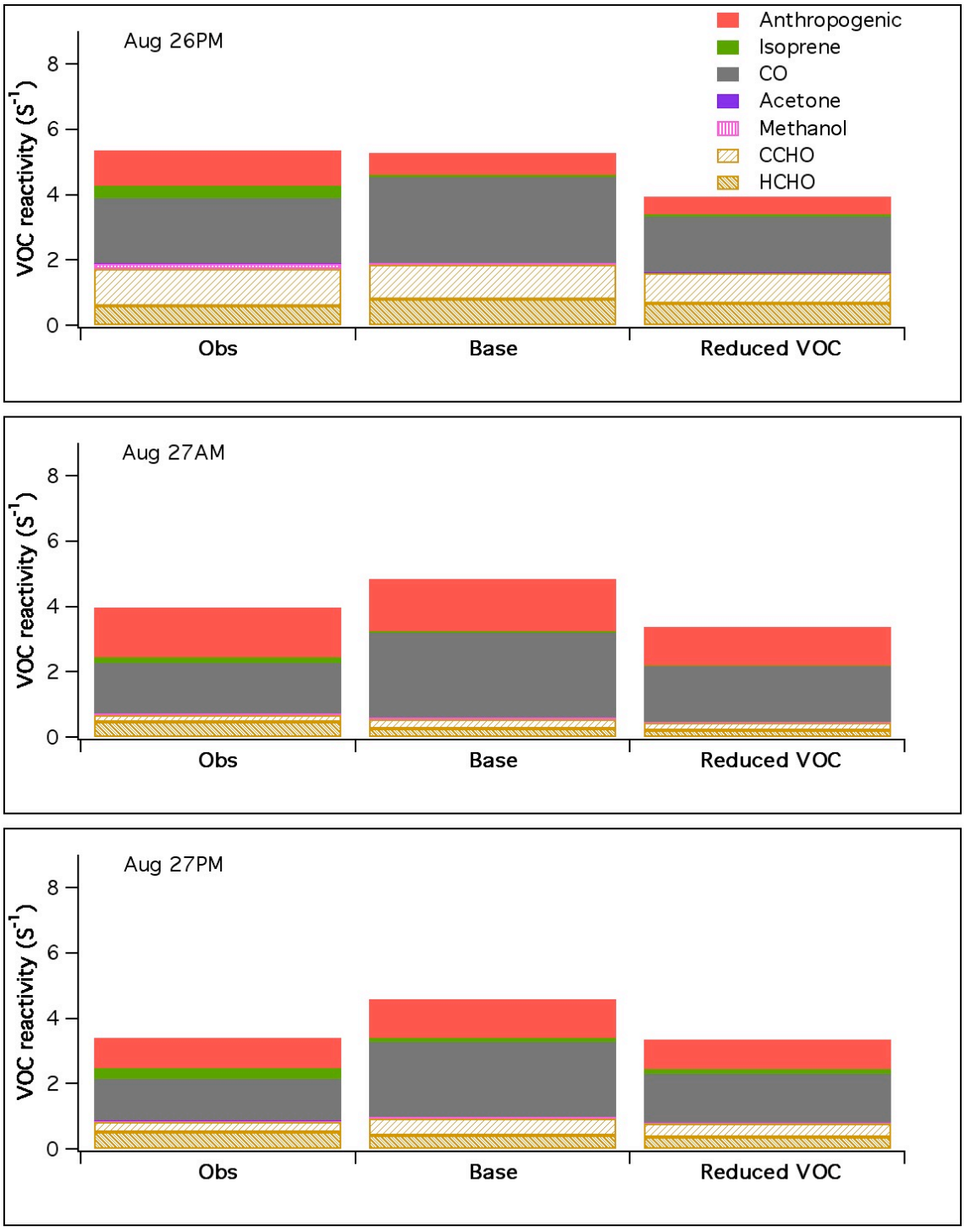


Figure 7. Components of the total VOC reactivity from measurements and from the standard and reduced VOC scenarios for Aug 26 PM, Aug 27 AM, and Aug 27 PM.

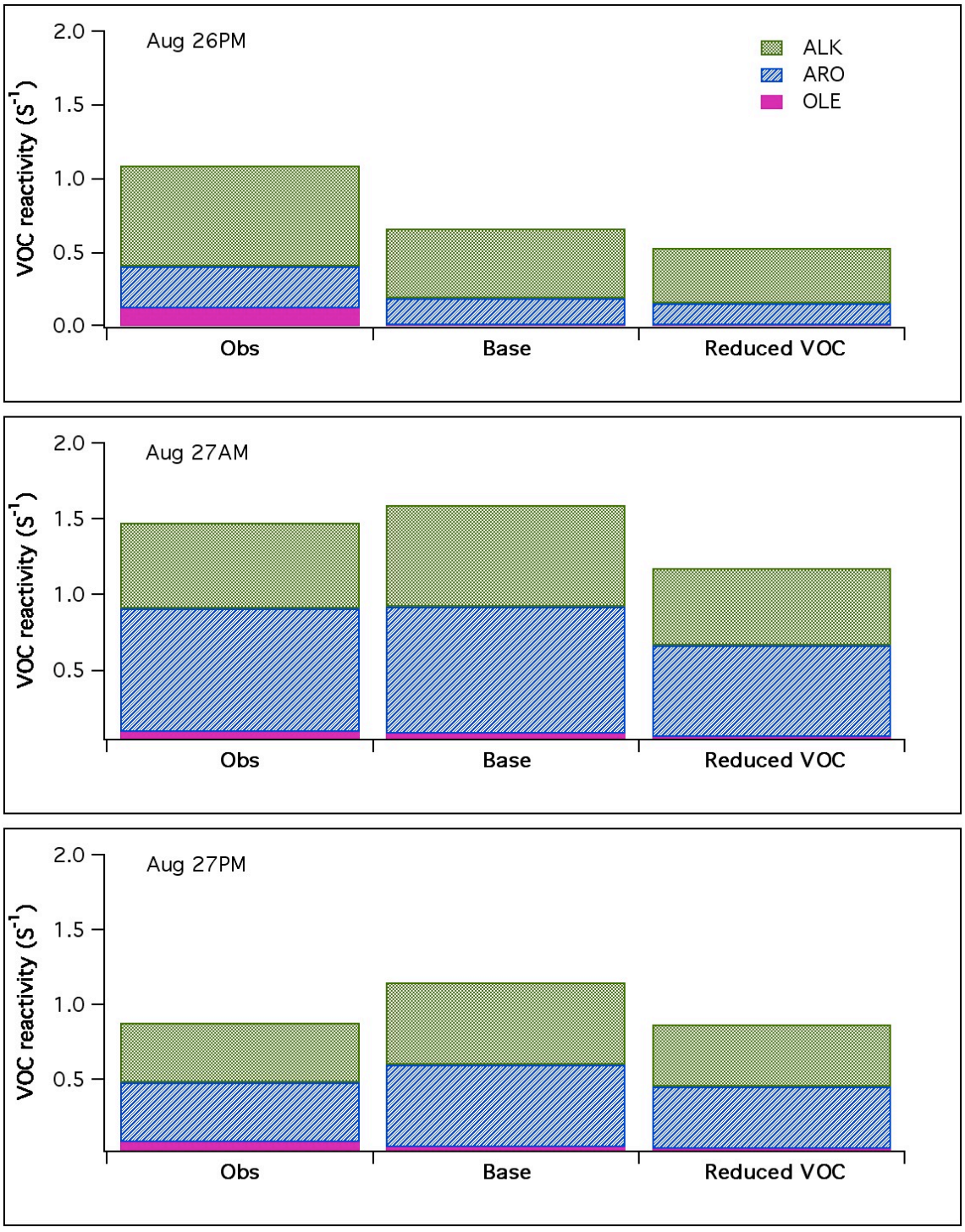


Figure 8. Components of anthropogenic VOC reactivity from measurements and from the standard and reduced VOC scenarios for Aug 26 PM, Aug 27 AM, and Aug 27 PM.

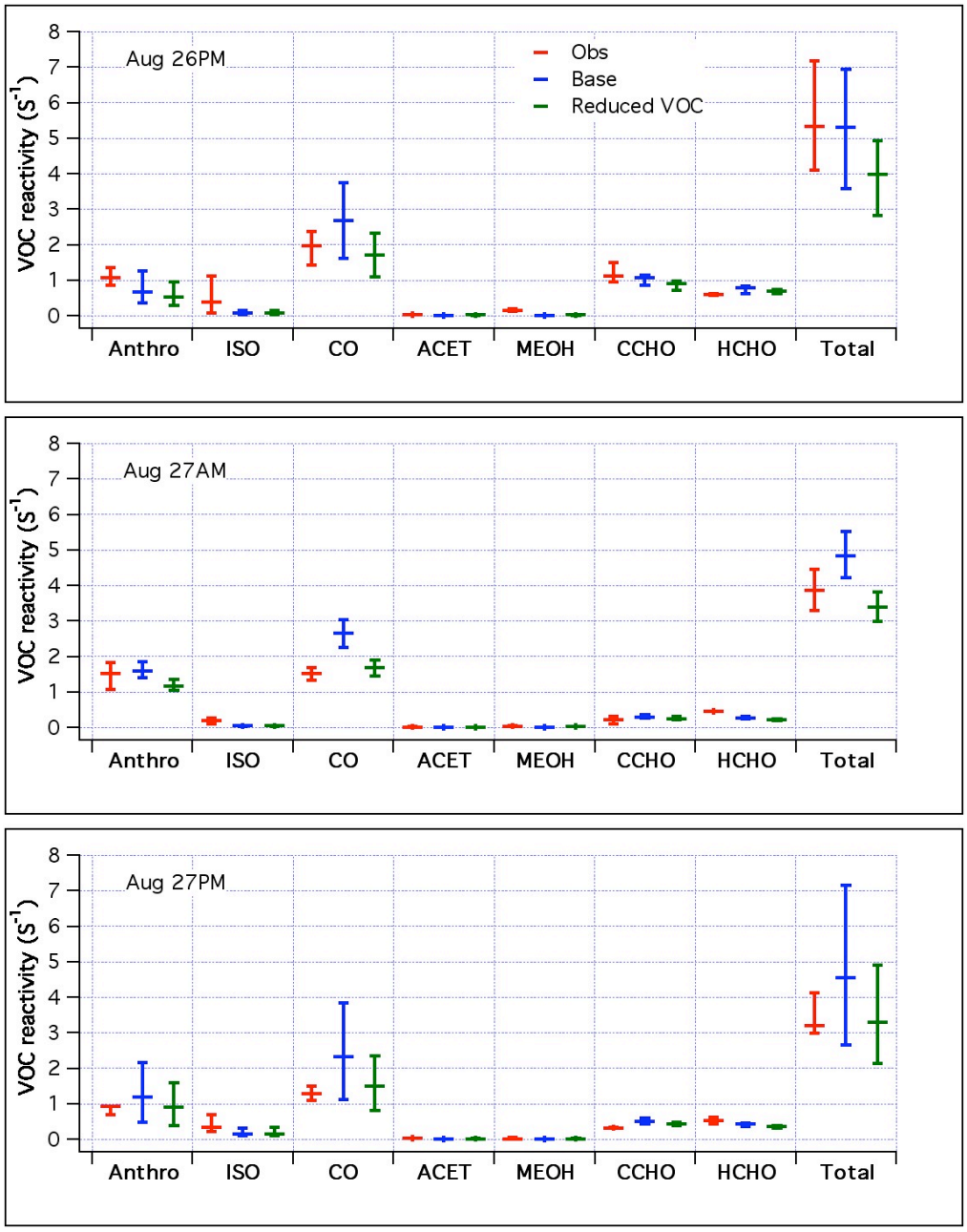


Figure 9. Components of the total VOC reactivity from measurements and from the standard and reduced VOC scenarios for Aug 26 PM, Aug 27 AM, and Aug 27 PM. The top and bottom bars represent the maximum and minimum values, and the center bar represents the median values.

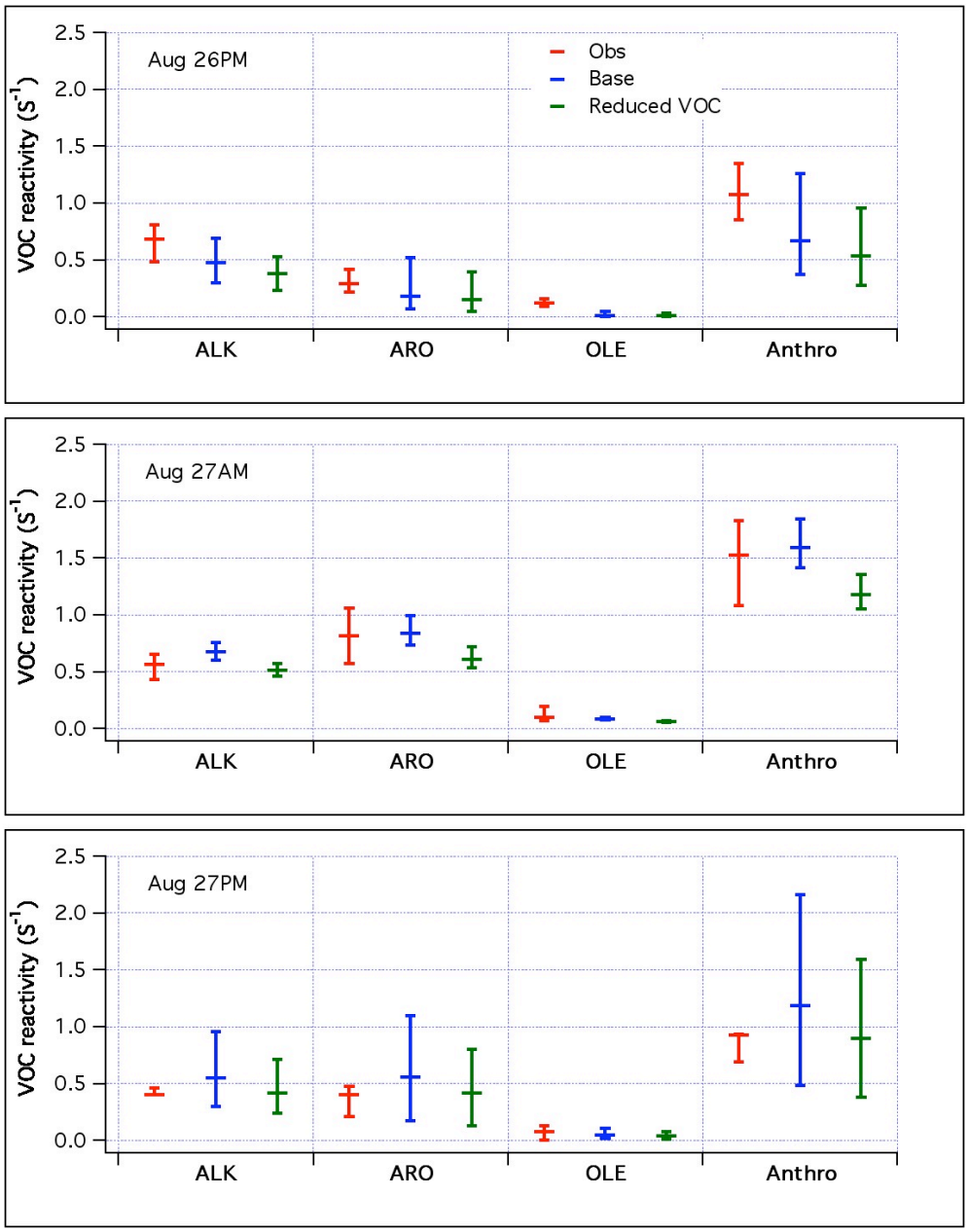


Figure 10. Components of the anthropogenic VOC reactivity from measurements and from the standard and reduced VOC scenarios for Aug 26 PM, Aug 27 AM, and Aug 27 PM. (The plot is in same style as Figure 9.)

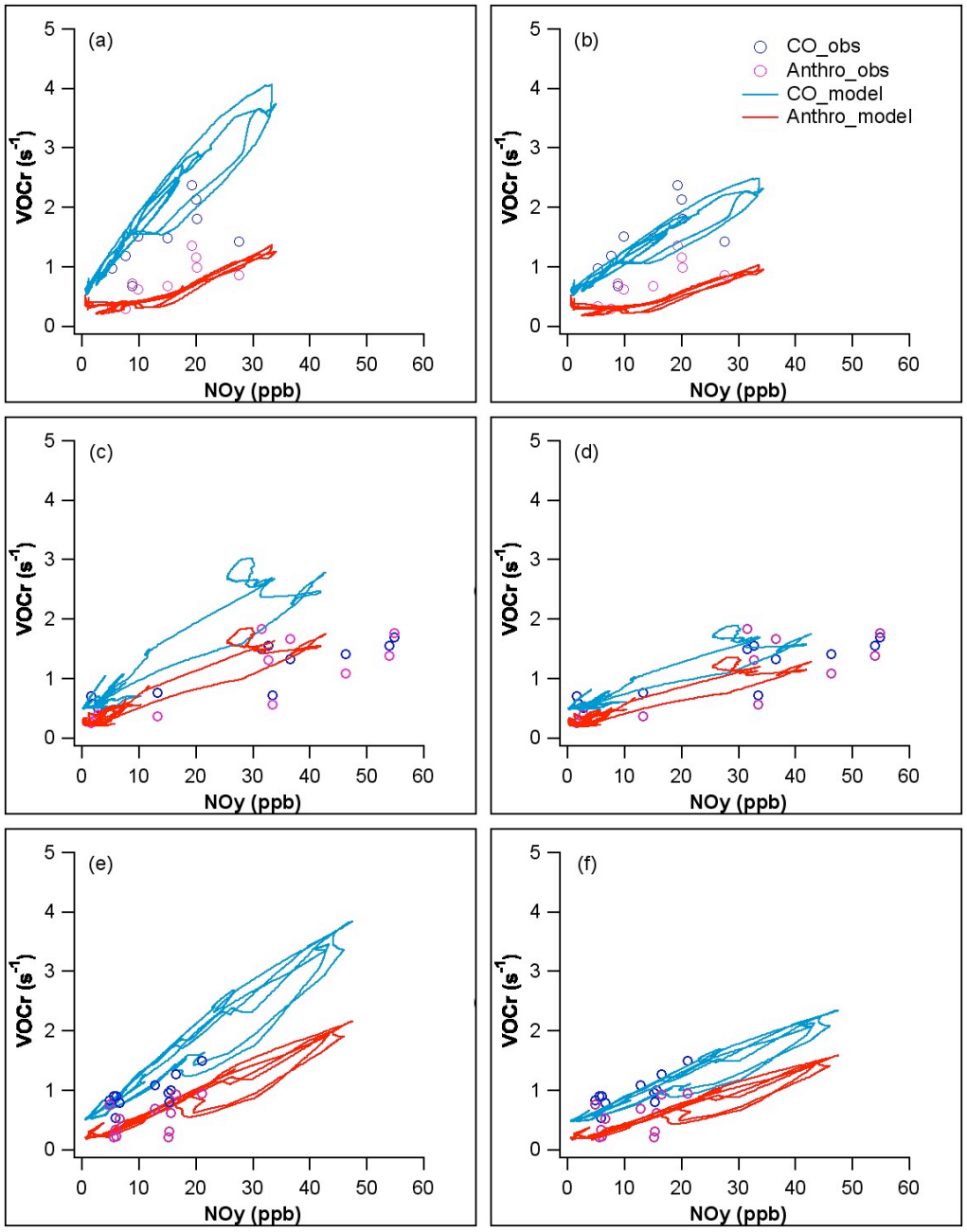


Figure 11. CO and anthropogenic VOC reactivity versus $NO_y$ from measurements and from the standard and reduced VOC scenarios for: a) standard scenario on Aug 26 PM, b) reduced VOC scenario on Aug 26 PM, c) standard scenario on Aug 27 AM, d) reduced VOC scenario on Aug 27 AM, e) standard scenario on Aug 27 PM, and f) reduced VOC scenario on Aug 27 PM.

Table 1. Summary of typical summer weekday emissions in the modeling domain.

| | Anthropogenic, Base (tons/day) | | Biogenic (tons/day) |
|---|---|---|---|
| ALK | 916 | ALK | 888 |
| ARO | 319 | OLE | 215 |
| OLE | 138 | Isoprene | 1235 |
| HCHO | 22 | Terpenes | 2451 |
| CCHO | 6 | NO | 41 |
| ACET | 9 | | |
| MEOH | 1 | | |
| VOC | 1559 | VOC | 4789 |
| $NO_x$ | 1336 | | |
| CO | 11390 | | |
| $SO_2$ | 553 | | |
| VOC/$NO_x$ | 1.2 | | |

Table 2. Mapping modeled and observed chemical compounds.

| Lumped species in SAPRC99 | Measured compounds in PNW2001 | % in SAPRC99 mixture | % measured in PNW2001 | Recalculated $k_{OH}$ ($cm^3$ $mole^{-1}$ $s^{-1}$) |
|---|---|---|---|---|
| ALK2 | propane | 59% | 59% | 1.15 |
| ALK3 | n-Butane | 68% | 98% | 2.39 |
| | Isobutane | 30% | | |
| ALK4 | Iso-Pentane | 45% | 91% | 4.46 |
| | n-Pentane | 18% | | |
| | 2-Methyl Pentane | 11% | | |
| | 3-Methylpentane | 8% | | |
| | Methylcyclopentane | 5% | | |
| | n-Hexane | 4% | | |
| ALK5 | 3-Methyl Hexane | 10% | 34% | 7.99 |
| | n-Heptane | 7% | | |
| | 2,3-Dimethyl Pentane | 6% | | |
| | Methylcyclohexane | 4% | | |
| | n-Octane | 4% | | |
| | 2-Methyl Hexane | 3% | | |
| ARO1 | Toluene | 70% | 87% | 5.71 |
| | Ethyl | 10% | | |
| | Benzene | 7% | | |
| ARO2 | m-Xylene | 22% | 87% | 25.88 |
| | o-Xylene | 20% | | |
| | p-Xylene | 22% | | |
| | 1,3,5-Trimethyl | 14% | | |
| | 1,2,4-Trimethyl | 9% | | |
| OLE1 | Propene | 29% | 29% | 26.3 |

Table 3. Summary of model-predicted $O_3$ and $NO_y$ levels compared with observed values for the three flights. Note that "Base" refers the standard scenario, and "07V" refers to the reduced VOC scenario.

| | Aug 26 PM (Sunday) | Aug 27 AM (Monday) | Aug 27 PM (Monday) |
|---|---|---|---|
| $O_3$ (Obs) | Peak: ~80 ppb (south and southeast of Seattle)<br>Background: ~40 ppb | Residue layer: 30-50 ppb<br>Touch-and-go profile: below 20 ppb | Peak: 40-50 ppb<br>Background: ~30 ppb |
| $O_3$ (Base) | Over-predictions of the peak by ~20 ppb | Under-predictions in the residual layer | Under-predictions to the east of Seattle |
| $O_3$ (07V) | Better agreement with the observed peak than the base case | Same as the base case | Slightly lower than the base case |
| $NO_y$ (Obs) | Peak: ~40 ppb<br>Background: a few ppb | Touch-and-go profile: up to 55 ppb | Peak: ~20 ppb<br>Background: a few ppb |
| $NO_y$ (Base) | Good agreement with the observed values | Some under-predictions within the touch-and-go profile | Over-predictions to the east of Seattle |
| $NO_y$ (07V) | Same as the base case | Same as the base case | Same as the base case |

Table 4. Distributions of $O_3/NO_y$ values from the standard and the reduced VOC scenarios and from previous studies[a].

| Location | VOC-sensitive locations | | $NO_x$-sensitive locations | |
|---|---|---|---|---|
| | 50th percentile | 95th percentile | 5th percentile | 50th percentile |
| Seattle, standard | 4.7 | 7.0 | 7.9 | 11.7 |
| Seattle, reduced VOC | 4.3 | 6.6 | 7.7 | 11.7 |
| Nashville | 3.6 | 5.6 | 7.1 | 10.8 |
| Nashville,high dep. | 5.3 | 7.2 | 8.7 | 13.9 |
| Northeast Corridor | 5.4 | 6.5 | 8.2 | 12.7 |
| Lake Michigan | 5.2 | 6.6 | 7.2 | 11.7 |
| Atlanta | 5.1 | 7.2 | 8.1 | 14.3 |
| Los Angeles (Godowitch) | 3.2 | 6.0 | 7.2 | 10.4 |
| Los Angeles (Chock) | 5.4 | 9.1 | 5.9 | 18 |
| San Joaquin (Sillman) | 7.3 | 11.6 | 15 | 26 |
| San Joaquin (Chang) | 7.7 | 12.3 | 12.5 | 22 |

[a]$O_3/NO_y$ for previous studies are from *Sillman and He* [2002].

Table 5. Comparisons of CO and VOC versus $NO_y$ ratios from observations and those versus $NO_x$ ratios from the emission inventory.

| Compound/$NO_y$ ($NO_x$) | Obs | Emissions inventory | Reactivity-weighted compound/$NO_y$ ($NO_x$) | Obs | Emissions inventory |
|---|---|---|---|---|---|
| ALK | 0.144 | 0.188 | ALK | 0.562 | 0.750 |
| ARO | 0.067 | 0.072 | ARO | 0.834 | 1.062 |
| OLE | 0.004 | 0.005 | OLE | 0.100 | 0.128 |
| Anthropogenic | 0.216 | 0.265 | Anthropogenic | 1.497 | 1.940 |
| CO | 6.49 | 11.58 | CO | 1.494 | 2.664 |
| ACET | 0.068 | 0.003 | ACET | 0.015 | 0.001 |
| MEOH | 0.034 | 0.001 | MEOH | 0.033 | 0.001 |
| CCHO | 0.017 | 0.004 | CCHO | 0.269 | 0.060 |
| HCHO | 0.047 | 0.015 | HCHO | 0.441 | 0.143 |
| | | | Total VOC | 3.75 | 4.81 |

# CHAPTER FOUR

## Investigating the impact of high resolution meteorological input and emissions on modeling ozone in the Pacific Northwest

Ying Xie and Brian Lamb
*Washington State University, Department of Civil and Environmental Research*

## Abstract

Air quality in the Pacific Northwest is strongly influenced by complex terrain and unique meteorological conditions within and near the Columbia River Gorge and the Cascade Mountain range. Topographical features interact closely with the regional flow, and therefore have an important impact on the transport of pollutants. In addition, there is significant spatial variability in urban emissions within the metropolitan areas. In this study, we used the MM5/SMOKE/CMAQ modeling system for nested 4 km and 1 km domains encompassing the Portland, OR metropolitan area and the Columbia River Gorge for an ozone episode that occurred during July, 1998, to investigate the effects of using high resolution meteorological and emissions inputs to a photochemical modeling simulation of $O_3$ for the region. We first evaluated meteorological model performance, and found that finer grid resolution generally results in improved model predictions, especially for wind direction and wind speed. We then compared the effects of high resolution meteorological input with those of high resolution emissions by running CMAQ at 4 km and 1 km for three scenarios: 1) with both MM5 meteorology and emissions at 4 km grid cells; 2) with 1 km MM5 meteorology, but 4 km emissions; and 3) with both MM5 meteorology and emissions at 1 km. Results showed that using high resolution meteorological input alone had a larger impact on the position and peak levels of the $O_3$ plume. $O_3$ concentrations were higher in the 1 km case compared to the 4 km case in areas along the Columbia River Gorge and the foothills of the Cascade mountain range where the terrain effects are substantial. Using high resolution emissions tended to affect small-scale features in $O_3$ concentration patterns mainly within the urban area. Areas with either $O_3$ increases or decreases occurred which were missing when using

coarse resolution emissions. Model evaluations for $O_3$ using measurements from available monitoring sites showed little difference in performance for the various cases, partly due to the sparse measurement network in the region.

## 1. Introduction

The Cascadia region of the Pacific Northwest periodically experiences elevated $O_3$ levels downwind of major urban areas. Air quality in the region is strongly influenced by complex terrain and unique meteorological conditions within and near the Columbia River Gorge and the Cascade Mountain range, and therefore model simulations are often difficult. A number of meteorological modeling studies have found that increasing grid resolution is beneficial for improving model results in regions strongly influenced by orographic flows or diurnal circulations. *Mcqueen et al.* [1995] found that a horizontal grid size of 2.5 km and a first vertical layer at 12 m produced the best agreement with the observations compared to using coarse grids in the Regional Atmospheric Modeling System (RAMS). *Colle and Mass* [2000] showed improved realism by decreasing the horizontal grid spacing from 12 to 1.33 km and increasing the number of vertical layers when simulating the gap flow through the Strait of Juan de Fuca with Mesoscale Meteorological model Version 5 [MM5, *Grell et al.*, 1994]. The Columbia River Gorge is the only near sea-level passage in the Cascades Mountains in Washington and Oregon, and *Sharp and Mass* [2002] found that a horizontal grid size of 1.33 km or less in the MM5 model is required to resolve the Columbia River Gorge and to predict realistic flow patterns during winter storm conditions. The general findings in those regions are that local scale forcing interacts closely with the regional flow, so that the accuracy of simulation relies directly upon resolving the topographical features.

The demand for high resolution modeling also comes from the need for resolving small scale variability in precursor emissions. It is well known that $O_3$ chemistry is highly nonlinear with complex photochemical reactions involving VOC and $NO_x$

precursors, and the sensitivity of air quality modeling to grid size has attracted the attention of a number of researchers. *Chang et al.* [1993] found more spatial features for $O_3$ and its precursors, but similar $O_3$ peaks using the SARMAP model at 12 and 4 km in California. *Gillani and Pleim* [1996] discussed the uncertainties related to anthropogenic emissions and pointed out that there is a subgrid scale uncertainty due to the nonlinear chemistry of $NO_x$ and odd hydrogen radicals. They demonstrated that urban emissions and VOC/$NO_x$ ratios are highly spatially variable, and large point source emissions are often $NO_x$-rich and very diffusion-limited. However, in grid models the emissions are dispersed into the grid volume instantaneously, and therefore, the results are often shifted to a different chemical regime from reality. They found that for urban emissions, there is progressive improvement in the resolution of VOC/$NO_x$ ratio as grid spacing is decreased below 20 km, and suggested using fine nested grids (~1-4 km) in metropolitan sub-domains and the plume-in-grid method for large point sources. *Jang et al.* [1995a and 1995b] used RADM with 80, 40, and 20 km resolution to study the effects of grid resolution on $O_3$ and its contributing processes using process analysis. They found over the same source area that the coarse grid tends to chemically produce more $O_3$ but less $NO_2$, while vertically exporting more $O_3$ and NO, but less $NO_2$. Therefore, the total amount of odd oxygen remained unaffected by the grid resolution. By demonstrating that grid resolution could significantly impact the competing rates for $NO_x$ emissions between chemistry and vertical transport, they concluded that vertical grid resolution is also important. *Ching et al.* [2006] studied subgrid scale variability using the CMAQ model at 36, 12, 4 and 1.33 km. They found more fine-scale features for $O_3$ and $NO_x$ with smaller grids, and different patterns when aggregating results from fine grids compared to

those from the native coarse grids. They also attempted to determine and parameterize the distribution of subgrid variability, but found these parameters tend to be highly variable. *Cohan et al.* [2006] studied the impact of grid resolution on ozone sensitivity using a direct sensitivity analysis with grid resolution of 36, 12, and 4 km. They found that results using a 12 km grid size were the same as for 4 km grids in terms of sensitivity response, except for local scale features.

Despite the need for high resolution modeling, weather forecasting and air quality simulations in the Pacific Northwest region have been and are routinely applied with grid sizes of 36, 12 and/or 4 km [*Mass et al.*, 2002; *Vaughan et al.*, 2004; *O'Neill et al.*, 2005; *Chen et al.*, 2008]. There have been only a few meteorological modeling studies conducted with horizontal grid sizes near or less than 1 km [*Colle and Mass*, 1998 and 2000; *Sharp and Mass*, 2002]; the effect of high model resolution on air quality simulations and $O_3$ predictions remains unknown. It is also not clear whether high resolution meteorological input or emissions will have a larger impact on air quality simulations if not applied simultaneously.

In this study, the MM5/SMOKE/CMAQ modeling system was used for nested 4 km and 1 km domains encompassing the Portland metropolitan area and the Columbia River Gorge for an ozone episode that occurred during July, 1998. The objectives are 1) to investigate the impact of high resolution meteorological and photochemical modeling on $O_3$ predictions for the region, and 2) to compare the relative effects of high resolution meteorological input versus high resolution emissions.

There are two key questions addressed in this work. First, given the complex terrain in the Pacific Northwest, does the use of high resolution 1 km MM5 simulations

improve air quality simulations for summertime $O_3$? Second, does the use of high resolution meteorological fields benefit from high resolution emission inventories for air quality simulations? Section 2 describes the methodology for meteorological and photochemical modeling. In section 3, we present the results starting with evaluation of meteorological model performance at different grid resolutions, followed by investigation of the effects of high resolution meteorological and photochemical modeling and comparing the relative effects on predicted $O_3$ spatial features. Finally, we evaluate model predictions at available $O_3$ monitoring sites and discuss the implications.

## 2. Methodology

### 2.1 Modeling domain and episode selection

MM5 was used to provide the 3-D meteorological field for air quality modeling. Four one-way nested domains with grid cell horizontal sizes of 36, 12, 4, and 1 km were applied. The 4 km domain covers a region encompassing the I-5 corridor of western Washington and Oregon and the innermost 1 km domain is focused upon the Portland metropolitan area and encompasses the Columbia River Gorge. For the 1 km domain, 297 x 193 grid cells were applied in the horizontal and 42 sigma layers were specified in the vertical. The 1 km emission and CMAQ domain was slightly windowed down from the 1 km MM5 domain with 280 x 176 grid cells in the horizontal. Vertically, 28 layers were applied with the first layer at 19 m and with 17 layers within 1500 m AGL.

The ozone episode from 27-28 July, 1998 was selected for the modeling study since it had the highest $O_3$ levels observed for the airshed in recent years. Multiple exceedances of both the 1-hr and 8-hr ozone standards were observed at various Oregon

and Washington monitoring sites, with 1-hr peaks close to 140 ppb. There were elevated temperatures over most of the period and light NW winds during the episode. As summarized by *Barna et al.* [2000], the typical synoptic conditions conducive to high $O_3$ concentrations in the region are characterized by the building of an upper-level ridge of high pressure over the west coast of North America and a thermal trough extending northward from California along the coast. This pattern was apparent in the surface weather map for 27 July, 1998 [*Lamb et al.*, 2006].

## 2.2 MM5

MM5 version 3.7 was used to develop the 3-D meteorology fields. NCEP ETA model analysis at 40 km grid was used to initialize the atmospheric condition and provide boundary conditions. Analysis nudging was applied in the 36 and 12 km domains and observational nudging was applied in the 4 km domain. For analysis nudging, 3D nudging was employed for winds, temperature, and moisture, with the boundary layer excluded for temperature and moisture. Surface nudging was applied for winds only. For observational nudging, wind speed and direction observations from available surface stations were used. 30-s the USGS global terrain and land use database was applied to resolve the terrain features and surface categories for the 4 and 1 km domains.

The MM5 physics options applied in the run included the Kain-Fritsch 2 cumulus parameterization scheme [*Kain*, 2004], the MRF PBL scheme [*Hong and Pan*, 1996], Reinser 1 moisture [*Reisner et al.*, 1998], CCM2 radiation [*Hack et al.*, 1993], and Noah Land Surface Model [*Chen and Dudhia*, 2001]. A 5-day simulation starting at 0000 UTC July 25, 1998 was completed for the 36/12/4 km domains first, and then the output from the 4 km domain was used to initialize the 1 km run at 1200 UTC 27 July, 1998 and to

provide the boundary conditions. A 15 min output frequency was specified for the 4 km domain, and a 5 min output frequency was specified for the 1 km domain.

Output from MM5 was processed by the Meteorology-Chemistry Interface Processor (MCIP) version 3 to provide the correct input to CMAQ. During the MCIP run, all planetary boundary layer (PBL) parameters and radiation fields were passed through from MM5 without re-calculation.

## 2.3 Emissions

The Sparse Matrix Operator Kernel Emissions (SMOKE) processor version 2.0 (http://www.smoke-model.org/index.cfm) was used to process area, onroad mobile, non-road mobile, and point source emissions. Point sources and area sources were based on the EPA 1999 National Emission Inventory (NEI) without back-casting. Local emissions estimates were used to update the 1999 NEI where appropriate. Non-road mobile sources such as lawn and garden and commercial construction equipment were estimated for year 1998 using EPA NONROAD model [*US. EPA*, 2005]. For non-road mobile sources that were not included in the NONROAD model (ships, locomotives, and aircraft), 1999 NEI estimates were used. For on-road vehicles, EPA MOBILE-6 [*US. EPA*, 2003] was used to determine emission factors with changes due to area-dependent Reid Vapor Pressure (RVP) and Inspection and Maintenance (I/M) plan taken into account. The resulting emission factors were assigned on a county level, and then multiplied by the Average Daily Vehicle Miles Traveled (ADVMT) for year 1998. For British Columbia, Year 2000 emissions data provided by the Greater Vancouver Regional District and Environment Canada [*GVRD*, 2002] were used directly for all anthropogenic source categories.

Initial anthropogenic emissions in annual estimates were temporally allocated by hour according to temporal profiles consisted of month, day of week, and hour of day. Spatially, surrogates at 4 km resolution were used to allocate the emissions for the 4 km domain and some source categories in the 1 km domain when surrogates at finer resolution weren't available. Surrogates available at 1 km resolution included population, mileage on roadways, major airport, livestock, and Oregon dry cleaners. Based on source category and pollutants type, the SAPRC99 chemical mechanism [*Carter*, 2000] was used to speciate the emissions.

Biogenic emissions from trees, plants, and crops were processed by the Biogenic Emissions Inventory System (BEIS) version 3.12. The model estimates VOC emissions from vegetation based on land-use categories and nitric oxide emissions from microbial activity based on soil types. The 1-km Biogenic Emissions Landcover Database, version 3 (BELD3), was used to generate normalized emissions, which were then used along with meteorological data and speciation profiles to compute gridded and speciated hourly biogenic emissions.

## 2.4 CMAQ

The U.S. EPA Models-3 Community Multi-scale Air Quality (CMAQ) Modeling System [*Byun and Schere*, 2006] version 4.6 was used for photochemical air quality modeling. It incorporates the output fields from the MM5/MCIP meteorological simulations and emissions derived from SMOKE, and then simulates the chemical transport using the CMAQ Chemical Transport Model (CCTM).

The SAPRC99 photochemical mechanism including aqueous chemistry and aerosol dynamics was employed. The Euler Backward Interactive (EBI) solver was used

to solve the chemical kinetic equations. The global mass-conserving scheme (yamo) was used as the advection scheme. Multi-scale and eddy diffusion were used as horizontal and vertical diffusion algorithms, respectively. For the 4 km domain, CMAQ boundary conditions were extracted from the MOZART-2 global atmospheric chemistry-transport model by matching the CMAQ boundary with the MOZART cells. The July average MOZART-2 values were derived by averaging over ten years of July runs (1990-1999) based upon a long-term climate simulation conducted as part of a separate analysis of the impact of global change on regional air quality at WSU [*Avise et al*., 2008]. Since MOZART-2 and CMAQ use different vertical grid structures, MOZART and CMAQ output were first converted to equivalent pressure coordinates, and then MOZART mixing ratios were linearly interpolated to CMAQ vertical layers [*personal communication, Jeremy Avise*]. For the 1 km domain, output from the 4 km run was used for initial and boundary conditions. A 4-day simulation starting at 1200 UTC July 25, 1998 was completed for the 4 km domain first, and then the output was used as initial and boundary conditions for a 2-day 1 km simulation starting at 1200 UTC 27 July, 1998. During the 1 km run, the default maximum synchronization step was reduced from 720 s to 65 s.

The effects of high resolution meteorological input were compared with those of high resolution emissions by running the CMAQ model at 4 km and 1 km for three cases. The first case employed both MM5 and emissions at 4 km. The second case incorporated 1 km MM5, but 4 km emissions, with the native 4 km emissions evenly divided into 16 grid cells to be applied. In the third case, both MM5 and emissions at 1 km were

incorporated. The results from the two runs with 1 km MM5, but different emissions were compared with each other and with those from the 4 km run.

## 3. Results

### 3.1 Meteorology model performance

MM5 was evaluated for surface wind and temperature (see Table 1) for all available meteorological stations within the 1 km modeling domain. The overall results show that mean absolute error (MAE) were about 3°C for 2 m temperatures, and 1 m/s and 55° for wind speed and wind direction. The performance is generally comparable to the real-time forecasting run operated at the University of Washington (http://www.atmos.washington.edu/~qcreport/verification_index.psp) and other air quality simulations in the Pacific Northwest [*Barna and Lamb*, 2000; *O'Neill and Lamb*, 2005].

Within various parameters, wind direction is mostly influenced by terrain and diurnal circulations and we found that there was substantial improvement with using finer grids. The mean bias (MB) and MAE in the 12 km domain were about 6° less than those in the 36 km domain. The 4 km domain showed marginally better performance in MAE (~1°) and more noticeable improvement in MB (~ 4°) over the 12 km domain, while the 1 km domain had some additional improvement (~ 4°) in both MB and MAE. *Mass et al.* [2002] compared the real-time forecasting run for the region at 36, 12, and 4 km grid spacing, and found very similar improvements in wind direction. For wind speed, all four domains showed very similar MAE but improved MB with finer grids. For temperature, the three domains between 1 and 12 km showed similar MAE which were

slightly improved from 36 km one, while the 12 km domain performed best for MB.

Model performance was also evaluated on an hourly basis as shown in Figure 1 for MAE and Figure 2 for MB. For wind direction, time series of MB and MAE suggested that the 1 km domain performed best for most of the hours. 4 km and 12 km results were relatively close, while 36 km showed substantially increased MB and MAE. In terms of wind speed, the four domains all had a tendency to under-predict during the day, while the results at night were more mixed. Higher resolution generally produced higher wind speeds and helped to reduce the model under-predictions in the daytime, with little bias from the 1 km domain in the afternoon to early evening hours. Similar to wind direction, there was more noticeable improvement while increasing grid resolution from 36 to 12 km and from 4 to 1 km, while the predictions from the 12 and 4 km domains were relatively close to each other. For temperature, there was an obvious diurnal pattern in the prediction, with warm tendencies in morning to early afternoon hours but cold bias at evening and night. Higher resolution helped slightly in the day, and showed more improvement at night.

## 3.2 CMAQ performance

### 3.2.1 $O_3$ spatial features with high resolution MM5

For CMAQ performance, we first compared the run with 1 km MM5, but 4 km emissions with the 4 km run for predicted $O_3$ spatial features to investigate the impact of high resolution meteorological input. Ozone surface contour plots at 15 LST on 27 July are shown in 3a and 3b for the 4 km run and 1 km run, respectively, with the difference plot (3b-3a) shown in 3c. Here the 1 km run ozone contours (3b) are the gridded means

aggregated from 1 km to 4 km grid cells, so that they can be compared with the 4 km results. Similar contours for 28 July are shown in Figure 3d-e.

Similar $O_3$ peaks were predicted by the two runs on 27 July, whereas on 28 July the 1 km run predicted slightly lower concentrations. When using high resolution MM5, the areas with elevated $O_3$ were reduced in size and shifted slightly further downwind. The maximum $O_3$ increases occurred along the Columbia River Gorge and the foothills of Cascades where the terrain effects are substantial. For example, transport of $O_3$ along the Gorge can be clearly identified, with $O_3$ increases around 20 ppb compared to the 4 km run. On the other hand, $O_3$ decreases, mostly around 10-25 ppb, were predicted closer to the source region when high resolution MM5 meteorology was used. As discussed in Section 3.1, increasing grid resolution generally helped to reduce the under-prediction of wind speed during the day. Comparing the 1 km and 4 km MM5 run (as shown in Figure 2b), higher wind speeds, by ~0.5 m/s, and smaller MB occurred in the 1 km run during the afternoon hours, which is likely to be the main factor contributing to the lower $O_3$ levels around the source region.

### 3.2.2 $O_3$ spatial features with high resolution emissions

The run with 1 km MM5 meteorology, but 4 km emissions was further compared with the run in which both high resolution MM5 meteorology and emissions were used for predicted $O_3$ spatial features. Ozone surface contour plots at 15 LST on 27 July are shown in Figure 4a for the run with high resolution MM5 only. Figure 4b shows similar contours for the run with both 1 km MM5 and emissions, with the difference plot (4b-4a) shown in 4c. Similar contours for 28 July are shown in Figure 4d-e.

The overall pattern and $O_3$ peaks were fairly similar between the two runs, but the run with both high resolution MM5 and emissions showed small-scale features which were missing when coarser emissions were used. Most of the differences occurred close to the source region such as along the I-5 corridor and within the Portland urban area with both increases and decreases in $O_3$ levels. $O_3$ decreases (mostly less than 15 ppb) mainly occurred in grid cells with large roadway emissions, where NO titration effects were better represented with fine-scale emissions. $O_3$ increases (mostly less than 10 ppb) were predicted in the surrounding cells next to these roadway emissions around the urban area, where NO emissions were artificially diluted when using 4 km emission surrogates. Increases in $O_3$ were also predicted further downwind of the source region, although the changes were mostly below 5 ppb.

### 3.2.3 Model performance for $O_3$

In the previous section, we illustrated the impact of high resolution meteorological and photochemical modeling in terms of predicted $O_3$ spatial features. We now evaluate the model runs and investigate if the differences in those spatial features can be verified by comparing to observed $O_3$ levels. There are 8 stations in the EPAAQS measurement network (http://www.epa.gov/ttn/airs/airsaqs) across the 1 km domain. $O_3$ concentrations were extracted from grid cells coincident with those measurement locations.

Model performances were first evaluated on an hourly basis (see Figure 5), and we found overall good performance, with all three runs capturing the peak and diurnal pattern of $O_3$ levels reasonably well at most of the monitoring sites.

At Castle Rock, Woodland, and Sauvie Island, three rural monitoring sites north of Portland along the I-5 corridor, moderately high $O_3$ levels between 80 to 100 ppb were observed. Comparing the three model simulations, the two runs with 1 km MM5 but different emissions predicted very similar temporal variations, which was also true at the other monitoring sites for most of the times. At Woodland and Sauvie Island, the two runs with 1 km MM5 input tended to predict slightly lower daytime peaks but a little higher nighttime levels compared to the run with 4 km meteorological fields. At Castle Rock, the daytime levels were similar in all three runs, while slightly higher nighttime levels from the 1 km simulations persisted. Compared to the observed $O_3$ levels, the runs with 1 km MM5 input performed better for daytime peaks, while the run with 4 km MM5 showed slightly better agreement for nighttime levels. The decrease of daytime peak $O_3$ mixing ratios from the high resolution run was consistent with lower $O_3$ levels close to the source region as discussed in Section 3.2.1, and was mostly likely due to higher wind speeds from the 1 km MM5 run. The differences in the nighttime levels also appeared to be mainly due to the changes in transport and dispersion process. This is because the slightly higher nighttime $O_3$ levels occurred when applying high resolution MM5 rather than high resolution emissions.

At Mt View and Milwaukie, two suburban sites with one close to Vancouver and the other slightly southeast of downtown Portland, the observed daytime peaks were close to 100 ppb while the nighttime $O_3$ levels were fairly low. At Mt view, all three runs captured the $O_3$ diurnal trend fairly well, although the model showed broader peaks compared to the observations. This has been related to CMAQ difficulties in simulating the evolution of nocturnal boundary layers and resulting impact on $O_3$ concentrations

[*Eder and Yu*, 2006]. At Milwaukie, observational data were missing on 27 July and part of 28 July. The 4 km run predicted the highest daytime peak, followed by the run with 1 km MM5 but 4 km emissions, while the run with both MM5 and emissions at 1 km showed the lowest daytime levels. This is the site where we see the largest difference between the two runs with up to about 8 ppb changes in the predicted $O_3$ peaks. This difference could be related to location near the urban center and is consistent with the small-scale feature changes discussed in Section 3.2.2

At Carus, another rural site located about 30 miles south of Portland at the foot of the mountains, a series of exceedances of the 1-hr and 8-hr ozone standards occurred on 27 through 28 of July, with 1-hr peak values of 133 and 137 ppb, respectively. All three model runs showed generally similar and good performance at this site.

Hockinson and Wishram are the two sites that are further away from the I-5 corridor and influenced heavily by complex terrain, with the former being 20 miles upwind of Portland close to the west slope of the Cascade Mountains and the latter along the east edge of the Columbia River Gorge. At Hockinson, moderately high $O_3$ values (close to 100 ppb) were observed. All three model runs appeared unable to capture the $O_3$ peaks on the two modeling days. At Wishram, $O_3$ values were moderate throughout the episode with maximum value of 77 ppb on 27 July. All three model runs captured the general trend of observed values, while the runs with 1 km MM5 meteorology predicted slightly higher $O_3$ levels most of the times, matching the observed values a little closer. As shown in Figure 3c and 3f, there were substantial $O_3$ increases along the Columbia River Gorge when high resolution MM5 meteorology was used. However, only small

differences were predicted at Wishram, since it's located on the east edge of the Gorge and therefore relatively far from the source region.

Hourly observed and predicted $O_3$ levels were used to calculate the 8-hr average concentrations and daily maximum 8-h (DM8H) values. The overall performance is summarized in Table 2. Data with observed $O_3$ mixing ratio less than 40 ppb were excluded to focus on the high $O_3$ levels. As expected from the close performance we described in the surface $O_3$ time series, the three model runs showed fairly close mean normalized bias (MNB) and mean normalized gross error (MNGE). For hourly 8-hr average, the 4 km run had marginally better MNB (8 %) compared to the two 1 km run (9% and 10%), while the 1 km runs performed slightly better for MNGE (17% versus 19%). For DM8H, the MNB (≤1%) was very close for all three runs, while the two runs with 1 km MM5 again improved slightly in MNGE (14% versus 17%). Compared to the other air quality simulations in the region [*Smyth et al.*, 2006; *O'Neill et al*., 2006, *Chen et al.*, 2008], the CMAQ runs showed fairly good performance here.

## 4. Conclusions

Air quality in the Pacific Northwest is strongly influenced by complex terrain and unique meteorological conditions within and near the Columbia River Gorge and the Cascade Mountain range. Topographical features interact closely with the regional flow, and therefore have an important impact on the dispersion of pollutants. In this study, the MM5/SMOKE/CMAQ modeling system was used for nested 4 km and 1 km domains encompassing the Portland metropolitan area and the Columbia River Gorge for an ozone episode that occurred at July, 1998 to investigate the effects of high resolution

meteorological and emissions inputs on photochemical modeling of $O_3$ predictions for the region. We first evaluated the effects of grid resolution on meteorological model performance. Then from an air quality perspective, the effects of high resolution meteorological input were compared with those of high resolution emissions by running CMAQ at 4 km and 1 km for three scenarios: 1) with both MM5 meteorology and emissions at 4 km; 2) with 1 km MM5 meteorology, but 4 km emissions; and 3) with both MM5 meteorology and emissions at 1 km.

MM5 performances were evaluated at four grid resolutions (36, 12, 4, and 1 km) and the results suggest that finer grid resolutions generally improve model performance, especially for wind direction and wind speed. More substantial differences occurred when grid spacing was reduced from 36 km to 12 km and from 4 km to 1 km, while the results from the 12 and 4 km domains were relatively similar. While comparing specifically between the 4 km and 1 km run, higher wind speed and reduced MB occurred in the afternoon to early evening hours and wind direction was improved for most of the time when finer grids were used.

For $O_3$ predictions, using high resolution meteorological input alone appeared to have a larger impact on the position and peak levels of the $O_3$ plume. $O_3$ concentrations were substantially higher (around 20 ppb) in the 1 km case compared to the 4 km case in areas along the Columbia River Gorge and the foothills of Cascades where the terrain effects are substantial. On the other hand, decreased levels were predicted close to the source region, largely due to the higher wind speed while finer grids were used. Using high resolution emissions appeared to affect small-scale features in $O_3$ concentration patterns mainly within the urban area. In that case, areas of either $O_3$ increases or

decreases occurred which were missing when using coarse resolution emissions. In contrast to the noticeable improvement with increased resolution in the meteorological model performance, photochemical model runs showed relatively similar levels of performance compared to observed $O_3$ values; this may be due, in part, to the fact that there were relatively few observation sites so that the effects of resolution cannot be discerned from the monitoring network. For surface $O_3$ time series and statistical performance at these sites, small differences occurred when high resolution meteorology input was used with slight improvement of daytime peaks at a few upwind sites, while the results didn't change when high resolution emissions were further applied.

The findings here suggest that high resolution meteorological input can have important effects on simulation of air quality impacts, especially in regions heavily influenced by orographical flows and diurnal circulations. Using high resolution emissions reveals small-scale features which are missing when coarse emission grids are used. These results can be important for characterizing subgrid variability, which is important for human exposure studies as well as model evaluation design. Meanwhile, the results here also call attention to more adequate evaluation of high resolution air quality modeling results, for example using mobile sampling devices in field experiments.

**References**


Avise, J., J. Chen, B. Lamb, C. Wiedinmyer, A. Guenther, E. Salathé, C. Mass (2008), Attribution of projected changes in US ozone and $PM_{2.5}$ concentrations to global changes, *Atmos. Chem. Phys. Discuss., 8*, 15131-15163.

Barna, M. G., and B. K. Lamb (2000), Improving ozone modeling in the regions of complex terrain using observational nudging in a prognostic meteorological model, *Atmos. Environ., 34*, 4889- 4906.

Byun, D. W., and K. L. Schere (2006), Review of the governing equations, computational algorithms, and other components of the Models-3 Community Multiscale Air Quality (CMAQ) modeling system, *Appl. Mech. Rev*., *59*, 51-77.

Carter, W. P. L. (2000), *Documentation of the SAPRC-99 Chemical Mechanism for VOC Reactivity Assessment*, No. 92 – 329, 95 – 308, Final Report to California Air Resources Board, Calif. Air Resour. Board, Riverside Calif. (Available at http://www.engr.ucr.edu/~carter/absts.htm#saprc99)

Chang J. S., K. H. Chang and S. Jin (1993), Two-way and one-way nested SARMAP air quality model, paper presented at International Conference on Regional Photochemical Measurement & Modeling Studies, A&WMA, San Diego, Calif., 8-12 November.

Chen, F., and J. Dudhia (2001), Coupling an advanced land surface–hydrology model with the Penn State–NCAR MM5 modeling system. Part I: Model implementation and sensitivity, *Mon. Wea. Rev., 129*, 569–585.

Chen, J., J. Vaughan, J. Avise, S. O'Neill, and B. Lamb (2008), Enhancement and evaluation of the AIRPACT ozone and PM2.5 forecast system for the Pacific Northwest, *J. Geophys. Res., 113*, D14305, doi:10.1029/2007JD009554.

Ching, J., J. Herwehe, and J. Swall (2006), On joint deterministic grid modeling and sub-grid variability conceptual framework for model evaluation, *Atmos. Envrion., 40*, 4935-4945.

Colle, B. A., and C. F. Mass (1998), Windstorms along the western side of the Washington Cascade Mountains. Part I: A high resolution observational and modeling study of the 12 February 1995 event, *Mon. Wea. Rev., 126*, 28–52.

Colle, B. A., and C. F. Mass (2000), High-resolution observations and numerical simulations of easterly gap flow through the Strait of Juan de Fuca on 9–10 December 1995, *Mon. Wea. Rev., 128*, 2398–2422.

Cohan, D. S., Yongtao H., Armistead G. R. (2006), Dependence of ozone sensitivity analysis on grid resolution, *Atmos. Environ., 40*, 126-135.

Eder, B., and S. C. Yu (2006), A performance evaluation of the 2004 release of Models-3 CMAQ, *Atmos. Environ., 40*, 4811 –4824.

Gillani, N. V., J. E. Pleim (1996), Sub-grid-scale features of anthropogenic emissions of NOx and VOC in the context of regional Eulerian models, *Atmos. Environ., 30* , 2043–2059.

Grell, A. G., J. Dudhia, and D. R. Stauffer (1994), A description of the fifth generation Penn State/NCAR mesoscale model (MM5), in *NCAR Tech. Note 3981STR*, 138 pp., Natl. Cent. Atmos. Res., Boulder, Colo. (Available at http://www.mmm.ucar.edu/mm5)

GVRD Canada (2002), *2000 Emission Inventory for the Lower Fraser Valley Airshed*, Policy and Planning Department Greater Vancouver Regional District, Fraser Valley Regional District, B. C., Canada. (Available at http://www.gvrd.bc.ca/air/inventory_reports.htm)

Jang, J. C., H. E. Jeffries, D. W. Byun, and J. E. Pleim (1995a), Sensitivity of ozone to model grid resolution: Part 1. Application of high-resolution regional acid deposition model, *Atmos. Environ., 29*, 3085–3100.

Jang, J. C., H. E. Jeffries, and S. Tonnesen (1995b), Sensitivity of ozone to model grid resolution: Part 2. Detailed process analysis for ozone chemistry, *Atmos. Environ., 29*, 3101– 3114.

Mass, C. F., D. Ovens, K. Westrick, and B. A. Colle (2002), Does Increasing Horizontal Resolution Produce More Skillful Forecasts?, *Bull. Amer. Meteor. Soc., 83*, 407-430.

McQueen, J. T., R. R. Draxler, and G. D. Rolph (1995), Influence of grid size and terrain resolution on wind field predictions from an operational mesoscale model, *J. Appl. Meteor., 34*, 2166–2181.

Hong, S.-Y., and H.-L. Pan (1996), Nonlocal boundary layer vertical diffusion in a medium-range forecast model, *Mon. Wea. Rev., 124*, 2322–2339.

Hack, J. J., B. A. Boville, B. P. Briegleb, J. T. Kiehl, P. J. Rasch, and D. L. Williamson (1993), Description of the NCAR Community Climate Model (CCM2), *NCAR Tech. Note*, *NCAR/TN-382+STR*, 108 pp., Natl. Cent. for Atmos. Res., Boulder, Colo.

Kain, J. S., (2004), The Kain-Fristch convective parameterization: An update, *J. Appl. Meteor., 43*, 170-181.

Lamb, B., Y. Xie, C. Bowman, S. Otterson, D. Schneider, K. Himes, J. Anderson, K.

Agyei, and B. Carper (2006), Modeling Analysis of Future Emission Scenarios for Ozone Impacts in the Puget Sound Area, Final report prepared for Puget Sound Clean Air Agency.

O'Neill, S. M. and B. K. Lamb (2005), Intercomparison of the Community Multiscale Air Quality Model and Calgrid using Process Analysis, *Environ. Sci. Technol., 39*, 5742-5753.

Smyth, S. C., W. M. Jiang, D. Z. Yin, H. Roth, and T. Giroux (2006), Evaluation of CMAQ $O_3$ and $PM_{2.5}$ performance using Pacific 2001 measurement data, *Atmos. Environ., 40*, 2735–2749.

Reisner, J., R. M. Rasmussen, and R. T. Bruintjes (1998), Explicit forecasting of supercooled liquid water in winter storms using the MM5 mesoscale model, *Quart. J. Roy. Metero. Soc., 124 B*, 1071-1107.

Sharp, J., and C. Mass (2002), Columbia Gorge gap flow: Insights from observational analysis and ultra-High-Resolution Simulation, *Bull. Amer. Meteor. Soc., 83*, 1757-1762.

U.S. EPA (2003), User's guide to MOBILE6.1 and MOBILE6.2 (Mobile source emission factor model), in *Rep. EPA420-R-03-010*, Off. of Transp. and Air Qual., Ann Arbor, Mich. (Available at http://www.epa.gov/otaq/m6.htm)

U.S. EPA (2005), Environmental Protection Agency Final 2005 Nonroad Model, [online] http://www.epa.gov/otaq/nonrdmdl.htm#model

Vaughan, J., et al. (2004), A numerical daily air quality forecast system for the Pacific Northwest, *Bull. Am. Meteorol. Soc., 85*, 549– 561.

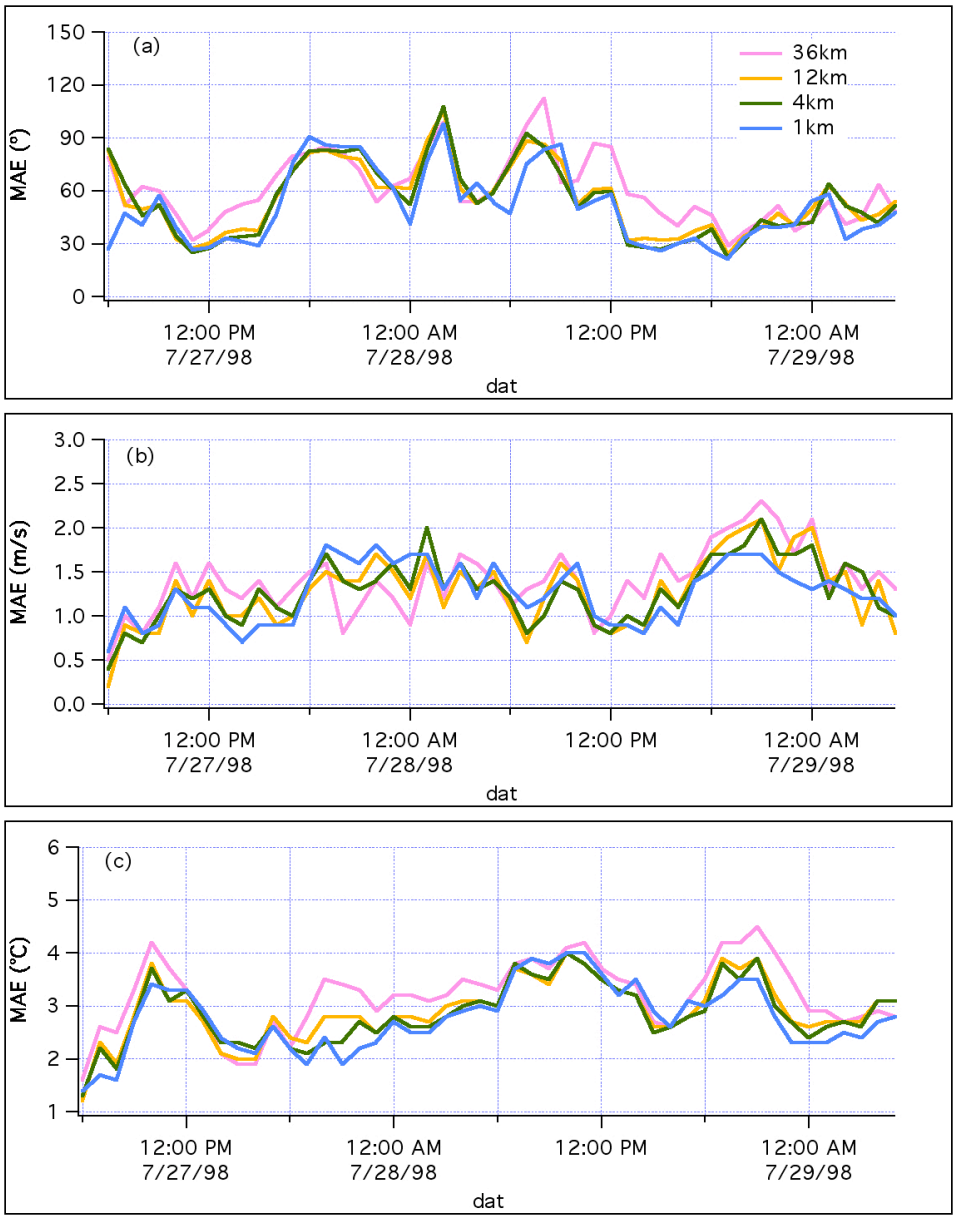


Figure 1. The MAE within the 1 km domain for a) wind direction; b) wind speed; and c) temperature.

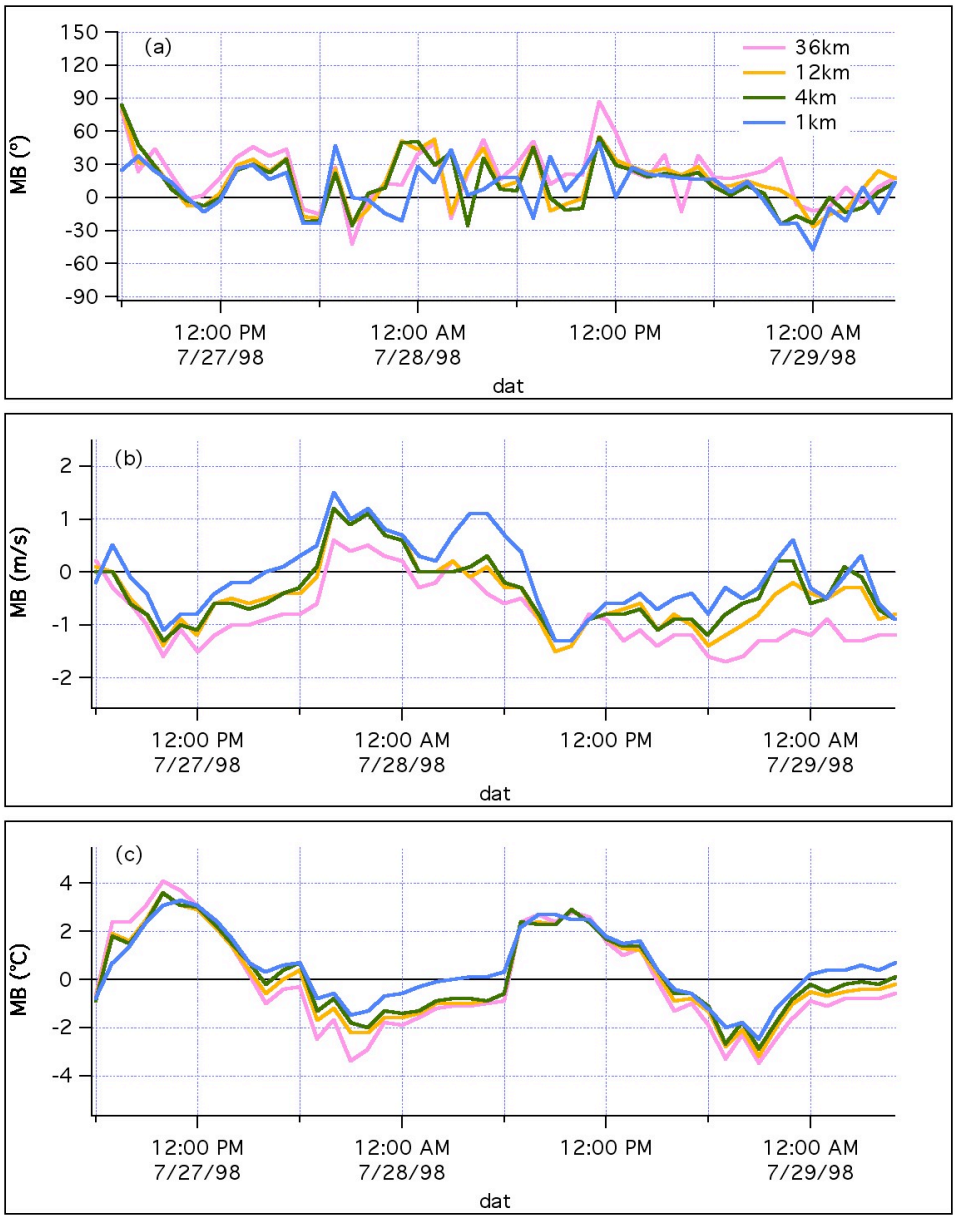


Figure 2. The MB within the 1 km domain for a) wind direction; b) wind speed; and c) temperature.

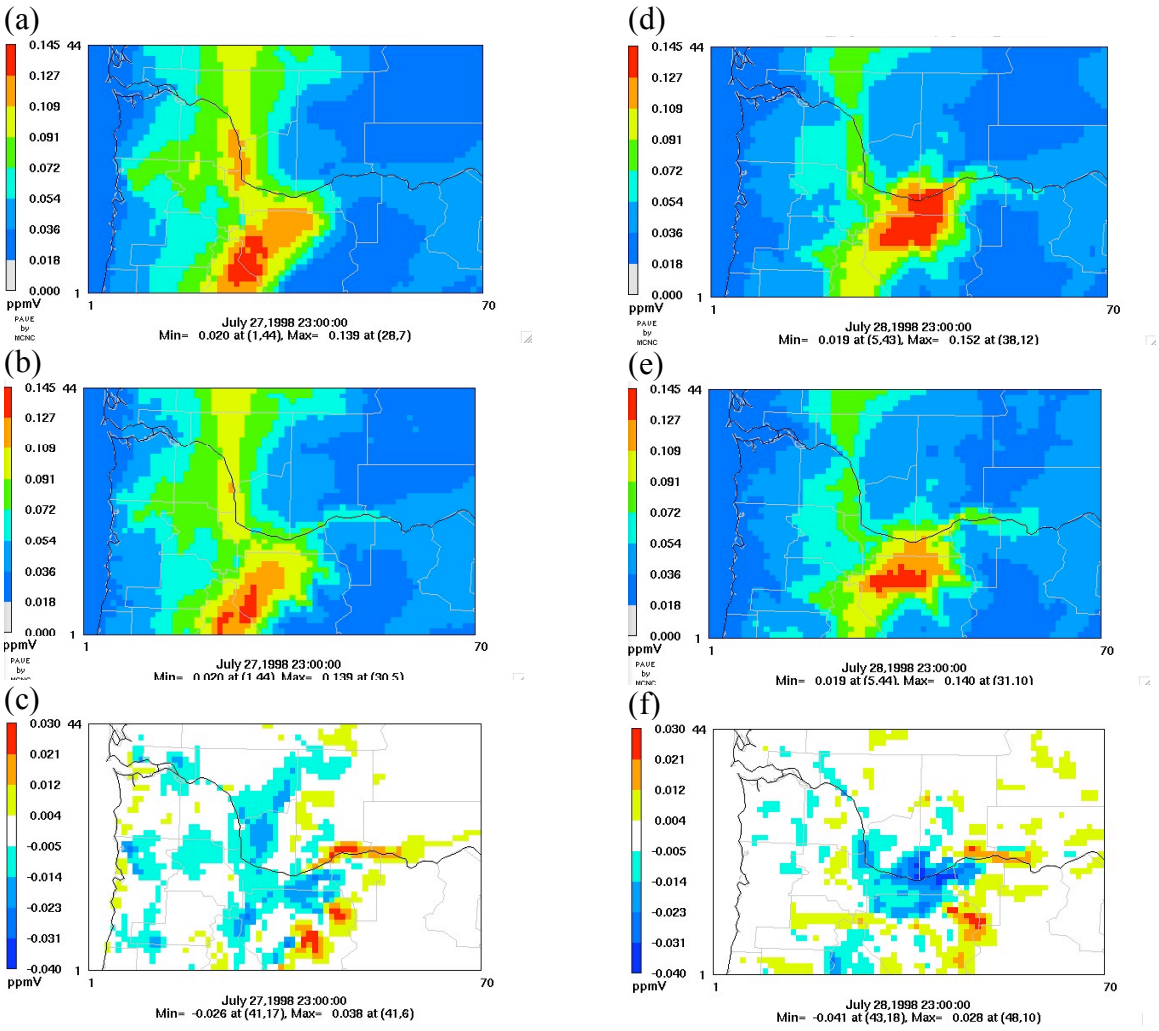


Figure 3. Surface ozone contours from CMAQ at 15 LST on 27 and 28 July, 1998. (a) 4 km run on 27 July. (b) 1 km run using 1 km MM5 but 4 km emissions on 27 July. (c) difference plot of "(b)-(a)". (d),(e), and (f) are similar plots for 28 July. (Note that (b) and (e) are the gridded mean concentrations aggregated from 1 km to 4 km grid cells.)

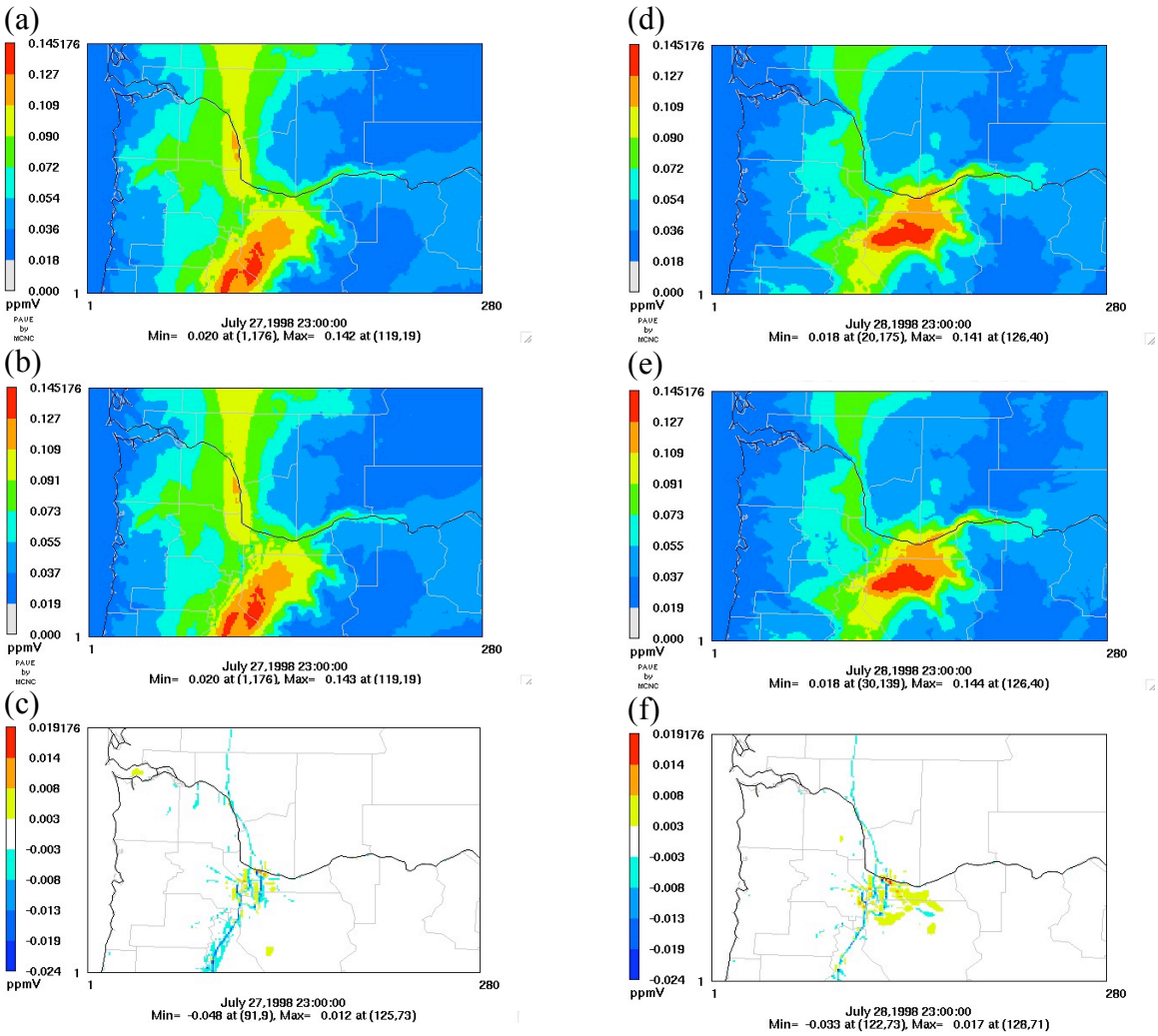


Figure 4. Surface ozone contours from CMAQ at 15 LST on 27 and 28 July, 1998. (a) 1 km run using 1 km MM5 but 4 km emissions on 27 July. (b) 1 km run using both 1 km MM5 and emissions on 27 July. (c) difference plot of "(b)-(a)". (d),(e), and (f) are similar plots for 28 July.

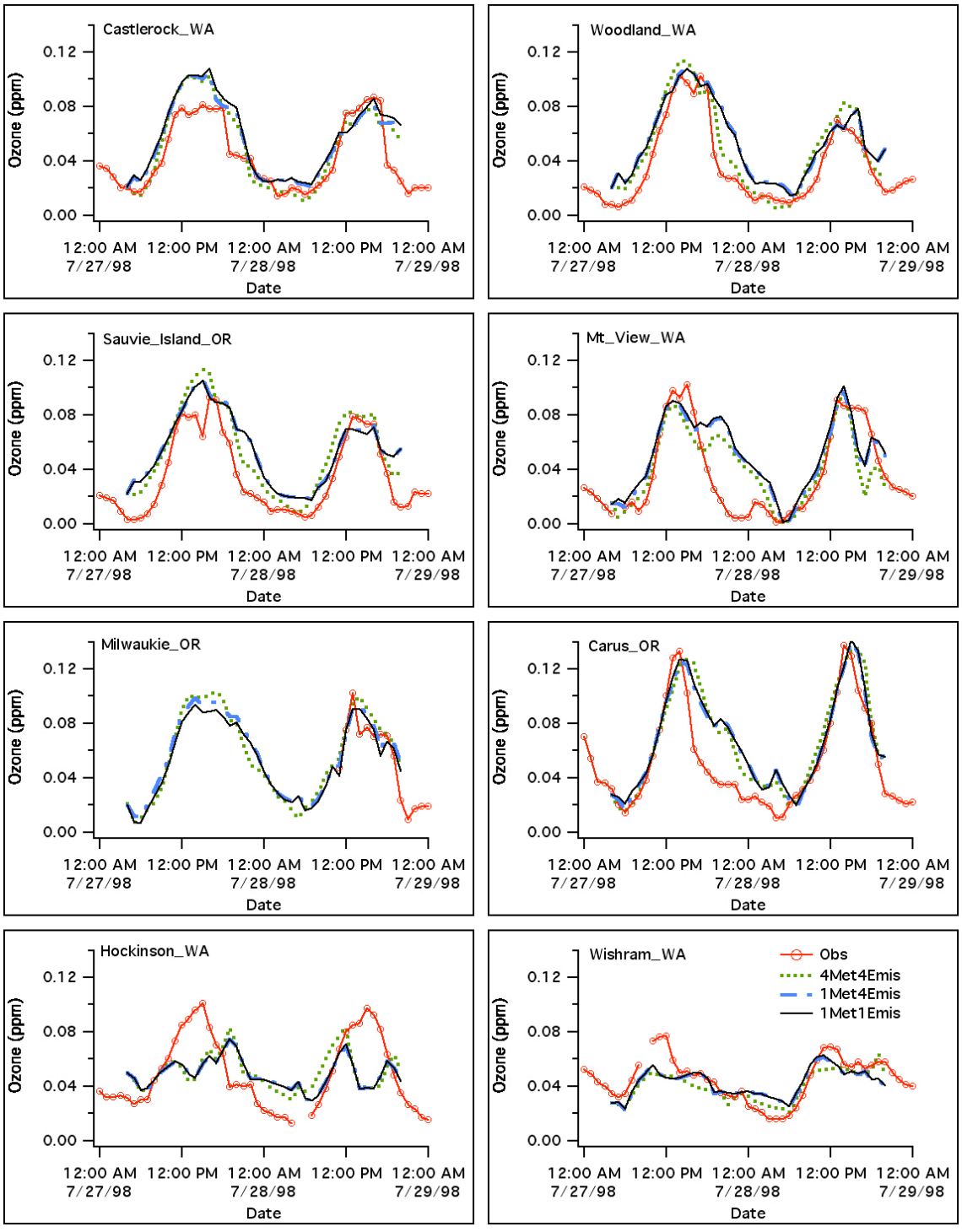


Figure 5. Observed surface $O_3$ levels compared with CMAQ predicted values from the 4 km run (4Met4Emis), the run with 1 km MM5 but 4 km emissions (1Met4Emis), and the run with both MM5 and emissions at 1 km (1Met1Emis) at surface sites.

Table 1. Summary of MM5 statistical performance with four grid resolutions.

| Resolution | Wind direction (°) | | Wind Speed (m/s) | | Temperature (°C) | |
|---|---|---|---|---|---|---|
| | MB | MAE | MB | MAE | MB | MAE |
| 1 km | 8 | 50 | -0.1 | 1.3 | 0.5 | 2.8 |
| 4 km | 12 | 54 | -0.4 | 1.3 | 0.2 | 2.9 |
| 12 km | 16 | 55 | -0.4 | 1.3 | 0.0 | 2.9 |
| 36 km | 21 | 61 | -0.8 | 1.4 | -0.1 | 3.2 |

Table 2. Summary of CMAQ statistical performance for 8-hr average and DM8H $O_3$ from the 4 km run (4Met4Emis), the run with 1 km MM5 but 4 km emissions (1Met4Emis), and the run with both MM5 and emissions at 1 km (1Met1Emis).

| | 8-hr average | | DM8H | |
|---|---|---|---|---|
| | MNB | MNGE | MNB | MNGE |
| 4Met4EI | 8% | 19% | 0% | 17% |
| 1Met4EI | 9% | 17% | 0% | 14% |
| 1Met1EI | 10% | 17% | 1% | 14% |

# CHAPTER FIVE

## Conclusions and future direction

This research employed the MM5/SMOKE/CMAQ modeling system to investigate ozone formation and fate in the Pacific Northwest region through three separate studies. In the first study, chemical features of instantaneous ozone production and the behavior of local photochemical indicators were examined. In the second study, the CMAQ model was evaluated for predicted $O_3$-$NO_x$-VOC chemistry by comparing to aircraft measurements collected during a field experiment in the Puget Sound region of western Washington. In the last study, the effects of using high resolution meteorological and emissions inputs to photochemical modeling simulation of $O_3$ were investigated.

Design and evaluation of ozone control strategies are largely dependent on photochemical modeling results. However, large uncertainties exist in model predictions due to the nonlinearity of ozone photochemistry and complex interactions between the governing physical and chemical processes. It is important to answer the following scientific questions in order to improve our future air quality simulations and abatement methods design for the region.

1) What are the chemical features that control $O_3$ formation for the region?
2) Does the current emission inventory correctly reflect $O_3$ precursor levels?
3) Can we use photochemical indicators to identify the sensitivity of $P(O_3)$ and $O_3$ to changes in $NO_x$ and VOC emissions for the region?
4) Are $P(O_3)$ and $O_3$ more responsive to $NO_x$ or VOC controls for each of the two major metropolitan areas within the region?

5) How do model predicted chemical features of ozone production and its sensitivity to $NO_x$ and VOC compare with the observed values?
6) Given the complex terrain in the region, does the use of high resolution MM5 simulations improve air quality simulations for summertime $O_3$?
7) Does the use of high resolution meteorological fields benefit from high resolution emission inventories for air quality simulations?

With the results from the three studies in this work, the answers to these questions are:

1) For the Portland area, maximum $P(O_3)$ was predicted to be 30-40 ppb $hr^{-1}$ downwind of the urban center, with $NO_x$ concentrations of 5-20 ppb and total VOC reactivity above 8 $s^{-1}$.
2) For the Puget Sound area, anthropogenic VOC and CO were the major contributors to odd oxygen photochemistry in the morning urban profile, while CO and oxygenated compounds accounted for two thirds of the measured reactivity in the afternoon aged plume according to the aircraft based measurements.
3) For the Puget Sound area, modeled $CO/NO_y$ and $VOC/NO_y$ ratios obtained with the current emission inventory were significantly higher than those observed from morning urban flights, with CO concentrations over-predicted by 80% and the total VOC reactivity over-predicted by 30%.
4) Both the instantaneous ($f_{OH+HC}$, $f_{HO2+NO}$, $P(H_2O_2)/P(HNO_3)$, $O_3/NO_x$, and $L_N/Q$) and cumulative ($O_3/NO_y$) photochemical indicators are closely related to VOC-

$NO_x$ sensitive conditions, with transitional values similar to those identified from the previous studies.

5) For the Puget Sound area, peak $O_3$ was associated with VOC-sensitive conditions, but these were not far from the transitional regime. For the Portland area, the greatest $P(O_3)$ (>30 ppb $hr^{-1}$) mostly occurred at transitional or $NO_x$-limited conditions.
6) For the Puget Sound area, comparisons of modeled and observed $O_3/NO_y$ slope indicated an overestimation of sensitivity to $NO_x$, probably due to too much VOC in the base emission inventory. In terms of VOC reactivity, the base case substantially overestimated the reactivity from CO. With the revised emission inventory, the model showed better agreement with measurements in terms of $O_3/NO_y$ correlations as well as the relative contributions to the total VOC reactivity.
7) Using high resolution meteorological input alone had a larger impact on the position and peak levels of the $O_3$ plume, with substantial increases in $O_3$ concentrations at places where complex terrain plays an important role. Using high resolution emissions tended to affect small-scale features in $O_3$ concentration patterns mainly within the urban area.

The findings from the CMAQ evaluation study suggested that both CO and oxygenated compounds play an important role in the regional photochemistry, however, their emissions are not well quantified. In the future, better methods should be developed for updating the current CO emission inventory, and more measurements are needed to

better characterize the sources of oxygenated compounds. However, these conclusions are based on measurements from three aircraft flights with limitations in the availability of measurements for certain useful species. For example, $NO_2$ was not measured and previous studies [*Tonnesen and Dennis*, 2000a, b; *Arnold et al*., 2003] have shown that accurate measurement of $NO_2$ can provide powerful probes ($O_3/NO_x$, $O_3/NO_z$, and $NO_z/NO_y$) for diagnostic evaluation of $O_3$ production and cycling processes. Meanwhile, more complete measurements of VOC species including light olefins, which were mostly not available in this work, are also needed to better characterize VOC reactivity in the atmosphere and access its impact on photochemical production of pollutants. Therefore, measurements of additional key species and comparisons with model results will further improve our understanding of the regional photochemistry and its representation in air quality models.

The evaluation of photochemical indicators suggests they are useful tools for distinguishing $NO_x$- and VOC-sensitive conditions and validating model predicted sensitivity. Meanwhile, we should keep in mind that the indicator values are highly dependent on the representation of photochemical mechanism, environmental conditions, removal processes such dry and wet deposition, and heterogeneous chemistry. Therefore, comparisons with results from different photochemical representations and different environment conditions, as well as comparisons with measurements such as smog chamber experiments are needed to improve our understanding of the derivation and usefulness of indicators.

In the high resolution modeling study, although substantial differences occurred in the ozone contour maps when different grid resolutions were used, model evaluation

using measurements from available monitoring sites showed little difference in ozone performance; this is partly due to the sparse measurement network in the region and the relatively short period we studied. In addition, generally similar model physics options were used in our coarse (4 km) and fine resolution (1 km) run, and the validity of these options at fine scale is currently not well known. Model simulations for longer time periods covering a wider range of conditions as well as more adequate model evaluations, for example using mobile sampling devices in field experiments, are essential to advance our knowledge of the merit and constraints of high resolution modeling.

## References

Arnold, J.R., R.L. Dennis, and G.S. Tonnesen (2003), Diagnostic evaluation of numerical air quality models with specialized ambient observations: testing the Community Multiscale Air Quality modeling system (CMAQ) at selected SOS 95 ground sites, *Atmos. Environ.,37*, 1185-1198.

Tonnesen, G. S., and R. L. Dennis (2000a), Analysis of radical propagation efficiency to assess ozone sensitivity to hydrocarbons and $NO_x$, 1, Local indicators of instantaneous odd oxygen production sensitivity, *J. Geophys. Res., 105*, 9213– 9226.

Tonnesen, G. S., and R. L. Dennis (2000b), Analysis of radical propagation efficiency to assess ozone sensitivity to hydrocarbons and $NO_x$, 2, Longlived species as indicators of ozone concentration sensitivity, *J. Geophys. Res., 105*, 9227– 9242.